Research Paper

GEOSPHERE

GEOSPHERE, v. 20, no. 2

https://doi.org/10.1130/GES02695.1

12 figures; 3 tables; 1 set of supplemental files

CORRESPONDENCE: wuchen@itpcas.ac.cn

CITATION: Liu, W., Wu, C., Li, J., Zhang, C., Jiang, T., Zuza, A.V., Haproff, P.J., Chen, X., and Yue, Y., 2024, Structure and provenance of the Cretaceous Pingshanhu Basin in the Hexi Corridor: Implications for Mesozoic tectonics in the northern Tibetan Plateau: Geosphere, v. 20, no. 2, p. 421–450, https://doi.org/10.1130/GES02695.1.

Science Editor: Christopher J. Spencer
Associate Editor: Jiyuan Yin

Received 21 June 2023
Revision received 18 October 2023
Accepted 7 December 2023

Published online 8 March 2024

Structure and provenance of the Cretaceous Pingshanhu Basin in the Hexi Corridor: Implications for Mesozoic tectonics in the northern Tibetan Plateau

Wenyou Liu[1,2], Chen Wu[1], Jie Li[3], Cunhui Zhang[1,4], Tian Jiang[5], Andrew V. Zuza[6], Peter J. Haproff[7], Xuanhua Chen[8], and Yahui Yue[1]

[1]State Key Laboratory of Tibetan Plateau Earth System and Resources Environment, Institute of Tibetan Plateau Research, Chinese Academy of Sciences, Beijing 100101, China
[2]School of Earth Sciences and Resources, China University of Geosciences (Beijing), Beijing 100083, China
[3]Chongqing Key Laboratory of Complex Oil and Gas Field Exploration and Development, Chongqing University of Science and Technology, Chongqing 401331, China
[4]University of Chinese Academy of Sciences, Beijing 100049, China
[5]School of Ocean Sciences, China University of Geosciences (Beijing), Beijing 100083, China
[6]Nevada Bureau of Mines and Geology, Nevada Geosciences, University of Nevada, Reno, Nevada 89557, USA
[7]Department of Earth and Ocean Sciences, University of North Carolina, Wilmington, North Carolina 28403, USA
[8]SinoProbe Center, Chinese Academy of Geological Sciences, Beijing 100037, China

ABSTRACT

The construction of Earth's largest highland, the Tibetan Plateau, is generally considered to have been generated by the Cenozoic India-Asia collision. However, the extent to which high topography existed prior to the Cenozoic remains unclear. The Hexi Corridor foreland basin of the northern Tibetan Plateau is an ideal region in which to investigate this history, given its widespread exposure of Early Cretaceous sedimentary sequences. In this study, we examined the Early Cretaceous strata in the northern Hexi Corridor to understand the relationships between pre-Cenozoic sedimentation and tectonic deformation and constrain the late Mesozoic tectonic setting of the adjacent Qilian Shan and Alxa blocks bordering the northern Tibetan Plateau. Results of sandstone petrology analyses, paleocurrent observations, and U-Pb geochronology suggest that the oldest Early Cretaceous sediments deposited in the northern Hexi Corridor were sourced from the southern Alxa block during the earliest Cretaceous. By the late Early Cretaceous, Hexi Corridor sediments were sourced from both the southern Alxa block to the north and the Qilian Shan to the south. Sandstone petrologic results indicate that the northern Hexi Corridor experienced a tectonic transition from contraction to extension during the Early Cretaceous. These findings suggest that the northern Tibetan Plateau region was partially uplifted to a high elevation during the late Mesozoic before the India-Asia collision.

1. INTRODUCTION

The tectonic evolution and formation mechanism(s) of the Tibetan Plateau and Asian tectonic system have profound implications for understanding the dynamics of intracontinental deformation (Figs. 1A and 1B; Burchfiel et al., 1991; Yin and Harrison, 2000; Tapponnier et al., 2001; Taylor et al., 2003; Royden et al., 2008; Yin, 2010; Clark, 2012; Ren et al., 2013; Wu et al., 2021b; Ding et al., 2022). Furthermore, deformation along the northernmost margin of the Tibetan Plateau is key to understanding how and when the plateau was constructed (e.g., Meyer et al., 1998; Clark et al., 2010; Clark, 2012; Duvall et al., 2011; Yuan et al., 2013; Zheng et al., 2017a; Li et al., 2019a, 2020b; Yu et al., 2019; Zuza et al., 2016, 2019; An et al., 2020; Wang et al., 2020a, 2022, 2023; Wu et al., 2021a, 2021b). Numerous investigations have focused on Cenozoic deformation across the northern Tibetan Plateau, which was induced by the India-Asia collision to the south. However, distributed faulting, overprinting relationships, relatively slow erosion, and limited exhumation in the northern Tibetan Plateau have hindered the use of traditional techniques, such as low-temperature thermochronology, to precisely resolve deformation kinematics, resulting in an incomplete understanding of the strain history (e.g., Chen et al., 2019a, 2019b; Zuza et al., 2019; Li et al., 2020a).

Two existing end-member models describe deformation along the northernmost Tibetan Plateau. In one model, deformation gradually propagated northward from the Himalayan collisional front to the northern plateau margin (e.g., Tapponnier et al., 2001; Clark, 2012; Wang et al., 2014, 2020a, 2020b; Zheng et al., 2017a; Yu et al., 2019). In the second model, deformation occurred across most of the Himalayan-Tibetan orogen shortly after the initial India-Asia collision, exploiting preexisting weaknesses, such as older suture zones. This was followed by out-of-sequence deformation along the northern Tibetan Plateau margin from the Eastern Kunlun Range in the south to the Hexi Corridor foreland basin in the northeast (Fig. 1B; e.g., Yin and Harrison, 2000; Chen et al., 2019a, 2020; Li et al., 2019a, 2020a; Wu et al., 2019b; Zuza et al., 2019, 2020; Bian et al., 2020). These two end-member models make predictions for the expansion directions of the thick and high Tibetan Plateau to the north and east, along with the kinematics and timing of intracontinental deformation and

Chen Wu https://orcid.org/0000-0003-0647-3530

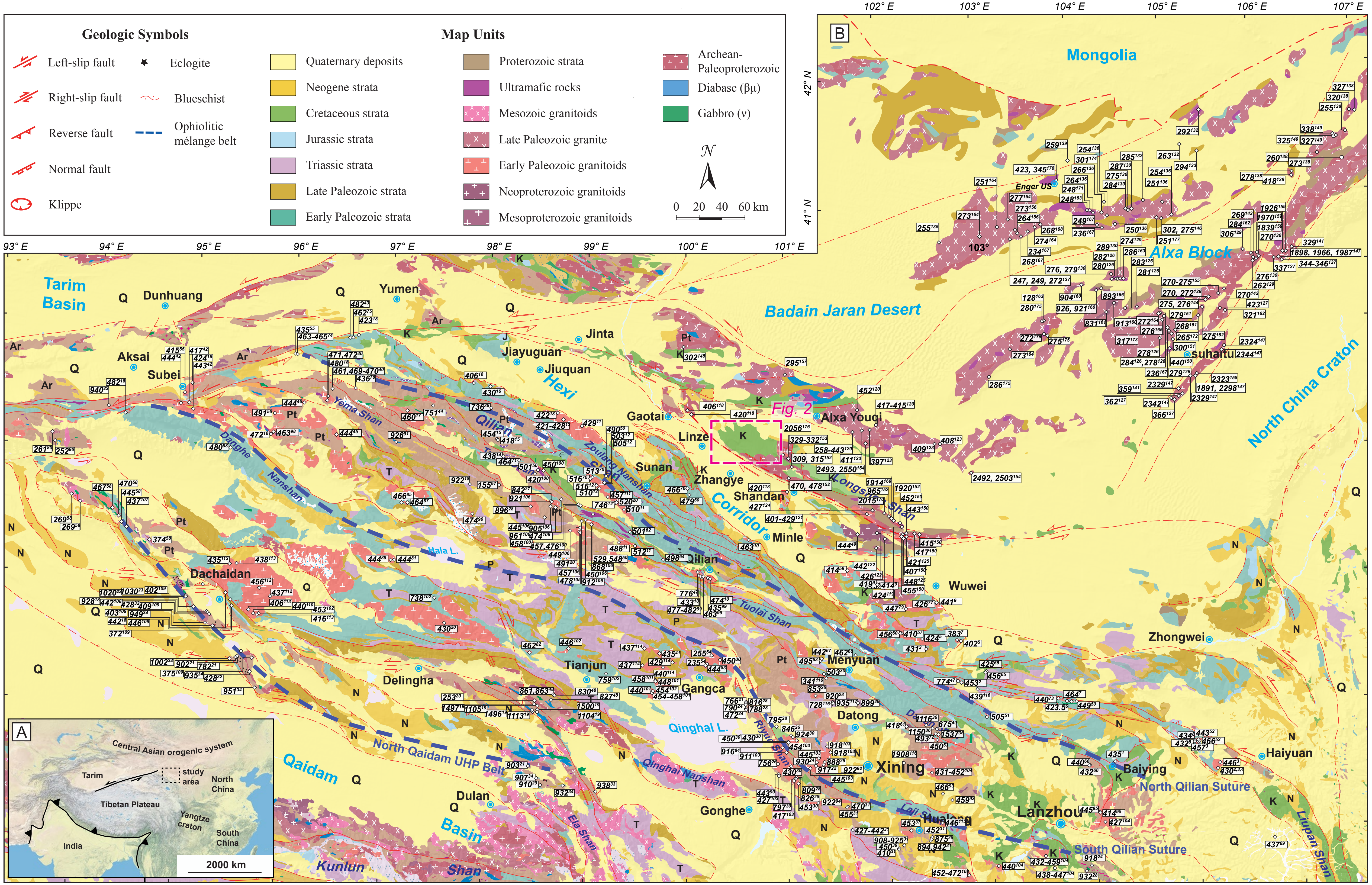

Figure 1. (A) Map of southern Asia showing the location of the study area in the northern Tibetan Plateau and Hexi Corridor foreland basin. (B) Geologic map of the northern Tibetan Plateau and Alxa block showing ages of magmatic rocks. The map is modified from Pan et al. (2004), Wu et al. (2022a), and Wang et al. (2022). The location of Figure 2 is shown by a pink dashed box. Data are compiled from: 1—Yang et al. (2020); 2—Tseng et al. (2009); 3—Yu et al. (2015); 4—Chen et al. (2016); 5—Xiong et al. (2012); 6—Qian et al. (1998); 7—Wu et al. (2004); 8—Chen et al. (2015b); 9—Zhang et al. (2017b); 10—Wu et al. (2011); 11—Wu et al. (2010); 12—Chen et al. (2014b); 13—Huang et al. (2017); 14—Chen et al. (2012); 15—Zhao et al. (2014); 16—Li et al. (2019b); 17—Mao et al. (2000); 18—Gehrels et al. (2003b); 19—Wang et al. (2021); 20—Li et al. (2021); 21—Peng et al. (2019); 22—Guo et al. (2000); 23—Wan et al. (2001, 2003); 24—Tung et al. (2007); 25—Xu et al. (2007); 26—Yong et al. (2008); 27—Xue et al. (2009); 28—Tung et al. (2013); 29—Yu et al. (2013); 30—Huang et al. (2015); 31—Yan et al. (2015); 32—Zhang et al. (2008); 33—Xu et al. (2011); 34—Song et al. (2012); 35—Liu et al. (2015); 36—Dong et al. (2015); 37—Guo et al. (2015a); 38—Li et al. (2015); 39—Zhang et al. (2015c); 40—Hou et al. (2015); 41—Shi et al. (2015); 42—Luo et al. (2015); 43—Song et al. (2004); 44—Su et al. (2004a); 45—Su et al. (2004b); 46—Su et al. (2004c); 47—Tseng et al. (2006); 48—Ma et al. (2018); 49—Song et al. (2016); 50—Song et al. (2013); 51—Qin et al. (2014a); 52—Qin et al. (2014b); 53—Liu et al. (2014); 54—Xie et al. (2014); 55—Li et al. (2010); 56—Huang et al. (2014); 57—Huang et al. (2018); 58—Wu et al. (2009); 59—Huang et al. (2010); 60—Ding and Huang (2019); 61—Wang et al. (2018a); 62—Wang et al. (2018b); 63—Peng et al. (2017); 64—Li et al. (2017); 65—Zhao et al. (2018); 66—Zhao et al. (2013); 67—Liu et al. (2019); 68—Guo et al. (2015b); 69—Wu et al. (2019b); 70—Zhang et al. (2018b); 71—Liu et al. (2018); 72—Liu et al. (2016a); 73—Zhang et al. (2019b); 74—Wang et al. (2017a); 75—Fan et al. (2020); 76—Bu et al. (2019); 77—Liu (2013); 78—Wang et al. (2017b); 79—Chen et al. (2019c); 80—Jia et al. (2017); 81—Zhang et al. (2018c); 82—Liao et al. (2014); 83—Shi et al. (2017); 84—Zhu et al. (2019); 85—Li et al. (2020b); 86—Hu et al. (2016); 87—Yu et al. (2018a); 88—Ji et al. (2019); 89—Yu et al. (2018b); 90—Zhang et al. (2012b); 91—Tao et al. (2017); 92—Gao et al. (2017); 93—Cao et al. (2019); 94—Lv et al. (2021); 95—Chen et al. (2008); 96—Zheng et al. (2017b); 97—Zhang et al. (2018a); 98—Qi (2012); 99—Chen (2009); 100—Zhang (2014); 101—Chang (2017); 102—Qin (2018); 103—Liu (2019); 104—Yang (2016); 105—An (2015); 106—Zuza et al. (2018); 107—Zhu et al. (2013); 108—Zhou et al. (2014); 109—Wu et al. (2007); 110—Lu et al. (2007); 111—Zhang et al. (2015b); 112—Zhu et al. (2016); 113—He et al. (2020); 114—Zhang et al. (2016b); 115—Cui et al. (2016); 116—Wu et al. (2021b); 117—Wu et al. (2022a); 118—Wang et al. (2020b); 119—Duan et al. (2015); 120—Liu et al. (2016c); 121—Tang (2015); 122—Zhang et al. (2017b); 123—Zhou et al. (2016); 124—Zhang et al. (2018d); 125—Qing (2012); 126—Dan et al. (2016); 127—Dan et al. (2014a); 128—Dan et al. (2014b); 129—Dan et al. (2015); 130—Feng et al. (2013); 131—Geng and Zhou (2012); 132—Hu et al. (2015); 133—Lin et al. (2014); 134—Peng et al. (2013); 135—Pi et al. (2010); 136—Ran et al. (2012); 137—Shi et al. (2014a); 138—Shi et al. (2014b); 139—Wang et al. (2015); 140—Wu et al. (2013); 141—Xu et al. (2013); 142—Zhang et al. (2013a); 143—Zhang et al. (2012a); 144—Zhang et al. (2015a); 145—Zhang et al. (2013c); 146—Zhang et al. (2014); 147—Zheng et al. (2014); 148—Dan et al. (2012); 149—Dan et al. (2014a); 150—Liu et al. (2016a); 151—Liu et al. (2016b); 152—Wu et al. (2022a); 153—Xue et al. (2017); 154—Zhang et al. (2013b); 155—Zhang et al. (2016c); 156—Chen et al. (2015a); 157—Chen et al. (2013); 158—Dong et al. (2007); 159—Geng et al. (2010); 160—Geng and Zhou (2010); 161—Li (2012); 162—Shi (2012); 163—Wang (2012); 164—Wu (2011); 165—Xiao et al. (2016); 166—Xiao et al. (2015); 167—Xie (2014); 168—Xie et al. (2015); 169—Xiu et al. (2002); 170—Xiu et al. (2004); 171—Xu et al. (2014); 172—Xu and Xiao (2015); 173—Xu and Xie (2015); 174—Yang et al. (2014); 175—Ye et al. (2016); 176—Zhang and Gong (2018); 177—Zhang et al. (2013d); 178—Zheng et al. (2016).

cooling and exhumation histories of the northern Tibetan Plateau. The out-of-sequence deformation model predicts that Cenozoic sedimentation occurred directly north of the Tibetan Plateau shortly after the India-Asia collision. Evidence in support of these predictions has come from both basinal sedimentology studies and bedrock thermochronology. For instance, the earlier uplift of the Qilian Shan in the north contradicts the long-established idea of a gradual northward progression within the Himalayan-Tibetan orogen. The northern Tibetan Plateau and Hexi Corridor to the northeast (Fig. 1A) experienced late Mesozoic tectonic activity, as evidenced by cooling ages in the Qilian Shan, which has complicated our understanding of Cenozoic tectonic evolution in that area (e.g., Li et al., 2019a, 2020a; An et al., 2020; Wu et al., 2021a). Early Cretaceous crustal uplift and shortening remain enigmatic but have been linked to the general absence of Cretaceous strata in the Qilian Shan and the widespread occurrence of early Cenozoic coarse-grained alluvial sediments in the Hexi Corridor (Fig. 1B; e.g., BGMR, 1969; Vincent and Allen, 1999; Chen et al., 2019a). The Cenozoic Qilian Shan–Nan Shan thrust belt developed shortly after the Cenozoic India-Asia collision (Fig. 1B; e.g., Yin et al., 2008a, 2008b; Clark et al., 2010; Clark, 2012; Duvall et al., 2011; Qi et al., 2016; Yu et al., 2017) and has remained active along the same northeastern Tibetan Plateau margin via out-of-sequence thrusting (e.g., George et al., 2001; Jolivet et al., 2001; Li et al., 2019a, 2020a; Wu e al., 2019a; Zuza et al., 2019). Subsequent Miocene deformation along the northeastern margin of the Tibetan Plateau may have affected the Hexi Corridor. The late Mesozoic spatiotemporal tectonic evolution of the Qilian Shan and Hexi Corridor remains poorly resolved, and characterization of this evolution can improve our understanding of the growth history and mechanisms of the northern Tibetan Plateau and its foreland.

Whether the present-day high topography formed during the Cenozoic or Mesozoic remains controversial, as researchers have suggested that the northern Tibetan Plateau experienced regional contraction and subsequent extension during the Mesozoic, despite significant Cenozoic overprinting and reactivation of older structures (Yin and Harrison, 2000; Chen et al., 2003, 2004, 2019a, 2019b; Horton et al., 2004; Pan et al., 2004; Yin et al., 2008a, 2008b; Yin, 2010; Gao et al., 2013; Zuza et al., 2018, 2019; He et al., 2019; Shao et al., 2019; Wu et al., 2021a; Wang et al., 2022). Late Mesozoic sedimentary successions are widespread in the Hexi Corridor, providing a key window to better understand the late Mesozoic deformation and sedimentation history of the northern Tibetan Plateau (Fig. 1B).

The Pingshanhu Basin of the northern Hexi Corridor contains Early Cretaceous siliciclastic strata that provide a record of tectonic events in the northern Tibetan Plateau (Figs. 1 and 2). In this contribution, we integrated geologic field mapping, detrital zircon U-Pb geochronology, sandstone petrographic composition analyses, Kolmogorov-Smirnov statistical tests, and multidimensional scaling analyses to document the late Mesozoic sedimentary provenance of the Pingshanhu Basin and tectonic history of the Hexi Corridor and adjacent mountain blocks. Our findings allow us to present a model for the Early Cretaceous tectonic evolution of the northern Tibetan Plateau.

2. REGIONAL GEOLOGICAL SETTING

The high elevation of the Tibetan Plateau was primarily attained in the Cenozoic as a result of the India-Asia collision (Yin and Harrison, 2000; Tapponnier et al., 2001; Royden et al., 2008; Ding et al., 2022), but there is evidence for prior Mesozoic crustal thickening, particularly along the southern and eastern plateau margins (e.g., Worley and Wilson, 1996; Murphy et al., 1997). The average elevation of the northeastern Tibetan Plateau (~3.5 km) is slightly lower than the rest of the plateau and sharply decreases to <1.5 km in the Hexi Corridor to the northeast (Fig. 1B). The Qilian Shan–Nan Shan thrust belt, located between the Alxa block and North China craton to the north and the Qaidam Basin to the south, marks the northeastern margin of the Tibetan Plateau (Fig. 1B). The Qilian Shan has a complex pre-Cenozoic tectonic history involving multiple phases of Proterozoic basement deformation, early Paleozoic orogeny, Mesozoic extension, and Cenozoic intracontinental deformation (e.g., Vincent and Allen, 1999; Yin and Harrison, 2000; Gehrels et al., 2003a, 2003b; Yin et al., 2007; Zuza et al., 2018). The development of the Qilian Shan–Nan Shan thrust belt is largely considered to have been a Cenozoic structural event; however, recent studies reported the occurrence of Early Cretaceous thrust faults in the northern Qilian Shan (Chen et al., 2019a; Wang et al., 2022). In addition, Jurassic–Cretaceous extensional and transtensional basins developed in the northern Tibetan Plateau, which were interpreted to have resulted from the far-field effects of the collision between the Lhasa and Qiangtang blocks to the south (e.g., Horton et al., 2004; Pan et al., 2004). Normal faults associated with Jurassic–Cretaceous extension do not appear to have been reactivated during Cenozoic contraction, as evidenced by both seismic reflection images (Yin et al., 2008a) and field observations (Zuza et al., 2019). Protracted cooling and deformation since the Early Cretaceous are recorded throughout the northern Tibetan Plateau and its foreland region (e.g., George et al., 2001; Jolivet et al., 2001; Li et al., 2019a, 2020a; An et al., 2020; Wu et al., 2021a). In this section, we describe the geology and tectonic setting of the Hexi Corridor, Qilian Shan to the south, and Alxa block to the north (Fig. 1B).

The early Paleozoic Qilian orogen exposed in the Qilian Shan contains several subparallel ophiolitic mélange belts of the North and South Qilian suture zones that separate the Qaidam continent to the south from the combined North Tarim and North China cratons to the north (Fig. 1B). In general, the primary tectonic domains of the early Paleozoic Qilian orogen include, from north to south (Fig. 1B): (1) the southern margin of the North China craton, including Paleoproterozoic metamorphic basement rocks and a Mesoproterozoic cover sequence, Neoproterozoic passive-margin strata, and postcollisional intrusions; (2) the North Qilian suture zone, consisting of discontinuously exposed, blueschist-facies ophiolitic rocks; (3) the Central Qilian terrane, consisting of Precambrian basement rocks intruded by early Neoproterozoic plutons; (4) the South Qilian suture zone, consisting of intermittently exposed ophiolitic rocks and widely exposed magmatic arc volcanic and plutonic rocks that overlie and/or intrude amphibolite-facies metamorphic rocks; and (5) the North Qaidam ultrahigh-pressure metamorphic rocks and Zongwulong ophiolitic

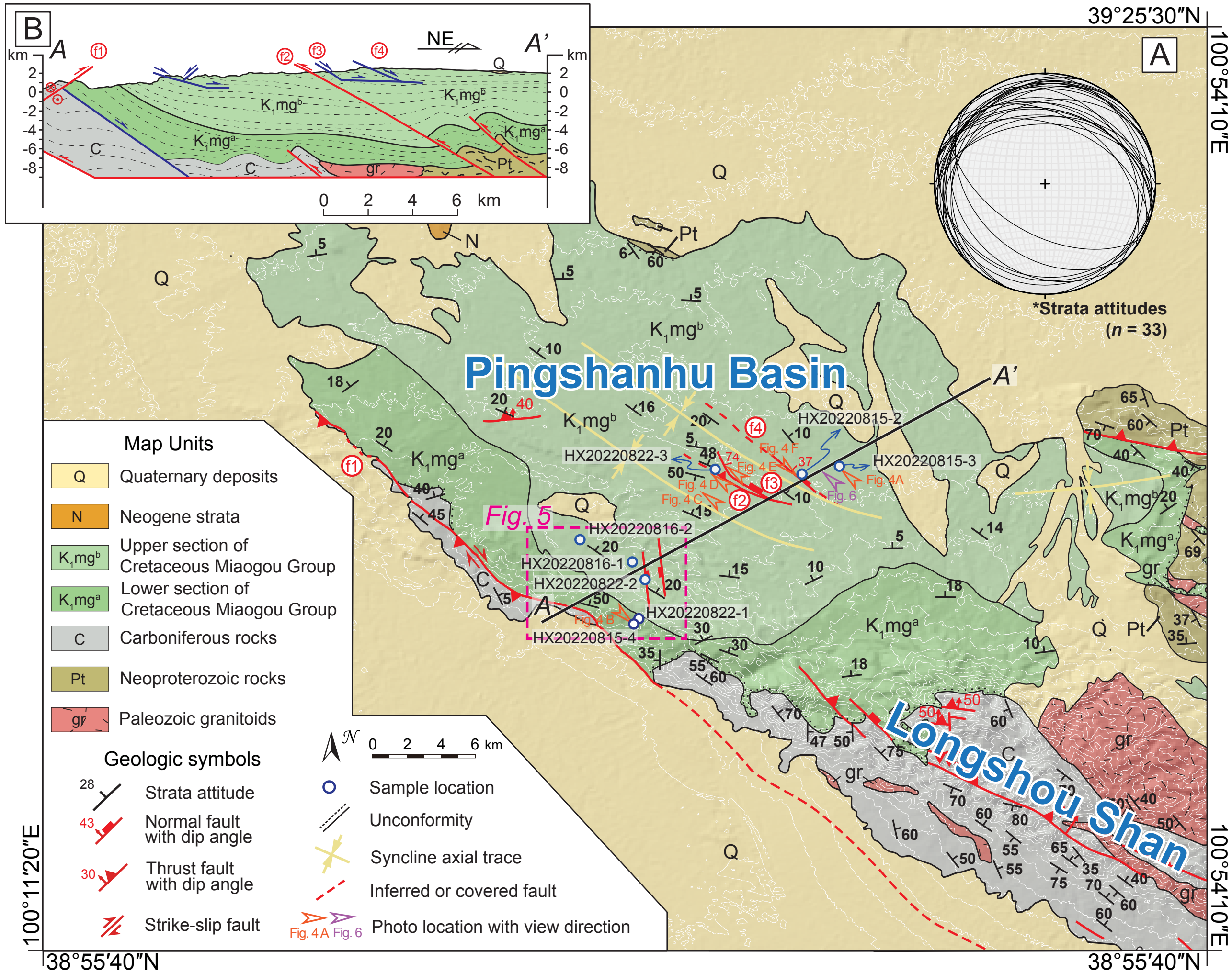

Figure 2. (A) Geologic map of the Pingshanhu Basin in the northern Hexi Corridor of northwestern China. The location of Figure 5 is shown by the pink dashed box. (B) Geological cross section (profile A–A′ in part A) across the Pingshanhu Basin.

complex. Key geologic relationships and rock ages of the Qilian Shan divided into northern, central, and southern segments have been summarized in simplified tectonostratigraphic columns and regional geologic maps by Wu et al. (2022a). The Qilian Shan experienced three periods of magmatism (Fig. 1B; Cowgill et al., 2003; Gehrels et al., 2003b; Wu et al., 2017, 2022a; Zuza et al., 2018), as evidenced by: (1) ca. 960–820 Ma plutons intruding Proterozoic basement rocks (Yin et al., 2007), (2) ca. 520–400 Ma magmatic arc plutons and volcanic rocks; and (3) less prevalent ca. 270 Ma plutons related to the Permian Kunlun arc magmatism scattered throughout the southern Qilian Shan and northern Qaidam Basin.

The Hexi Corridor foreland basin is located along the northeastern margin of the Tibetan Plateau, surrounded by the Tarim Basin to the west, Qilian Shan to the south, and Alxa block to the north (Fig. 1B). The Hexi Corridor contains folded and faulted late Mesozoic–Cenozoic sedimentary rocks that are predominantly exposed along the northern margin of the Qilian Shan and Longshoushan region to the north (Fig. 1B; Zhang et al., 2016a, 2017a). The Longshoushan has a long and complex tectonic history dating back to the Paleoproterozoic (Wu et al., 2022b). During the Neoproterozoic, continental rifting occurred in the Longshoushan region, as evidenced by the local occurrence of ca. 832–827 Ma (ultra)mafic intrusions (e.g., Li et al., 2004, 2005; Zhang et al., 2010; Tung et al., 2013; Tang et al., 2014). Ca. 444–414 Ma arc granitoids and ca. 424–421 Ma (ultra)mafic rocks were emplaced in the Longshoushan region during the Central Asian and Qilian orogenies (Fig. 1B; Duan et al., 2015; Zeng et al., 2016, 2021; Song et al., 2017; Zhang et al., 2017b; Zhang and Gong, 2018; Liu et al., 2020a, 2020b; Wang et al., 2020b; Wu et al., 2021a).

Since the late Mesozoic, the Hexi Corridor has experienced several periods of tectonic deformation and exhumation (Zhang et al., 2017a), including: (1) ca. 130 Ma exhumation and cooling due to the collision of the Lhasa and Qiangtang blocks, (2) early Cenozoic exhumation due to the India-Asia collision, and (3) deformation and exhumation since the late Cenozoic. Thermal-tectonic activity since the late Mesozoic, widely recorded in the Hexi Corridor, is also reported for the Longshoushan (Zhang et al., 2017a; Chen et al., 2019a, 2022; Wang et al., 2022).

The Alxa block of the western North China craton (Fig. 1B) was generated due to subduction, accretion, and collision processes of the Paleo-Asian Ocean domain (Zheng et al., 2014; Xiao et al., 2015). The Alxa block experienced four main magmatic-metamorphic events during the Precambrian (Fig. 1B; e.g., Geng et al., 2010; Dan et al., 2012; Gong et al., 2012; Zhang et al., 2013b; Wu et al., 2014; Zhang and Gong, 2018): (1) ca. 2.8–2.7 Ga crustal growth indicated by Hf isotope signatures (Zhang and Gong, 2018), (2) ca. 2.5 Ga tonalite-trondhjemite-granodiorite petrogenesis (Gong et al., 2012; Zhang et al., 2013b), (3) ca. 2.3–2.0 Ga multiphase magmatism (Dan et al., 2012; Gong et al., 2016), and (4) ca. 1.95–1.90 Ga and ca. 1.85 Ga high-grade metamorphism (Zhang et al., 2013b). During the Phanerozoic, the Alxa block experienced three main magmatic events associated with southward subduction of Paleo-Asian oceanic lithosphere (e.g., Feng et al., 2013; Zheng et al., 2014; Zhang et al., 2022): (1) Late Devonian–early Carboniferous magmatism related to subduction of Paleo-Asian oceanic lithosphere (Feng et al., 2013; Deng et al., 2022); (2) widespread late Carboniferous–late Permian magmatism in a back-arc basin along the northern margin of the Alxa block (Feng et al., 2013; Zhang et al., 2022); and (3) Early to Late Triassic magmatism, marking the final phase of Paleo-Asian oceanic subduction (Feng et al., 2013).

The southwestern Alxa block experienced Triassic intracontinental deformation related to the closures of the Paleo-Asian and Paleo-Tethys Oceans (Song et al., 2018; Zhang et al., 2021). During the Jurassic–Early Cretaceous, Permian–Triassic strata now exposed in the southwestern Alxa block (Fig. 1B) were exhumed and eroded, thereby supplying detritus to a proximal basin (Song et al., 2018). Basin sedimentation was followed by tectonic inversion during the Cretaceous (Song et al., 2018). During the Jurassic–Cretaceous, the southwestern Alxa block experienced tectonic burial and heating associated with the Mongol-Okhotsk orogeny and/or the Lhasa-Qiangtang block collision (Song et al., 2018).

3. GEOLOGY OF THE PINGSHANHU BASIN

3.1. Stratigraphy

The ~30 × 30 km Pingshanhu Basin is bounded by the right-slip Longshoushan fault to the south, Heli Shan to the west, and Beida Shan to the north (Figs. 1 and 2). Basement rocks of the Pingshanhu Basin, largely exposed in the Longshoushan area, consist of mostly Paleoproterozoic (ca. 2.69–1.76 Ga) granitic intrusions and granitic gneisses and a few Neoproterozoic metasedimentary rocks (Fig. 2; Gong et al., 2016; Wu et al., 2021b, 2022b). Middle Carboniferous strata of the Pingshanhu Basin consist of metasandstone, slate, phyllite, and lenticular crystalline limestone (Fig. 3; BGGP, 1973). Middle to Upper Carboniferous strata of the basin consist of crystalline limestone, sericite schist, and quartzite. Jurassic strata of the basin consist of fine-grained sandstone, siltstone, and sandy shale (Fig. 3).

Within the Pingshanhu Basin, widespread Lower Cretaceous strata overlie Middle to Upper Carboniferous strata along an angular unconformity. The Lower Cretaceous stratigraphy can be divided into a lower section, represented by the lower Miaogou Group (labeled K_1mg^a), which strikes northwest in the southern part of the basin, and an upper section, represented by the upper Miaogou Group (labeled K_1mg^b), which constitutes most of the basin (Fig. 3). The lower Miaogou Group has an average thickness of ~900 m and consists of blocky conglomerate and sandstone with minor gravels (Fig. 3; e.g., BGGP, 1973; Shao et al., 2019). The conglomerate is poorly sorted and contains mostly ~1–5 cm granitic clasts and angular, sandy gravels. These lithologies indicate an alluvial fan–fan delta sedimentary environment during the earliest Cretaceous Period. The upper Miaogou Group has an average thickness of ~1900 m and consists of claystone, fine-grained sandstone, and carbonaceous shale with trough cross-beds (Fig. 3; e.g., BGGP, 1973; Shao et al., 2019). The coarse- and fine-grained sandstones locally display well-developed, ~4-m-thick cross-beds (Fig. 4A). These strata were deposited in an alluvial environment that transitioned to a lacustrine environment (e.g., Vincent and Allen, 1999; Peng et al., 2011). Cretaceous strata are unconformably overlain by Miocene claystone and brick-red sandstone (BGGP, 1973). Quaternary alluvial fans, eolian deposits, and terrace sediments overlie older strata along unconformities (Fig. 3).

3.2. Structural Observations

3.2.1. Folds and Growth Strata

We observed northwest-trending folds in the Pingshanhu Basin mostly comprised of the Lower Cretaceous upper Miaogou Group strata (Fig. 2). These folds are open and symmetric, and they have wavelengths of ~0.5–1 km, axial trace lengths up to ~2 km, and plunges of ~5°–20° (Fig. 2).

Syntectonic growth strata in foreland basins offer a direct connection to tectonic deformation. Two sections of growth strata occur throughout the

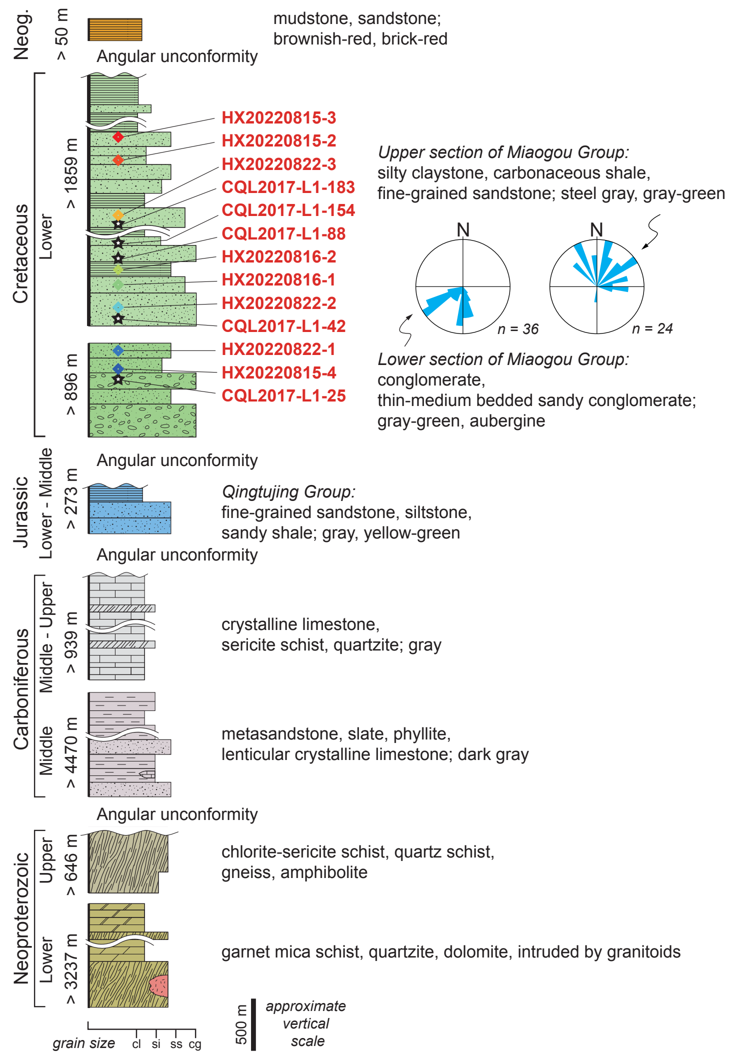

Figure 3. Lithostratigraphic column of the Pingshanhu Basin. The approximate locations of collected Early Cretaceous detrital zircon samples are shown in the column, along with rose diagrams of paleocurrent directions for the lower and upper Miaogou Group. Neog.—Neogene. The five black stars represent the locations of previously collected samples in our study area (Shao et al., 2019). Grain size: cl—clay; si—siltstone; ss—sandstone; cg—conglomerate.

Lower Cretaceous Miaogou Group, indicating two syndepositional tectonic events (Figs. 4B and 4C). Lower Cretaceous growth strata of the lower Miaogou Group occur along the margin of the Pingshanhu Basin and have dips of 12°–40° that shallow up section to the south (Fig. 4B). Pregrowth strata contain sediment grain sizes that transition from coarse at the basal section to fine at the uppermost section.

Lower Cretaceous growth strata of the upper Miaogou Group are localized to the southern limb of an anticline in the basin center and have dips of 17°–52° that shallow up section (Fig. 4C). Deposition of the growth strata was coeval with folding and thrusting, as the oldest growth strata suggest the initiation of anticlinal growth.

3.2.2. Faults

We used field observations and satellite imagery to map the extent of northwest-striking thrust and normal faults throughout the Pingshanhu Basin (Figs. 4D and 4F). For convenience of description, the faults are labeled f1 to f4 from south to north (Fig. 2A).

Fault 1 (f1 in Fig. 2) is a southwest-dipping, curvilinear thrust fault exposed along the southwestern margin of the Pingshanhu Basin, interpreted to be the along-strike continuation of the Longshoushan fault (Fig. 2A). Along its eastern segment, fault 1 juxtaposes Carboniferous strata over Lower Cretaceous strata of the lower Miaogou Group (K_1mg^a; Fig. 2). Fault 1 can be traced for ~15 km to the southeast to the southwestern margin of Longshoushan, where the fault is buried by Quaternary strata (Fig. 2A). Fault 2 (f2 in Fig. 2) is a northeast-dipping thrust fault (strike 115° and dip 42°N) exposed in the center of the Pingshanhu Basin (Fig. 2A). We identified three sets of marker beds characterized by gray-white sandstone and estimated their offsets by fault 2 (Fig. 4D). Along its northern segment, fault 2 juxtaposes hanging-wall strata that form an ~50-m-wide syncline over footwall growth strata (Fig. 4D). Fault 3 (f3 in Fig. 2) is a northeast-dipping normal fault that cuts the upper Miaogou Group (Fig. 4E). Hanging-wall strata dip 53°N, and footwall strata dip 43°N (Fig. 4E). Fault 3 has offset an ~0.5-m-thick, gray-white sandstone marker bed by ~1.5 m. Fault 4 (f4 in Fig. 2) is a northeast-dipping normal fault that cuts the upper Miaogou Group by ~20 m (Fig. 4F). Fault 4 is buried by Quaternary strata (Fig. 4F).

Several northwest-striking, normal right-slip faults cut the Lower Cretaceous upper Miaogou Group (Figs. 4G and 5). These normal right-slip faults may continue to the southeast for ~10 km and link with fault 1 (Fig. 5). Mapped separations and striations on fault surfaces indicate normal right-slip kinematics (Fig. 4H). Marker beds are offset by ~2–20 m along these faults (Figs. 4I and 4J). We also observed a domino-type extensional normal fault system that cuts the upper Miaogou Group (Fig. 4K). Elsewhere, we observed low-angle thrust faults cut by younger, high-angle normal faults within the upper Miaogou Group (Fig. 6). The photo locations and directions are also shown in Google Earth imagery in the figures (Fig. 5A).

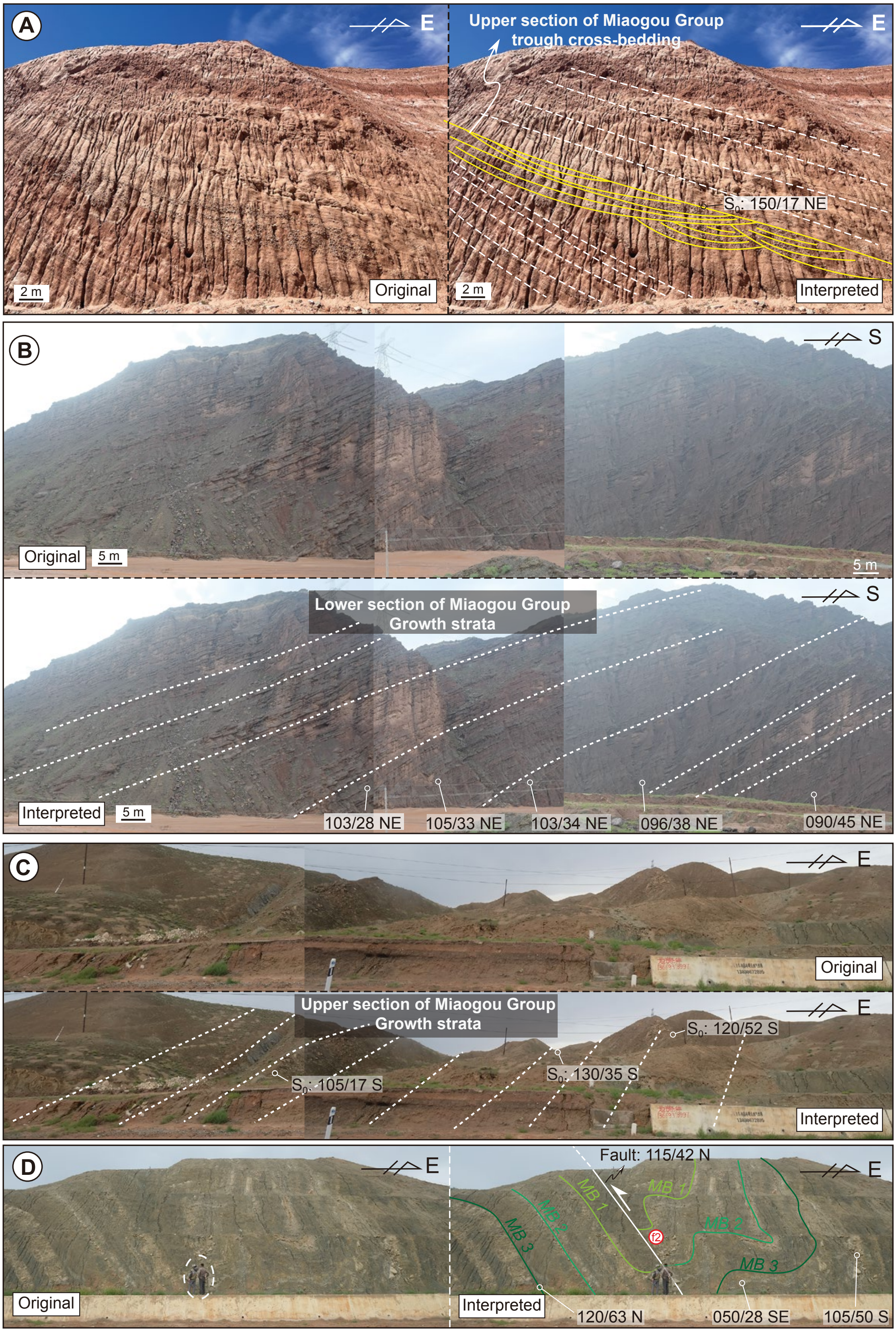

Figure 4. Original and interpreted field photographs of sedimentary and structural features of the Pingshanhu Basin discussed in the text. Photograph locations are shown in Figures 2 and 5. (A) Trough cross-bedding in the upper Miaogou Group (K_1mg^b). (B) Growth strata in the lower Miaogou Group (K_1mg^a). (C) Growth strata in the upper Miaogou Group. (D) A northeast-dipping thrust fault (labeled "f2"; strike 115° and dip 42°N). MB—marker bed. (*Continued on following two pages.*)

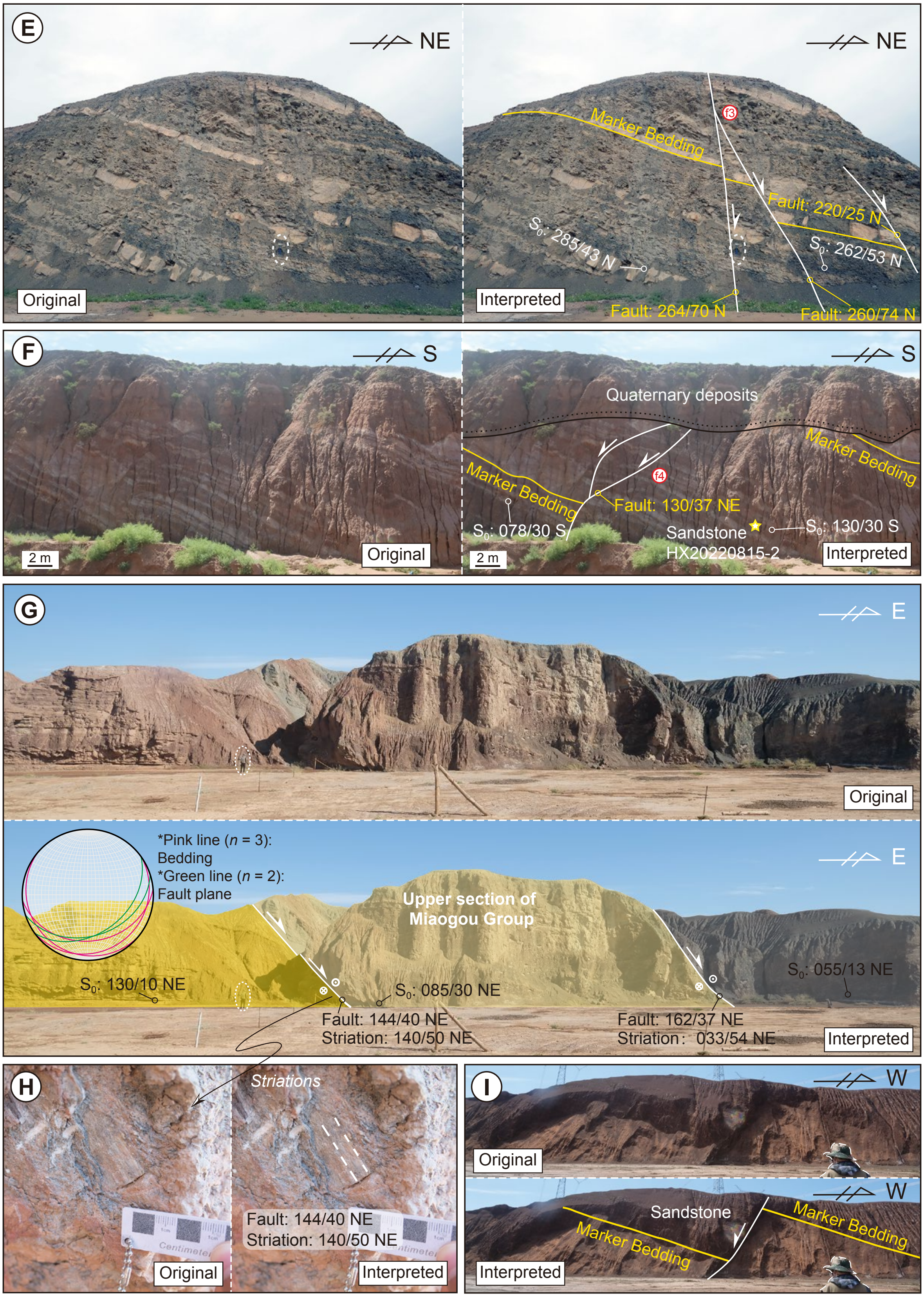

Figure 4 (*continued*). (E) Three north-dipping normal faults, including fault "f3," in the Miaogou Group. (F) Two northeast-dipping normal faults, including fault "f4," in the upper Miaogou Group (K_1mg^b) are overlaid by Quaternary alluvial-fan deposits. (G) Normal right-slip faults in the upper Miaogou Group (K_1mg^b). The inset stereonet plot shows the orientations of bedding and fault planes. (H) Striations on the fault surfaces in part G. (I) Kinematic indications of normal right-slip fault. (*Continued on following page.*)

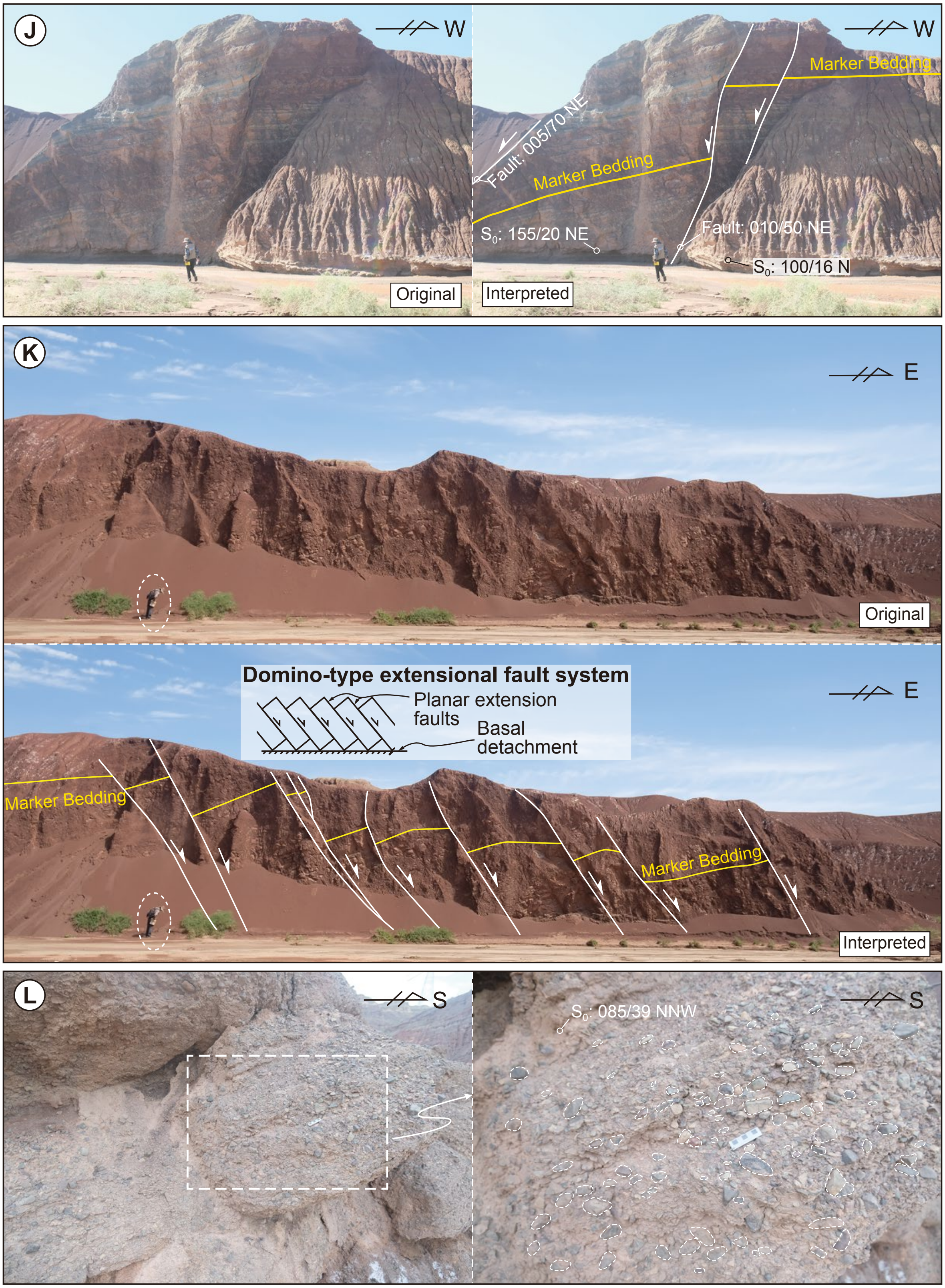

Figure 4 (*continued*). (J) East-dipping normal faults in Pingshanhu Basin. (K) East-dipping, domino-type extensional fault structure. (L) Pebbles and coarse-grained sands in the lower section of Miaogou Group.

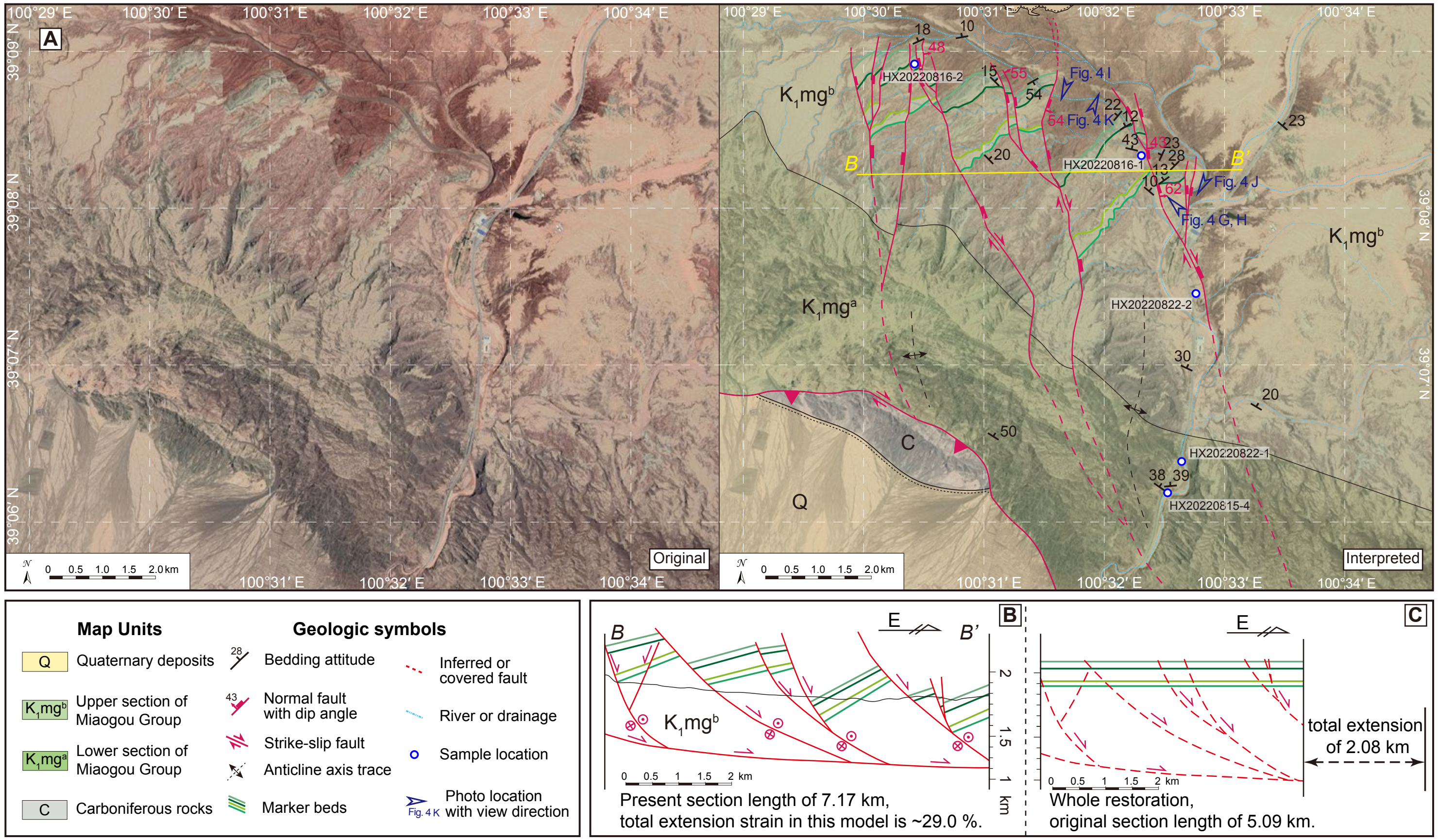

Figure 5. (A) Structural interpretation of the southern Pingshanhu Basin, based on observations in the field and from Google Earth imagery. (B) Geological cross section (profile B–B′) across regional right-slip fault systems. (C) Restored cross section of part B.

3.3. Balanced Cross-Section Restoration

Based on the results of geologic mapping, we constructed an east-west–oriented balanced cross section across the southwestern Pingshanhu Basin to calculate the local extension of the upper Miaogou Group (B-B′ in Figs. 5A and 5B). Restoration of the cross section was performed by measuring the line lengths of observed Cretaceous marker beds and retrodeforming slip along the faults to restore the marker beds to a continuous and subhorizontal configuration (Fig. 5C). The restoration yielded a magnitude of extension of 7.17 km across an original section length of 5.09 km (29% extensional strain; Figs. 5B and 5C). This strain estimate is a minimum given that our cross section only restored plane-strain normal-fault slip, thus ignoring any potential out-of-plane motion due to strike-slip or oblique-slip faulting.

3.4. Paleocurrent Analysis

Paleocurrent directions indicate sediment dispersal patterns and can be used to resolve sediment provenance (DeCelles et al., 1983; Amajor, 1987). We collected paleocurrent measurements in the upper and lower Miaogou Group following the method of DeCelles et al. (1983) (Figs. 4A and 4L). Sixty paleocurrent measurements were collected in the lower and upper Miaogou

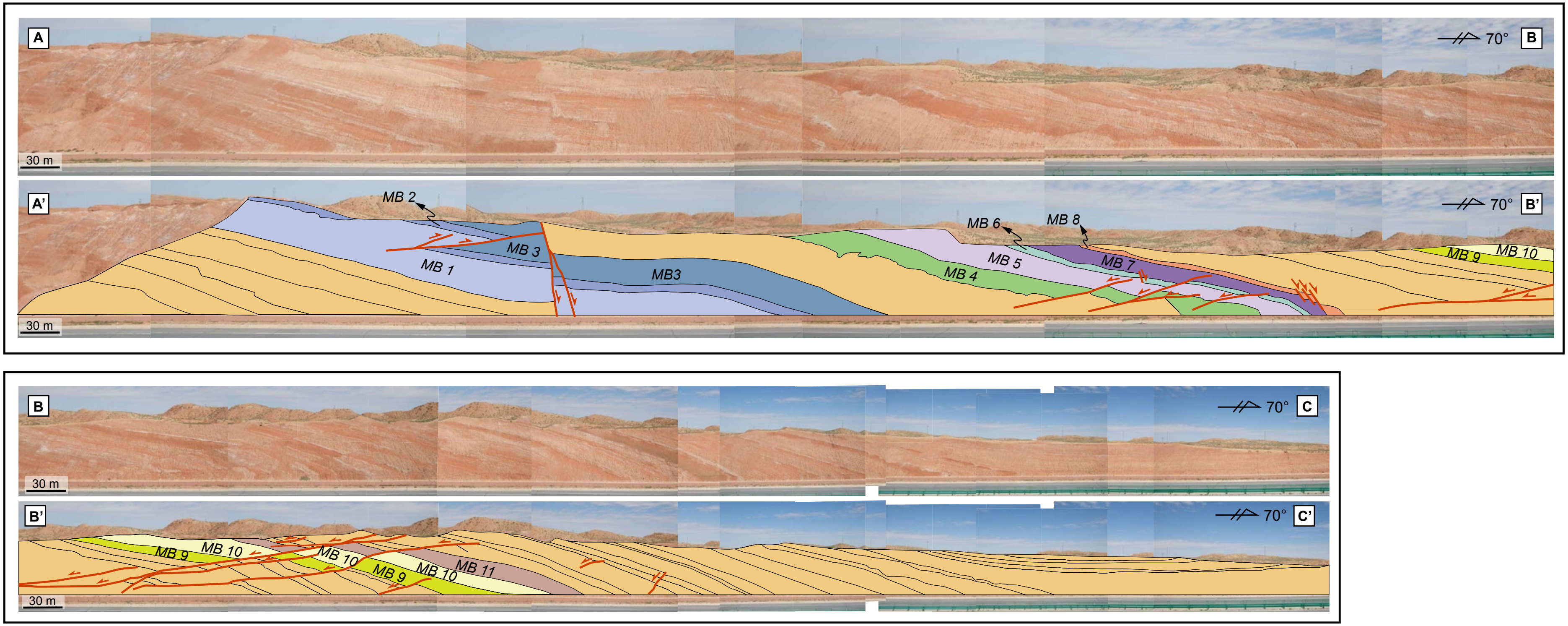

Figure 6. Field photographs of Pingshanhu Basin strata showing thrust faults crosscut by younger normal faults. MB—marker bed. The photo location and view direction can be found in Figure 2B.

Group, which were measured on one stratigraphic section. The first group of paleocurrent data was collected in the lower Miaogou Group with 36 measurements (Fig. 4L). The second group of paleocurrent data was collected in the upper Miaogou Group with 24 measurements (Fig. 4A). Horizontal bedding rotations were corrected, and the results are shown in rose diagrams (Fig. 3). Strata-corrected paleocurrent flow directions are directed southwestward for the lower Miaogou Group, but they are predominantly directed northward, with some minor southward measurements, for the upper Miaogou Group (Fig. 3).

4. SAMPLING STRATEGY AND ANALYTICAL METHODS

We collected two coarse-grained sandstone samples (HX20220815–4 and HX20220822–1) from the lower Miaogou Group and six fine-grained sandstone and silty claystone samples (HX20220815–2, HX20220815–3, HX20220816–1, HX20220822–2, HX20220822–3, and HX20220816–2) from the upper Miaogou Group to examine sediment compositions for provenance and tectonic setting determinations. Sample locations are listed in Table 1 and shown in Figure 2A.

4.1. Sandstone Composition

We performed quartz–feldspar–lithic fragment (Qt-F-L) composition analyses for seven sandstone samples and one silty claystone sample (HX20220815–2; HX20220815–3; HX20220815–4; HX20220816–1; HX20220816–2; HX20220822–1; HX20220822–2; HX20220822–3) using the Gazzi-Dickinson method to determine whether sediment of the Early Cretaceous Miaogou Group was derived from stable continental blocks, recycled orogens, and/or magmatic arcs (Dickinson, 1970, 1985). To eliminate the effects of grain size, grains larger than 0.625 mm were counted as monocrystalline (Fig. 7; Dickinson, 1970, 1985; Ingersoll et al.,

TABLE 1. SUMMARY OF SAMPLE LOCATIONS AND DETRITAL ZIRCON U-Pb RESULTS FOR THE PINGSHANHU BASIN

Sample number	Description	Latitude (°N)	Longitude (°E)	Elevation (m)	Sample site	*n*
HX20220815-2	Sandstone	39°10′56.50″	100°38′51.50″	1758	Upper section of Cretaceous Miaogou Group	81 of 100
HX20220815-3	Sandstone	39°11′20.10″	100°40′46.10″	1853	Upper section of Cretaceous Miaogou Group	74 of 84
HX20220816-1	Sandstone	39°08′23.90″	100°32′17.70″	1619	Upper section of Cretaceous Miaogou Group	75 of 100
HX20220816-2	Silty claystone	39°08′58.70″	100°30′25.90″	1663	Upper section of Cretaceous Miaogou Group	66 of 100
HX20220822-2	Sandstone	39°07′27.82″	100°32′43.54″	1580	Upper section of Cretaceous Miaogou Group	80 of 100
HX20220822-3	Sandstone	39°10′59.74″	100°35′32.89″	1719	Upper section of Cretaceous Miaogou Group	71 of 100
HX20220822-1	Sandstone	39°06′24.41″	100°32′36.85″	1584	Lower section of Cretaceous Miaogou Group	84 of 100
HX20220815-4	Sandstone	39°06′14.60″	100°32′28.80″	1572	Lower section of Cretaceous Miaogou Group	90 of 100

1984). Monocrystalline quartz (Qm), polycrystalline quartz (Qp), plagioclase (P), K-feldspar (K), volcanic/metavolcanic lithic fragments (Lv), and sedimentary/metasedimentary lithic fragments (Ls) were differentiated optically in petrographic thin sections. Based on the petrologic compositions, total quartzose grains (Qt = Qm + Qp), feldspar grains (F = P + K), total unstable lithic fragments (L = Lv + Ls), and total lithic fragments (Lt = L + Qp) were calculated. Detailed sample locations and results are listed in Tables 1 and 2, respectively.

4.2. Detrital Zircon U-Pb Geochronology

We performed detrital zircon U-Pb geochronology on eight sedimentary rock samples to determine the magmatic record of the northern Tibetan Plateau and provenance of the Lower Cretaceous Miaogou Group strata. Whole-rock samples were initially processed via standard crushing and sieving. Detrital zircon grains (Table S1 in the Supplemental Material[1]) were separated from sieved material using typical heavy liquids and magnetic separation techniques. Zircon grains were randomly picked under a microscope and mounted in epoxy resin. Cathodoluminescence images of zircon grains were collected using a scanning electron microscope to identify their internal texture and determine laser-ablation (LA) spot targets. We analyzed one spot for each zircon grain. We targeted the clear growth zoning to obtain the youngest crystallization age. Detrital zircon U-Pb age and trace-element compositions were measured via LA–inductively coupled plasma–mass spectrometry (LA-ICP-MS) at the Key Laboratory of Continental Collision and Plateau Uplift, Chinese Academy of Sciences, Beijing, China. Reference standard zircon grains Plešovice and 91500 zircon, and glass reference materials NIST SRM 610 and NIST SRM 612 (Wiedenbeck et al., 1995; Pearce et al., 1997; Sláma et al., 2008) were each measured between 10 unknown sample analyses. An ATL 193 nm ArF excimer laser-ablation system and Agilent 7500a ICP-MS instrument were used to ablate zircon grains and acquire element ion-signal intensities, respectively. The Plešovice and NIST SRM 612 reference standard zircon grains were used for matrix-matched calibration and trace-element content calibration, respectively. Isotope ratios and trace-element concentrations were calculated using the program Iolite 4.0 (Paton et al., 2010, 2011). The program ComPbCon#3.17 (Andersen, 2002) was used for common Pb corrections and ages. Concordia plots were generated using the program Isoplot (Ludwig, 2003). We report $^{207}Pb/^{206}Pb$ ages for zircon grains older than 1000 Ma and $^{206}Pb/^{238}U$ ages for zircon grains younger than 1000 Ma (Black et al., 2003; Ludwig, 2003; Table S1).

[1]Supplemental Material. Table S1: Detailed results of detrital zircon U-Pb analyses for sandstone samples from Pingshanhu Basin. Table S2: Summary of geochronology results for magmatic rocks in the Qilian Shan and the Alxa block. Please visit https://doi.org/10.1130/GEOS.S.25008647 to access the supplemental material, and contact editing@geosociety.org with any questions.

4.3. Kolmogorov-Smirnov Statistical Tests and Multidimensional Scaling

We calculated Kolmogorov-Smirnov nonparametric statistics to quantify the age similarity of two detrital zircon samples. The maximum difference in ages between samples is defined as the *D* value, and α = 0.01 or 0.05. Typically, the null hypothesis (H_0) that the two samples were drawn from the same population can be rejected when $D_{observed}$ is greater than $D_{critical}$ (α = 0.05). For α = 0.05, the $D_{critical}$ value is calculated as

$$D_{critical} = 1.36\sqrt{\frac{N_1 + N_2}{N_1 N_2}}, \quad (1)$$

where N_1 and N_2 are the numbers of zircon grain analyses for the two samples, respectively (Saylor and Sundell, 2016; Wu et al., 2019a). In the Kolmogorov-Smirnov test, the *P* value is the threshold of the significance level at which to reject the null hypothesis (H_0). Thus, a *P* value >0.05 corresponds to a >95% confidence level that the two samples are derived from the same parent distribution. Because the random sampling of a large population distorts the distributions introduced, relatively large sample sizes are required to reject the null hypothesis (H_0) (Saylor and Sundell, 2016).

We performed multidimensional scaling (MDS; Vermeesch, 2013) to visualize the dissimilarity between the ages of detrital samples (e.g., Wu et al., 2019a; Liu et al., 2023) and eliminate inherent bias stemming from sediment

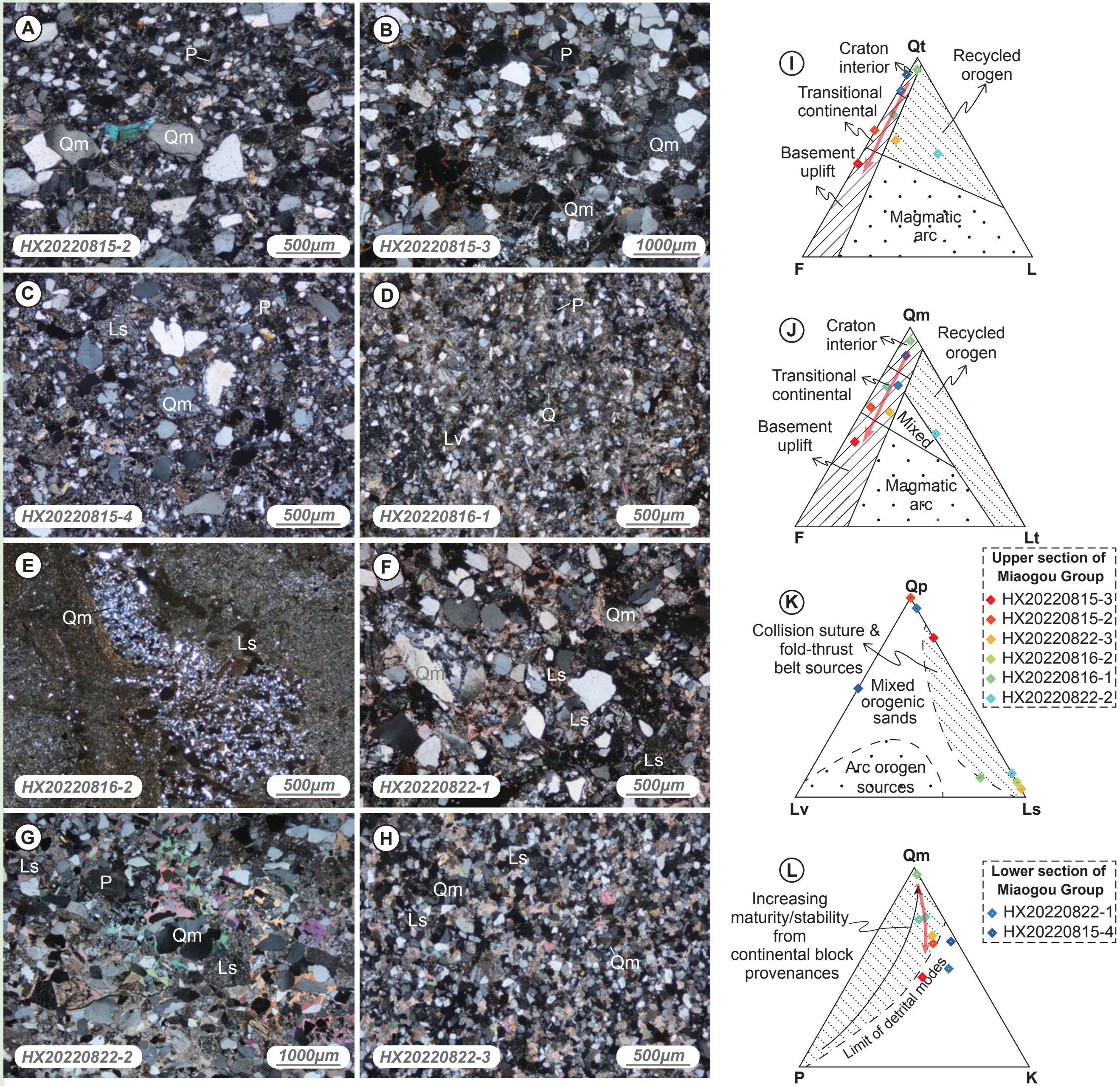

Figure 7. (A–D, F–H) Photomicrographs of the sandstone samples in this study. (E) Photomicrograph of the claystone sample in this study. (I–L) Triangular modal compositional diagrams of sandstone samples analyzed in this study (Dickinson, 1985). The salmon-colored arrow indicates the transition of sediment provenance from the lower Miaogou Group (K_1mg^a) to the upper Miaogou Group (K_1mg^b). Qm—monocrystalline quartz; Qp—polycrystalline quartz; Qt—total quartzose grains; Q—quartz; P—plagioclase; K—K-feldspar; F—feldspar grains; L—total unstable lithic fragments; Lt—total lithic fragments; Lv—volcanic/metavolcanic lithic fragments; Ls—sedimentary/metasedimentary lithic fragments.

TABLE 2. MODAL COMPOSITIONS OF THE SANDSTONE SAMPLES IN THIS STUDY

Strata	Sample	Component											Total
		Qm	Qp	Lv	Ls	Lm	P	K	Qt	F	L	Lt	
Upper section of Cretaceous Miaogou Group	HX20220815-2	240 (60.15%)	12 (3.01%)	0 (0%)	0 (0%)	0 (0%)	42 (10.53%)	105 (26.32%)	252 (63.16%)	147 (36.84%)	0 (0%)	12 (3.01%)	399
	HX20220815-3	180 (42.86%)	16 (3.81%)	0 (0%)	4 (0.95%)	0 (0%)	96 (22.86%)	124 (29.52%)	196 (46.67%)	220 (52.38%)	4 (0.95%)	20 (4.76%)	420
	HX20220816-1	296 (70.48%)	2 (0.48%)	3 (0.71%)	15 (3.57%)	0 (0%)	44 (10.48%)	60 (14.29%)	298 (70.95%)	104 (24.76%)	18 (4.29%)	20 (4.76%)	420
	HX20220816-2	336 (93.07%)	1 (0.28%)	0 (0%)	12 (3.32%)	0 (0%)	2 (0.55%)	10 (2.77%)	337 (93.35%)	12 (3.32%)	12 (3.32%)	13 (3.6%)	361
	HX20220822-2	183 (46.92%)	18 (4.62%)	0 (0%)	129 (33.08%)	0 (0%)	18 (4.62%)	42 (10.77%)	201 (51.54%)	60 (15.38%)	129 (33.08%)	147 (37.69%)	390
	HX20220822-3	225 (57.84%)	2 (0.51%)	0 (0%)	45 (11.57%)	0 (0%)	32 (8.23%)	85 (21.85%)	227 (58.35%)	117 (30.08%)	45 (11.57%)	47 (12.08%)	389
Lower section of Cretaceous Miaogou Group	HX20220815-4	192 (48.61%)	6 (1.52%)	5 (1.27%)	172 (43.54%)	0 (0%)	8 (2.03%)	12 (3.04%)	198 (50.13%)	20 (5.06%)	177 (44.81%)	183 (46.33%)	395
	HX20220822-1	152 (39.9%)	72 (18.9%)	0 (0%)	115 (30.18%)	0 (0%)	32 (8.4%)	10 (2.62%)	224 (58.79%)	42 (11.02%)	115 (30.18%)	187 (49.08%)	381

Notes: Total = Qm + Qp + Lv + Ls + Lm + P + K. Abbreviations: monocrystalline quartz (Qm), polycrystalline quartz (Qp), plagioclase (P), K-feldspar (K), volcanic/metavolcanic lithic fragments (Lv), sedimentary/metasedimentary lithic fragments (Ls), and metamorphic lithic fragments (Lm). Total quartzose grains (Qt) = Qm + Qp, feldspar grains (F) = P + K, total unstable lithic fragments (L) = Lv +Ls, and total lithic fragments (Lt) = L + Qp.

recycling and/or variations in zircon fertility in age comparisons (Nordsvan et al., 2020). In multidimensional Cartesian space, the greater distance between sample points corresponds to more dissimilarity between the samples. MDS results can be used to interpret stratigraphic correlations, constrain maximum depositional ages, and understand broader tectonic histories (e.g., Cawood et al., 2012; Gehrels, 2014). MDS analyses were conducted on a compilation of the zircon ages of our samples and potential source areas to interpret the provenance of the Early Cretaceous Miaogou Group of the Pingshanhu Basin. We compared the Cretaceous strata with bulk compilations of Qilian Shan and Alxa block magmatic rocks in MDS to avoid missing some important age populations. We also used the Kolmogorov-Smirnov statistic to compare the Miaogou Group ages with the published ages of 8 samples from the Qilian Shan and Alxa block to investigate their depositional relationships (Yang et al., 2009; Zhang et al., 2016b; Zhao et al., 2016; Song et al., 2017, 2021; Li et al., 2021).

5. RESULTS

5.1. Sandstone Petrography

The detrital materials of eight sandstone and silty claystone samples from the Lower Cretaceous Miaogou Group of the Pingshanhu Basin are moderately sorted and rounded grains and composed of monocrystalline (~42%–93%) and polycrystalline quartz (~3%–18%), feldspar (~5%–52%), and unstable lithic fragments (~1%–44%) defined by volcanic (~0.7%–1.2%) and sedimentary (~1%–43%) fragments (Fig. 7). Petrologic compositional fields and detrital mode triangular diagrams suggest different sources for the samples (Dickinson and Suczek, 1979; Dickinson et al., 1983). In the Qt-F-L and Qm-F-Lt diagrams, the sandstone and silty claystone compositions generally plot within the recycled orogen field and continental block field, respectively (Figs. 7I and 7J). Furthermore, the sandstone and silty claystone compositions indicate a provenance transition from the craton interior to basement uplift, indicating that the maturity and/or stability of the source decreased. In the Qp-Lv-Ls diagram, collisional sutures or fold-and-thrust belts are shown as potential sources of the sandstone and silty claystone material (Fig. 7K). In the Qm-P-K diagram, the sandstone and silty claystone compositions generally plot within the Qm region, but the data show a trend of decreasing provenance maturity and/or stability with the Miaogou Group strata becoming younger (Fig. 7L).

5.2. Detrital Zircon U-Pb Geochronology

Zircon grains from the samples of the Miaogou Group were mostly subhedral and colorless except for a few elongated, euhedral grains (Fig. 8). Zircon grains were ~50–200 μm long and had aspect ratios of 1:1–3:1. Cathodoluminescence images of zircon grains showed clear growth zoning (Fig. 8).

The chondrite-normalized rare earth element patterns of the analyzed zircon grains (Figs. 9A and 9B; Table 1) show heavy rare earth element enrichment with a positive Ce anomaly and negative Eu anomaly. These patterns suggest that the grains were mostly sourced from igneous rocks, with few grains sourced from metamorphic rocks (Belousova et al., 2002; Corfu et al., 2003; Hoskin, 2005). The Th/U values of the zircon grains were mostly >0.1, except for 11 zircon grains with Th/U values <0.1 (Fig. 9C; Table S1). These values suggest that most of the zircon grains came from a magmatic origin (Belousova et al., 2002; Corfu et al., 2003).

5.2.1. Lower Miaogou Group

Sandstone sample HX20220815–4 was collected from the lower Miaogou Group in the southern part of the Pingshanhu Basin (Figs. 2 and 5A).

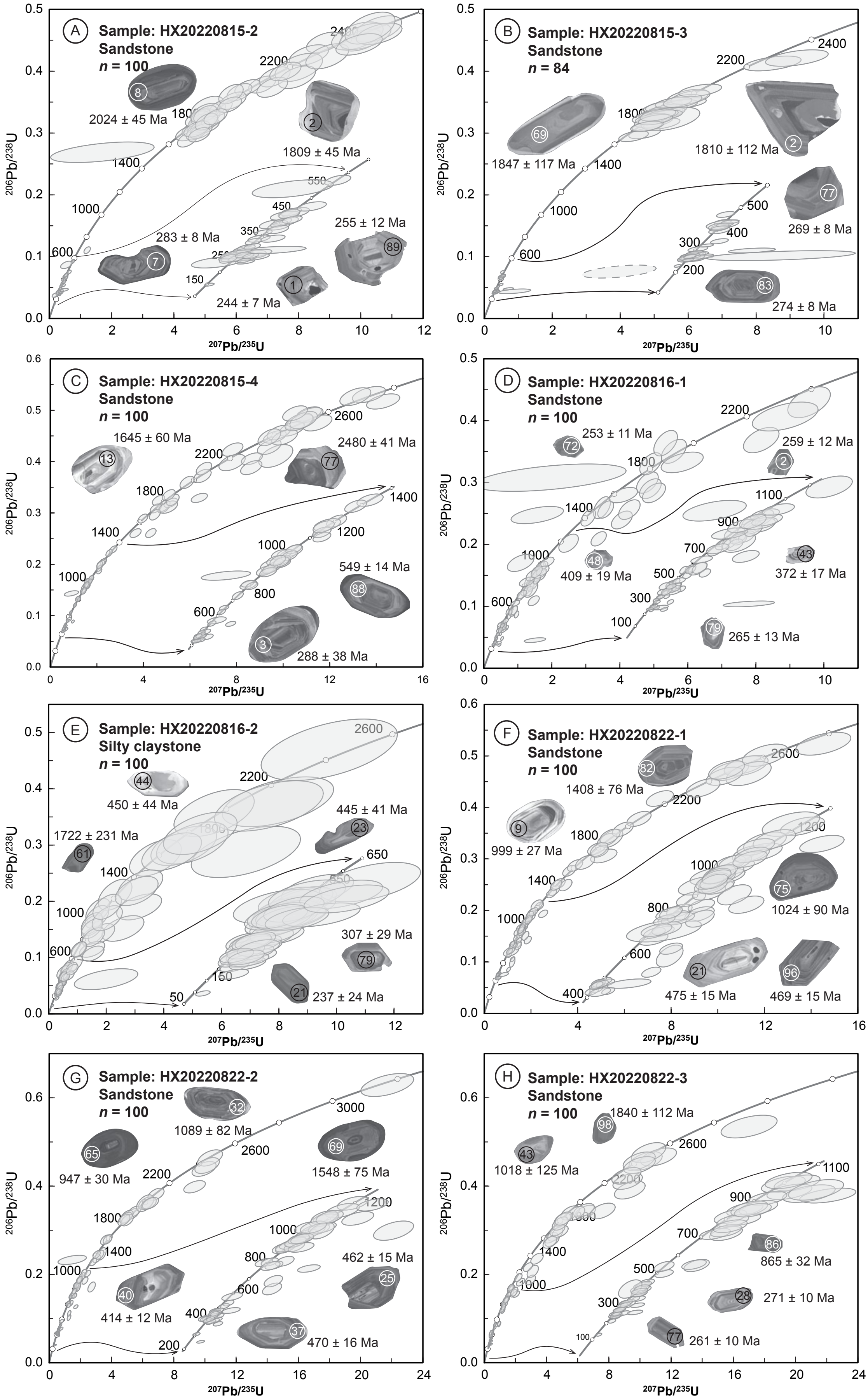

Figure 8. (A–H) U-Pb concordia diagrams showing age results of single-shot zircon grain analyses and representative cathodoluminescence images and age results of zircon grains for each sample. Error ellipses are 2σ. Circles with number represent ~30 μm diameter analyzed spots for U-Pb dating as a scale.

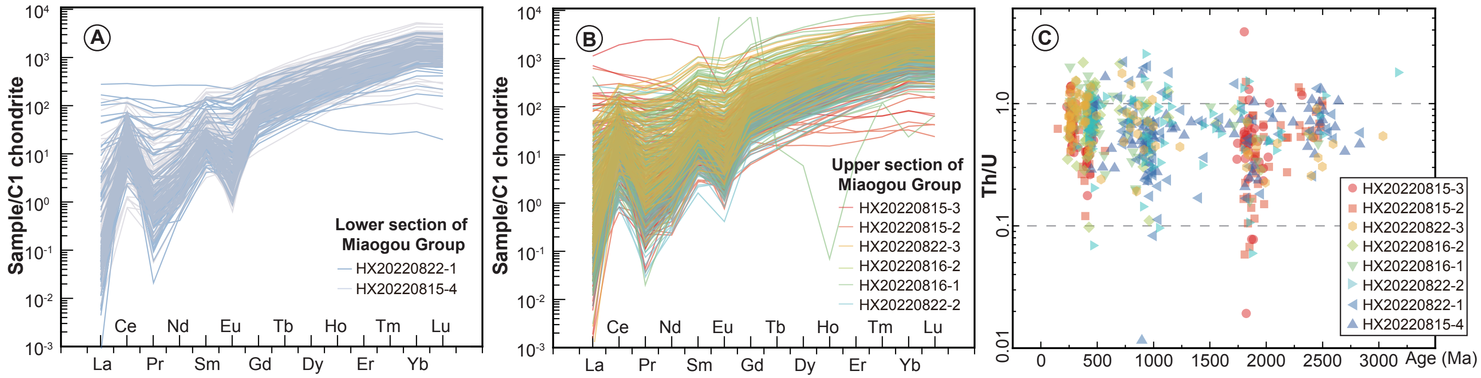

Figure 9. (A–B) Trace-element concentrations of zircon grains from the lower (A) and upper (B) sections of the Miaogou Group. Normalization values are from McDonough and Sun (1995). (C) Th/U versus U-Pb age diagram of zircon grains in this study.

One-hundred zircon grain analyses yielded U-Pb ages ranging ca. 2830–430 Ma (Fig. 10A). The dominant age population of this sample (Figs. 3 and 10A) is ca. 480–400 Ma with a ca. 461 Ma peak (Fig. 10A). A second age population occurs ca. 1000–800 Ma with a ca. 908 Ma peak (Fig. 10A). Minor age populations occur ca. 2500–2400 Ma (Fig. 10A).

Sandstone sample HX20220822–1 was collected from the lower Miaogou Group in the southern part of the Pingshanhu Basin (Figs. 2 and 5A). One-hundred zircon grains analyses yielded U-Pb ages ranging ca. 2837–431 Ma (Fig. 10A). The dominant age population of this sample (Figs. 3 and 10A) is ca. 480–400 Ma with a ca. 464 Ma peak (Fig. 10A). A second age population occurs ca. 1000–800 Ma with a ca. 972 Ma peak (Fig. 10A).

Sandstone sample CQL2017-L1–25 was collected from the lower Miaogou Group (Fig. 3; Shao et al., 2019). Eighty zircon grains yielded U-Pb ages ranging ca. 3215–283 Ma (Fig. 10A). The dominant age population of this sample (Fig. 10A) is ca. 600–400 Ma with a ca. 470 Ma peak (Fig. 10A). Two second age populations occur ca. 1000–800 Ma with a ca. 952 Ma peak (Fig. 10A) and ca. 2600–2400 Ma with a ca. 2466 Ma peak.

5.2.2. Upper Miaogou Group

Sandstone sample HX20220815–2 was collected from the upper Miaogou Group in the center of the Pingshanhu Basin (Fig. 2). One-hundred zircon grains yielded U-Pb ages ranging ca. 2499–149 Ma (Fig. 10B). The dominant age population of this sample (Figs. 3 and 10B) occurs ca. 300–250 Ma with a ca. 272 Ma peak (Fig. 10B). Two other age populations occur ca. 480–400 Ma with a ca. 438 Ma peak and ca. 1900–1800 Ma with a ca. 1852 Ma peak (Fig. 10B). Few ages are clustered ca. 2500–2400 Ma (Fig. 10B).

Sandstone sample HX20220815–3 was collected from the upper Miaogou Group in the center of the Pingshanhu Basin (Fig. 2). Eighty-four zircon grains yielded U-Pb ages ranging ca. 2419–230 Ma (Fig. 10B). The dominant age population of this sample (Figs. 3 and 10B) occurs ca. 300–250 Ma with a ca. 275 Ma peak (Fig. 10B). Two other age populations occur ca. 480–400 Ma with a ca. 412 Ma peak and ca. 1900–1800 Ma with a ca. 1849 Ma peak.

Sandstone sample HX20220816–1 was collected from the upper Miaogou Group in the southern part of the Pingshanhu Basin (Figs. 2 and 5A). One-hundred zircon grains yielded U-Pb ages ranging ca. 2461–234 Ma (Fig. 10B). The dominant age population of this sample (Figs. 3 and 10B) occurs ca. 480–400 Ma with a ca. 418 Ma peak (Fig. 10B). A second age population occurs ca. 1000–800 Ma with a ca. 933 Ma peak (Fig. 10B).

Silty claystone sample HX20220816–2 was collected from the upper Miaogou Group in the southern part of the Pingshanhu Basin (Figs. 2 and 5A). One-hundred zircon grains yielded U-Pb ages ranging ca. 2377–237 Ma (Fig. 10B). The dominant age population of this sample (Figs. 3 and 10B) occurs ca. 480–400 Ma with a ca. 418 Ma peak (Fig. 10B). A second age population occurs ca. 300–250 Ma with a ca. 285 Ma peak (Fig. 10B).

Sandstone sample HX20220822–2 was collected from the upper Miaogou Group in the southern part of the Pingshanhu Basin (Fig. 2). One-hundred zircon grains yielded U-Pb ages ranging ca. 3171–310 Ma (Fig. 10B). The dominant age population of this sample (Figs. 3 and 10B) occurs ca. 480–400 Ma with a ca. 456 Ma peak (Fig. 10B). A second age population occurs ca. 1000–800 Ma with a ca. 929 Ma peak (Fig. 10B).

Sandstone sample HX20220822–3 was collected from the upper Miaogou Group in the center of the Pingshanhu Basin (Fig. 2). One-hundred zircon grains yielded U-Pb ages ranging ca. 3037–241 Ma (Fig. 10B). The dominant age population of this sample (Figs. 3 and 10B) occurs ca. 300–250 Ma with a

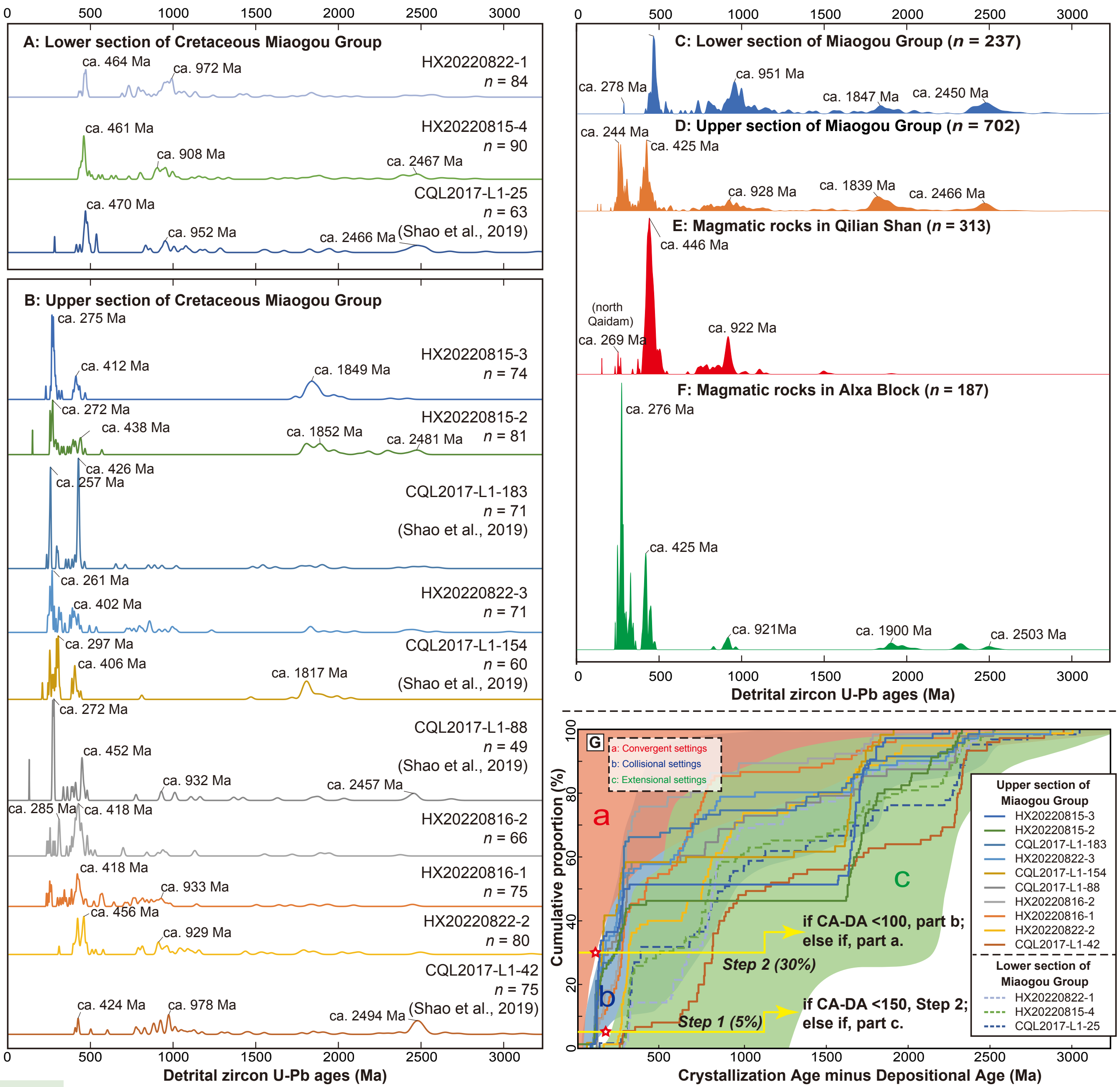

Figure 10. (A–D) Normalized relative probability plots of detrital zircon U-Pb ages from Cretaceous strata samples. Data are from this study and Shao et al. (2019). (E–F) Magmatic ages from the Qilian Shan (E) and Alxa block (F) (Table S2; see text footnote 1). (G) Cumulative distribution curves of detrital zircon ages from the Lower Cretaceous strata of the Pingshanhu Basin. Colored areas represent distinct tectonic settings of deposition according to Cawood et al. (2012). CA-DA—crystallization age minus deposition age.

ca. 261 Ma peak (Fig. 10B). A second age population occurs ca. 480–400 Ma with a ca. 402 Ma peak (Fig. 10B).

Sandstone sample CQL2017-L1–42 was collected from the upper Miaogou Group (Fig. 3; Shao et al., 2019). Eighty zircon grains yielded U-Pb ages ranging ca. 3116–424 Ma (Fig. 10B). The age population of this sample (Fig. 10B) is ca. 480–400 Ma with a ca. 424 Ma peak. Second age populations occur ca. 1000–800 Ma with a ca. 978 Ma peak and ca. 2600–2400 Ma with a ca. 2494 Ma peak.

Sandstone sample CQL2017-L1–88 was collected from the upper Miaogou Group (Fig. 3; Shao et al., 2019). Forty-nine zircon grains yielded U-Pb ages ranging ca. 2976–129 Ma (Fig. 10B). The age population of this sample (Fig. 10B) is ca. 300–200 Ma with a ca. 272 Ma peak, with a second population ca. 500–400 Ma with a ca. 452 Ma peak.

Sandstone sample CQL2016-L1–154 was collected from the upper Miaogou Group (Fig. 3; Shao et al., 2019). Seventy-five zircon grains yielded U-Pb ages ranging ca. 2776–209 Ma (Fig. 10B). The age population of this sample (Fig. 10B) is ca. 300–200 Ma with a ca. 297 Ma peak, with second populations ca. 500–400 Ma with a ca. 406 Ma peak and ca. 2000–1800 Ma with a ca. 1817 Ma peak.

Sandstone sample CQL2017-L1–183 was collected from the upper Miaogou Group (Fig. 3; Shao et al., 2019). Seventy-five zircon grains yielded U-Pb ages ranging ca. 2617–236 Ma (Fig. 10B). The age population of this sample (Fig. 10B) is ca. 300–200 Ma with a ca. 257 Ma peak, with a second population ca. 500–400 Ma with a ca. 426 Ma peak.

5.3. Statistical Results

5.3.1. Lower Miaogou Group

We used the Kolmogorov-Smirnov statistic and MDS tests to compare the ages of Miaogou Group samples with those of Qilian Shan and Alxa block plutons (Fig. 11; Table 3). Large P values (i.e., 0.902 and 0.194) correspond to sample HX20220815–4 and Silurian and Ordovician strata of the Alxa block (Table 3). The D values for the ages of sample HX20220815–4 compared to those of Alxa block strata are 0.084 and 0.164, respectively, which are less than $D_{critical}$ (α = 0.05). Sample HX20220822–1 and Alxa block samples deposited in the Neoproterozoic, Cambrian, and Ordovician yielded P values of 0.282, 0.066, and 0.481, respectively (Table 3). The D values for the ages of sample HX20220822–1 compared to those of Cambrian, Ordovician, and Neoproterozoic strata of the Alxa block are 0.143, 0.196, and 0.130, respectively, which are less than $D_{critical}$ (α = 0.05).

5.3.2. Upper Miaogou Group

The P values of 0.136 and 0.429 were calculated for sample HX20220822–2 and Silurian strata of the Alxa block and Devonian strata in the Qilian Shan (Table 3). The D values for the ages of sample HX20220822–2 compared to those of Silurian strata of the Alxa block and Devonian strata of the Qilian Shan are 0.176 and 0.133, respectively, which are less than $D_{critical}$ (α = 0.05). Sample HX20220816–1 and Devonian strata of the Qilian Shan yielded a P value of 0.055 (Table 3). The D value for the ages of sample HX20220816–1 compared to those of Devonian strata of the Qilian Shan is 0.226, which is less than $D_{critical}$ (α = 0.05). Sample HX20220816–2 and Permian strata of the Alxa block yielded a P value of 0.267 (Table 3). The D value for the ages of sample HX20220816–2 compared to those of Permian strata of the Alxa block is 0.172, which is less than $D_{critical}$ (α = 0.05). Sample HX20220815–2 and Cretaceous and Triassic strata of the Qilian Shan yielded P values of 0.220 and 0.390 (Table 3). The D values for sample HX20220815–2 compared to those of Cretaceous and Triassic strata of the Qilian Shan are 0.163, and 0.134, which are less than $D_{critical}$ (α = 0.05). Sample HX20220815–3 and the Cretaceous and Triassic strata of the Qilian Shan yielded P values of 0.260 and 0.313 (Table 3), which are consistent with sample HX20220815–2. The D values for the ages of sample HX20220815–3 compared to those of Cretaceous and Triassic strata of the Qilian Shan are 0.160 and 0.147, which are less than $D_{critical}$ (α = 0.05). Given the P and $D_{critical}$ values being larger than the D values, the null hypothesis (H_0) can be accepted.

The Shepard plot shows the dissimilarities between the upper Miaogou Group and the plutons in the Alxa block and Qilian Shan pluton, with a low-stress value of 0.31316 (left panel in Fig. 11). The two-dimensional MDS plot shows a systematic similarity in sediment provenance between the lower Miaogou Group and the Alxa block plutons (i.e., Carboniferous, Ordovician, Cambrian, and Proterozoic plutons) and the Qilian pluton (i.e., Ordovician, Cambrian, and Proterozoic plutons). The upper Miaogou Group has an inherent connection with the Alxa block plutons (i.e., Triassic, Permian, Carboniferous, Devonian, and Silurian plutons) and Qilian plutons (i.e., Permian, Devonian, Silurian, and Cambrian plutons; right panel in Fig. 11).

6. DISCUSSION

6.1. Sediment Sources of the Early Cretaceous Pingshanhu Basin

In the following sections, we discuss the implications of our field observations, compilation of detrital zircon U-Pb ages (Fig. 10), results of petrologic compositional analyses (Fig. 7), and results of Kolmogorov-Smirnov (Table 3) and MDS analyses (Fig. 11) on tectonic setting and depositional systems of the Hexi Corridor and the northern Tibetan Plateau during the Cretaceous.

6.1.1. Lower Cretaceous Lower Miaogou Group

Three samples collected from the lower Miaogou Group of the Pingshanhu Basin contained five prominent age populations with peaks at ca. 278 Ma, ca. 471 Ma, ca. 951 Ma, ca. 1847 Ma, and ca. 2450 Ma (Fig. 10C). Plutons with Triassic ages occur along the north margin of Qaidam Basin (Figs. 1B and 10E).

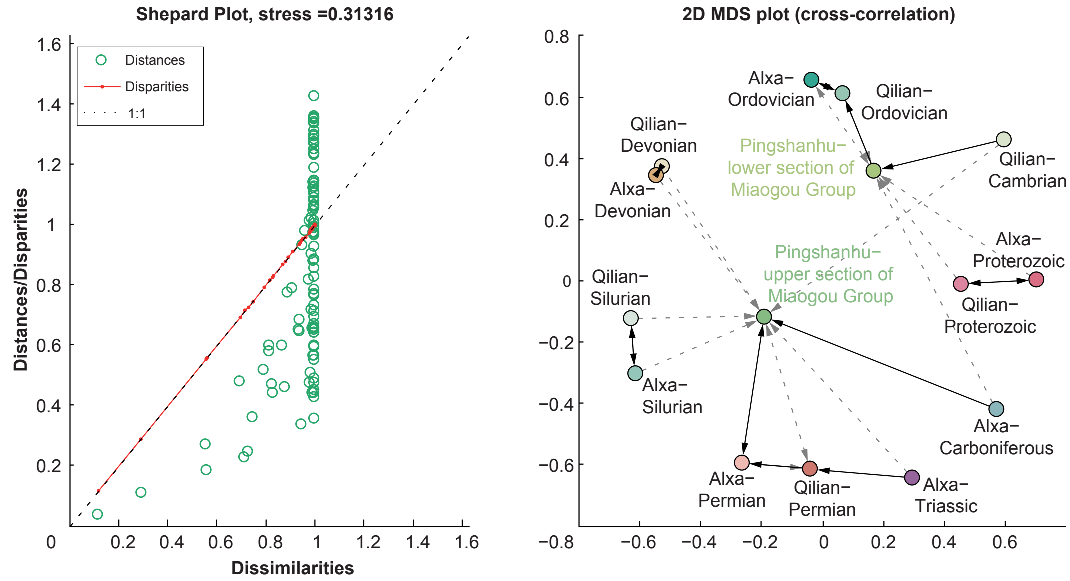

Figure 11. Shepard and two-dimensional multidimensional scaling (2D MDS) plots for detrital zircon samples and adjacent magmatic samples from the Pingshanhu Basin. Dissimilarity is based on the complement of the cross-correlation. The black solid lines and gray dashed lines in the MDS plot represent the point from each sample to its closest neighbor and second closest neighbor, respectively.

TABLE 3. TWO-SAMPLE KOLMOGOROV-SMIRNOV TEST RESULTS FOR THE SAMPLES COLLECTED FROM THE PINGSHANHU BASIN AND ADJACENT REGION

P values/ *D* values	HX2022 0815-2	HX2022 0815-3	HX2022 0815-4	HX2022 0816-1	HX2022 0816-2	HX2022 0822-1	HX2022 0822-2	HX2022 0822-3	Qilian-Cretaceous	Qilian-Triassic	Qilian-Devonian	Alxa-Permian	Alxa-Silurian	Alxa-Ordovician	Alxa-Cambrian	Alxa-Neoproterozoic
HX0815-2	–	**0.350**	0.000	0.000	0.000	0.000	0.000	0.000	**0.220**	**0.390**	0.000	0.000	0.000	0.000	0.000	0.000
HX0815-3	**0.150**	–	0.000	0.000	0.000	0.000	0.000	0.005	**0.260**	**0.313**	0.000	0.000	0.000	0.000	0.000	0.000
HX0815-4	0.366	0.453	–	0.000	0.000	**0.268**	**0.309**	0.000	0.000	0.000	0.002	0.000	**0.902**	**0.194**	0.006	0.002
HX0816-1	0.441	0.373	0.379	–	**0.067**	0.000	0.014	**0.148**	0.001	0.000	**0.055**	0.001	0.000	0.000	0.000	0.000
HX0816-2	0.477	0.406	0.495	**0.246**	–	0.000	0.000	**0.130**	0.000	0.000	0.001	**0.267**	0.000	0.000	0.000	0.000
HX0822-1	0.388	0.471	**0.152**	0.426	0.637	–	0.009	0.000	0.000	0.000	0.000	0.000	0.020	**0.481**	**0.066**	**0.282**
HX0822-2	0.345	0.352	**0.148**	0.275	0.402	0.257	–	0.000	0.000	0.000	**0.136**	0.000	**0.429**	0.004	0.000	0.000
HX0822-3	0.348	0.289	0.496	**0.204**	**0.209**	0.514	0.400	–	0.028	0.005	0.000	0.007	0.000	0.000	0.000	0.000
Qilian-Cretaceous	**0.163**	**0.160**	0.479	0.327	0.362	0.496	0.411	0.235	–	0.090	0.000	0.000	0.000	0.000	0.000	0.000
Qilian-Triassic	**0.134**	**0.147**	0.446	0.351	0.386	0.457	**0.371**	0.268	0.182	–	0.000	0.000	0.000	0.000	0.000	0.000
Qilian-Devonian	0.462	0.365	0.276	**0.226**	0.333	0.406	0.176	0.419	0.428	0.380	–	0.000	0.006	0.000	0.000	0.000
Alxa-Permian	0.520	0.463	0.632	0.344	**0.172**	0.706	0.483	0.271	0.407	0.442	0.443	–	0.000	0.000	0.000	0.000
Alxa-Silurian	0.369	0.449	**0.084**	0.379	0.459	0.228	**0.133**	0.498	0.482	0.449	0.248	0.597	–	0.026	0.000	0.000
Alxa-Ordovician	0.377	0.459	**0.164**	0.542	0.643	**0.130**	0.276	0.509	0.484	0.445	0.437	0.705	0.221	–	**0.329**	**0.284**
Alxa-Cambrian	0.444	0.514	0.252	0.608	0.743	**0.196**	0.374	0.576	0.523	0.526	0.510	0.836	0.336	**0.142**	–	**0.435**
Alxa-Neoproterozoic	0.444	0.513	0.263	0.522	0.756	**0.143**	0.385	0.572	0.523	0.527	0.508	0.837	0.340	**0.143**	**0.122**	–

Notes: Bold indicates *P* and $D_{critical}$ values are larger than *D* values, the null hypothesis (H_0) can be accepted. Triangular area on the upper-right of the table represents the *P* values. Triangular area on the lower-left of the table represents the *D* values.

Therefore, the Triassic zircon grains in the Lower Cretaceous lower Miaogou Group were likely sourced from the Alxa block to the north via southward flow (Fig. 10F). These age populations are consistent with reported magmatic ages for the Alxa block to the north (Fig. 10F; e.g., Wei et al., 2013; Duan et al., 2015; Tang, 2015; Liu et al., 2016b, 2017; Zhou et al., 2016; Zhang et al., 2017b, 2018d; Wang et al., 2020b; Table S2). In addition, paleocurrent results in the lower Miaogou Group indicate southward flow (Fig. 10C). These constraints suggest that the provenance of sediment in the Pingshanhu Basin during the earliest Cretaceous was the Alxa block to the north. This interpretation is consistent with the sedimentary records and detrital age compositions of the Early Cretaceous strata of the Yumu Shan in the southern Hexi Corridor (Wang et al., 2022).

6.1.2. Lower Cretaceous Upper Miaogou Group

The detrital zircon age distributions of the sandstone samples collected from the basal portion of the upper Miaogou Group (i.e., CQL2017-L1–42, HX20220822–2; Figs. 10A and 10B) are comparable to those of sandstone samples collected from the lower Miaogou Group. This similarity implies that the Miaogou Group sediment continued to be sourced from the Alxa block during the late Early Cretaceous. The detrital zircon ages of other samples from the upper Miaogou Group (Figs. 10B and 10D) are consistent with the ages from both the northern Qilian Shan and Alxa block (Figs. 10E and 10F). Particularly, the detrital zircon age peaks at ca. 928 Ma, ca. 1839 Ma, and ca. 2466 Ma in samples from the upper Miaogou Group allow us to suggest that Cretaceous sediments of the Pingshanhu Basin were partially sourced from late Paleozoic magmatic rocks related to subduction of Paleo-Asian oceanic lithosphere. Detrital zircon ages for the upper Miaogou Group show a slight increase in grains younger than 300 Ma compared to samples from the lower Miaogou Group. This transition in detrital ages may reflect an increased contribution of sediment from the Qilian Shan in response to regional extension in the northern Tibetan Plateau at that time.

In contrast to the Lower Cretaceous lower Miaogou Group, paleocurrent results in the upper Miaogou Group suggest predominantly northward flow, with minor southward flow (Figs. 3 and 12). These findings suggest that the sediment provenance of the Pingshanhu Basin changed as the basin margins evolved and igneous rocks in the adjacent Beida Shan and Longshoushan were exhumed to the surface. Some metamorphic zircons found in the Miaogou Group sediments may have been derived from Precambrian metamorphic rocks in the Alxa block. This indicates that the Alxa block might have been a continuous source of the sediments. Taken together, we interpret that the Miaogou Group sediments of the Pingshanhu Basin were sourced from the north during the earliest Cretaceous and from both the north and south during the late Early Cretaceous. This interpretation is consistent with the results of our Kolmogorov-Smirnov statistical test (Table 3) and MDS analyses (Fig. 11).

6.2. Tectonic Evolution of the Hexi Corridor and Northern Tibetan Plateau

A qualitative evaluation of the tectonic setting of the Pingshanhu Basin can be conducted based on the detrital zircon ages minus the host depositional ages plotted in synthetic relative probability diagrams (Cawood et al., 2012). A significant proportion of the detrital zircon ages is within 150 m.y. of the host depositional ages, which correspond to a continental collision setting (Fig. 10G; Cawood et al., 2012). Three samples from the lower Miaogou Group and two samples from the upper Miaogou Group suggest an extensional setting (Fig. 10G). In contrast, eight samples from the upper Miaogou Group correspond to a continental collision setting (Fig. 10G). Cumulative probability curves demonstrate the transition in the sedimentary environment from an extensional basin to a continental collision setting during the Early Cretaceous (Fig. 10G). However, extension is not reported for the northern Tibetan Plateau and Alxa block during the Late Jurassic and Early Cretaceous. Rather, the northern Tibetan Plateau and Alxa block experienced contraction and uplift during this time, related to the closure of the Mongol-Okhotsk Ocean and the Lhasa-Qiangtang block collision (Zhang et al., 2017a, 2021; Song et al., 2018; Chen et al., 2019a, 2019b; Wang et al., 2022; Han et al., 2023). Furthermore, the upper Miaogou Group contains an appreciable percentage of Permian-aged zircon grains. This is consistent with the tectonic setting and sedimentary environment in the Yumu Shan of the southern Hexi Corridor (Wang et al., 2022), implying that the same tectonic-sedimentary environment was present throughout the Hexi Corridor during the Early Cretaceous.

Based on new and previously published constraints, we propose the following model for the Mesozoic tectonic evolution of the Hexi Corridor (Fig. 12): During the Late Jurassic, the southwestern Alxa block was uplifted and exhumed in response to the Mongol-Okhotsk orogeny (Song et al., 2018). During earliest Cretaceous contraction, the northern Hexi Corridor received sediment from the Alxa block to the north, as evidenced by growth strata and paleocurrent indicators in the Miaogou Group (Figs. 3, 4B, and 12). Mesozoic unroofing of the southwestern Alxa block supplied sediment with ample Paleozoic zircon grains to the Hexi Corridor (Fig. 12). By ca. 130 Ma, the continued Lhasa-Qiangtang block collision resulted in contraction and exhumation of the Longshoushan (Zhang et al., 2017a). During this time, the Longshoushan contributed detrital materials to the Hexi Corridor. Early Cretaceous regional contraction was succeeded by ~2 km of extension (~29% strain) and right-slip faulting in the Hexi Corridor (Figs. 5C and 12; Wang et al., 2022). This extensional event is also evidenced in the Jiuquan and Yin'e basins (Chen et al., 2014a; Zhang et al., 2019a, 2020; Hou et al., 2020). During this time, both the northern Qilian Shan to the south and Alxa block to the north supplied sediment to the Hexi Corridor, with a progressively more dominant detrital input from the Qilian Shan (Fig. 12). Thus, the present-day topography of the northern Tibetan Plateau can be traced back to tectonic activity since the Cretaceous (Feng et al., 2023).

Our findings for the Pingshanhu Basin in the northern Hexi Corridor suggest that the northern Tibetan Plateau experienced a complex deformation history during the Mesozoic. Specifically, field observations and detrital zircon

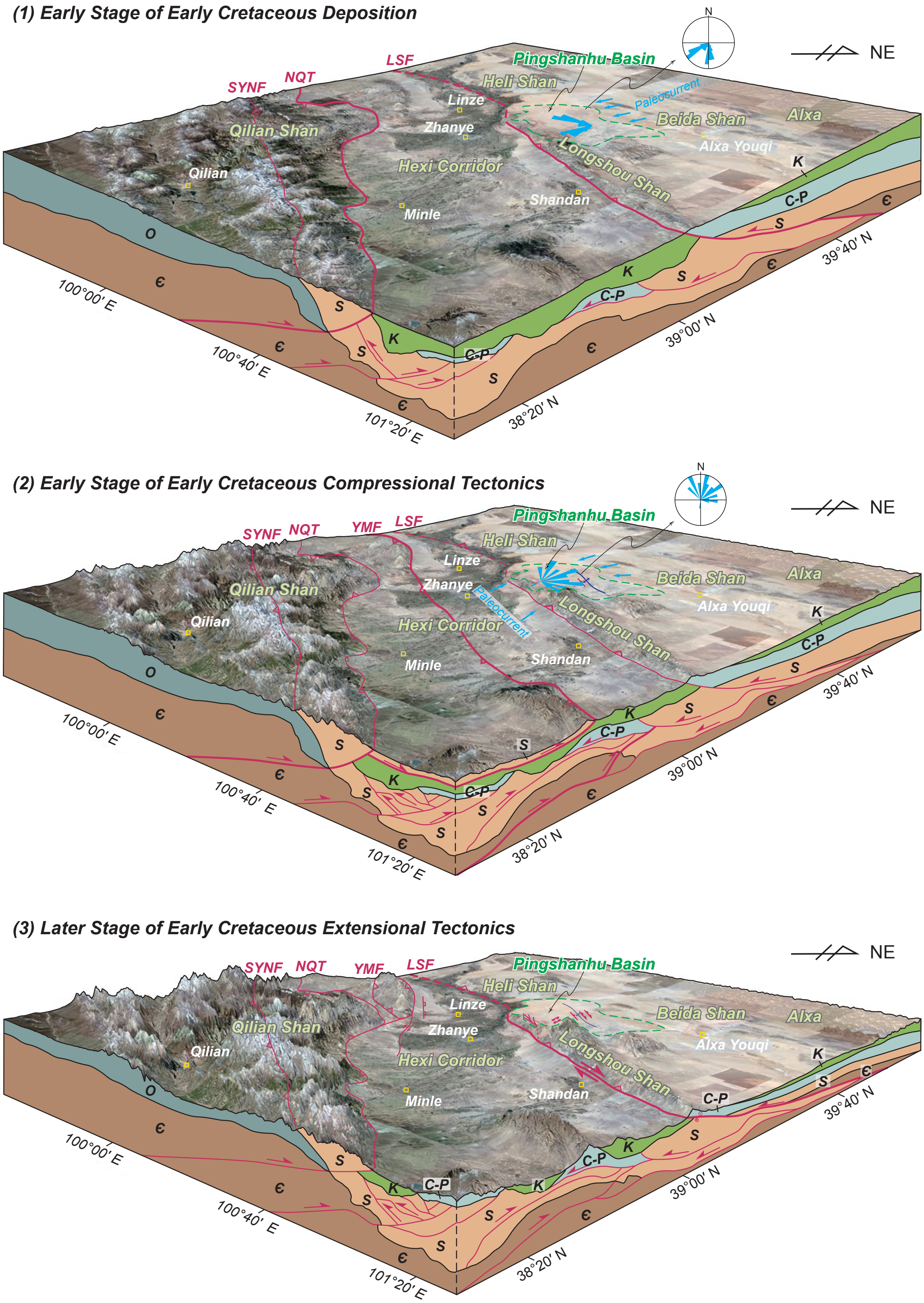

Figure 12. Three-stage tectonic evolution model of the northern Tibetan Plateau during the Early Cretaceous. (1) During the early stage of Early Cretaceous deposition, the northern Hexi Corridor basin received sediment from the Alxa block to the north. (2) Continued collision of the Lhasa and Qiangtang blocks resulted in ca. 130 Ma contraction and exhumation of the Pingshanhu Basin. (3) Early Cretaceous regional contraction was succeeded by extension and right-slip faulting in the Hexi Corridor basin. K—Lower Cretaceous; C–P—Carboniferous–Permian; S—Silurian; O—Ordovician; Є—Cambrian; SYNF—South Yeniugou fault; NQT—North Qilian thrust; YMF—Yumushan fault; LSF—Longshoushan fault.

ages suggest that the Hexi Corridor underwent regional contraction and subsequent extension during the Early Cretaceous (Shao et al., 2019; Wang et al., 2022). At the onset of the Early Cretaceous, the depositional environment of the Pingshanhu Basin remained relatively stable with sediment sourced from the southern Alxa block, which had been uplifted since the Triassic (Song et al., 2018). Due to the far-field effects of the Qiangtang-Lhasa block collision, the Qilian Shan was uplifted during the late Early Cretaceous and contributed detrital materials to the Hexi Corridor. Uplift of the Qilian Shan was accommodated via ~48 km of slip along the North Qilian thrust system (Wang et al., 2022). Our model also suggests that deformation in the northern Tibetan Plateau beginning in the Mesozoic may also have continued into the Cenozoic after the initial India-Asia collision as out-of-sequence thrusting.

The Qilian Shan was the dominant sediment source for the Hexi Corridor during the Early Cretaceous, suggesting that tectonic activity was focused in the Qilian Shan at that time. Sedimentary structures within the Pingshanhu Basin suggest the occurrence of a prograding deltaic system (Peng et al., 2011; Wang et al., 2022). Closures of the Tethys and Paleo-Asian Ocean systems (Peng et al., 2013; Zhang et al., 2021; Wang et al., 2022) and normal and right-slip faulting occurred in the Pingshanhu Basin and surrounding areas (Vincent and Allen, 1999; Wang et al., 2022). The notable absence of Late Cretaceous strata in the Hexi Corridor may have resulted from uplift and erosion throughout the northern Tibetan Plateau as a result of the Cenozoic India-Asia collision.

7. CONCLUSIONS

Structural, petrologic, and geochronologic data collected from the Cretaceous section of the Pingshanhu Basin in the Hexi Corridor foreland basin led to the following key findings:

(1) The Early Cretaceous Miaogou Group exhibits five prominent age populations at ca. 300–250 Ma, ca. 480–400 Ma, ca. 1000–800 Ma, ca. 1900–1800 Ma, and ca. 2500–2400 Ma.

(2) Pingshanhu Basin strata were sourced from the Alxa block to the north during the earliest Cretaceous. During the late Early Cretaceous, Pingshanhu Basin strata were predominantly sourced from the Qilian Shan to the south, with minor continued sediment contribution from the Alxa block to the north.

(3) Field observations, petrologic compositions, and provenance interpretations from detrital zircon ages of Pingshanhu Basin strata indicate that the northern Hexi Corridor experienced regional contraction and subsequent extension (~2 km, ~29%) during the Early Cretaceous.

(4) During the late Mesozoic, the uplift of the Qilian Shan in the northern Tibetan Plateau resulted in sediment dispersal throughout the Hexi Corridor.

ACKNOWLEDGMENTS

We thank Science Editor Christopher Spencer, Associate Editor Jiyuan Yin, and four anonymous reviewers for their critical, careful, and very constructive reviews. This research was financially supported by the National Natural Science Foundation of China (grants 41988101 and 42072001), the Second Tibetan Plateau Scientific Expedition and Research Program (grant 2019QZKK0708), and the Tectonics Program of the U.S. National Science Foundation (EAR-1914503 and EAR-1914501), and Geological Exploration Project of Qinghai (2023085027ky002).

REFERENCES CITED

Amajor, L.C., 1987, Paleocurrent, petrography and provenance analyses of the Ajali Sandstone (Upper Cretaceous), southeastern Benue Trough, Nigeria: Sedimentary Geology, v. 54, p. 47–60, https://doi.org/10.1016/0037-0738(87)90003-0.

An, K.X., Lin, X.B., Wu, L., Yang, R., Chen, H.L., Cheng, X.G., Xia, Q.K., Zhang, F.Q., Ding, W.W., Gao, S.B., Li, C.Y., and Zhang, Y., 2020, An immediate response to the Indian-Eurasian collision along the northeastern Tibetan Plateau: Evidence from apatite fission track analysis in the Kuantan Shan–Hei Shan: Tectonophysics, v. 774, p. 228–278, https://doi.org/10.1016/j.tecto.2019.228278.

An, Y.L., 2015, Geochemistry, Geochronology of the Dandeer Intrusive Rocks in the Middle Section of the Central Qilian Mountain and their Tectonic Significance [M.A. thesis]: Beijing, China University of Geosciences (Beijing), 57 p.

Andersen, T., 2002, Correction of common lead in U-Pb analyses that do not report ^{204}Pb: Chemical Geology, v. 192, p. 59–79, https://doi.org/10.1016/S0009-2541(02)00195-X.

Belousova, E., Griffin, W., O'Reilly, S.Y., and Fisher, N., 2002, Igneous zircon: Trace element composition as an indicator of source rock type: Contributions to Mineralogy and Petrology, v. 143, p. 602–622, https://doi.org/10.1007/s00410-002-0364-7.

Bian, S., Gong, J.F., Chen, L., Zuza, A.V., Chen, H.L., Lin, X.B., Cheng, X.G., and Yang, R., 2020, Diachronous uplift in intra-continental orogeny: 2D thermo-mechanical modeling of the India-Asia collision: Tectonophysics, v. 775, https://doi.org/10.1016/j.tecto.2019.228310.

Black, L.P., Kamo, S.L., Allen, C.M., Aleinikoff, J.N., Davis, D.W., Korsch, R.J., and Foudoulis, C., 2003, TEMORA 1: A new zircon standard for Phanerozoic U-Pb geochronology: Chemical Geology, v. 200, p. 155–170, https://doi.org/10.1016/S0009-2541(03)00165-7.

Bu, T., Wang, G.Q., Tang, Z., Luo, G.G., Zhu, T., Ji, B., and Guo, L., 2019, Petrogenesis of the middle Ordovician granite in the Yaodonggou area of the North Qilian orogenic belt: Constraints from zircon U-Pb geochronology and geochemistry: Acta Petrologica et Mineralogica, v. 38, p. 145–159 [in Chinese with English abstract].

Burchfiel, B.C., Zhang, P.Z., Wang, Y.P., Zhang, W.Q., Song, F.M., Deng, Q.D., Molnar, P., and Royden, L., 1991, Geology of the Haiyuan fault zone, Ningxia-Hui Autonomous Region, China, and its relation to the evolution of the northeastern margin of the Tibetan Plateau: Tectonics, v. 10, p. 1091–1110, https://doi.org/10.1029/90TC02685.

Bureau of Geology of Gansu Province, (BGGP, First Regional Geological Survey), 1973, Geologic Map of Zhangye Region: Beijing, China, Ministry of Geology of China, scale 1:200,000.

Cao, J., Li, W., Wang, G., and Zhang, X., 2019, The acid-intermediate intrusive rocks in the east section of middle Qilian orogenic belt: LA-ICP-MS zircon U-Pb age and tectonic implications: Geology and Resources, v. 28, p. 423–433 [in Chinese with English abstract].

Cawood, P.A., Hawkesworth, C.J., and Dhuime, B., 2012, Detrital zircon record and tectonic setting: Geology, v. 40, p. 875–878, https://doi.org/10.1130/G32945.1.

Chang, P.Y., 2017, Analysis of Jiermeng Granite Pluton Zircon U-Pb Age and Tectonic Environments, South Qilian [M.A. thesis]: Beijing, China University of Geosciences (Beijing), 69 p.

Chen, G.C., Shi, J.Z., Jiang, T., Zhang, H.Y., Li, W., and Wang, B.W., 2015a, LA-ICP-MS zircon U-Pb dating and geochemistry of granitoids in Tamusu, Alxa Right Banner, Inner Mongolia: Geological Bulletin of China, v. 34, p. 1884–1896 [in Chinese with English abstract].

Chen, J.L., Xu, X.Y., Zeng, Z.X., Xiao, L., Wang, H.L., Wang, Z.Q., and Xiao, S.W., 2008, Geochemical characters and LA-ICPMS zircon U-Pb dating constraints on the petrogenesis and tectonic setting of the Shichuan intrusion, east segment of the Central Qilian, NW China: Acta Petrologica Sinica, v. 24, p. 841–854 [in Chinese with English abstract].

Chen, L., Liu, L.J., Capitanio, F.A., Gerya, T.V., and Li, Y., 2020, The role of pre-existing weak zones in the formation of the Himalaya and Tibetan Plateau: 3-D thermomechanical modelling: Geophysical Journal International, v. 221, p. 1971–1983, https://doi.org/10.1093/gji/ggaa125.

Chen, Q.L., 2009, The Petrology of Niuxinshan Granitoids in the North Qilian and Their Zircon SHRIMP Dating [M.A. thesis]: Beijing, Capital Normal University, 64 p.

Chen, S., Wang, H., Wei, J., Lv, Z.Y., Gan, H.J., and Jin, S.D., 2014a, Sedimentation of the Lower Cretaceous Xiagou Formation and its response to regional tectonics in the Qingxi Sag, Jiuquan Basin, NW China: Cretaceous Research, v. 47, p. 72–86, https://doi.org/10.1016/j.cretres.2013.11.006.

Chen, S., Niu, Y.L., Sun, W.L., Zhang, Y., Li, J.Y., Guo, P.Y., and Sun, P., 2015b, On the origin of mafic magmatic enclaves (MMEs) in syn-collisional granitoids: Evidence from the Baojishan pluton in the North Qilian orogen, China: Mineralogy and Petrology, v. 109, p. 577–596, https://doi.org/10.1007/s00710-015-0383-5.

Chen, S., Niu, Y.L., Li, J.Y., Sun, W.L., Zhang, Y., Hu, Y., and Shao, F.L., 2016, Syn-collisional adakitic granodiorites formed by fractional crystallization: Insights from their enclosed mafic magmatic enclaves (MMEs) in the Qumushan pluton, North Qilian orogen at the northern margin of the Tibetan Plateau: Lithos, v. 248–251, p. 455–468, https://doi.org/10.1016/j.lithos.2016.01.033.

Chen, W., Zhou, W.P., Chen, K.X., Liu, M.W., Wang, T., Fang, M., He, H.Y., and Zhang, B., 2013, Subduction-related early Permian granodiorite in Jinchangshan of Alashan, Inner Mongolia: Evidences from zircon U-Pb geochronology and geochemistry: Journal of Mineralogy and Petrology, v. 33, p. 53–60 [in Chinese with English abstract].

Chen, X.H., Yin, A., Gehrels, G.E., Cowgill, E.S., Grove, M., Harrison, T.M., and Wang, X.F., 2003, Two phases of Mesozoic north-south extension in the eastern Altyn Tagh range, northern Tibetan Plateau: Tectonics, v. 22, p. 1053, https://doi.org/10.1029/2001TC001336.

Chen, X.H., Shao, Z.G., Xiong, X.S., Gao, R., Liu, X.J., Wang, C.F., Li, B., Wang, Z.Z., and Zhang, Y.P., 2019a, Fault system, deep structure and tectonic evolution of the Qilian orogenic belt, northwest China: Geology in China, v. 46, p. 995–1020 [in Chinese with English abstract].

Chen, X.H., Shao, Z.G., Xiong, X.S., Gao, R., Xu, S.L., Zhang, Y.P., Li, B., and Wang, Y., 2019b, Early Cretaceous overthrusting of Yumu Mountain and hydrocarbon prospect on the northern margin of the Qilian orogenic belt: Acta Geoscientica Sinica, v. 40, p. 377–392 [in Chinese with English abstract].

Chen, X.H., Dong, S.W., Shi, W., Ding, W.C., Zhang, Y.P., Li, B., Shao, Z.G., and Wang, Y., 2022, Construction of continental Asia in the Phanerozoic: A review: Acta Geologica Sinica (English Edition), v. 96, p. 26–51, https://doi.org/10.1111/1755-6724.14867.

Chen, Y.J., Yang, K., Wu, B., Zhao, R.Y., Wang, G., and Gou, X.M., 2019c, Zircon U-Pb dating and its geological implications in Beidaban granite, northern Qilian, Gansu Province: Journal of East China University of Technology (Natural Sciences), v. 42, p. 108–115.

Chen, Y.X., Xia, X.H., and Song, S.G., 2012, Petrogenesis of Aoyougou high-silica adakite in the North Qilian orogen, NW China: Evidence for decompression melting of oceanic slab: Chinese Science Bulletin, v. 57, p. 2289–2301, https://doi.org/10.1007/s11434-012-5069-3.

Chen, Y.X., Song, S.G., Niu, Y.L., and Wei, C.J., 2014b, Melting of continental crust during subduction initiation: A case study from the Chaidanuo peraluminous granite in the North Qilian suture zone: Geochimica et Cosmochimica Acta, v. 132, p. 311–336, https://doi.org/10.1016/j.gca.2014.02.011.

Chen, Z.L., Wang, X.F., Yin, A., Chen, B.L., and Chen, X.H., 2004, Cenozoic left-slip motion along the central Altyn Tagh fault as inferred from the sedimentary record: International Geology Review, v. 46, p. 839–856, https://doi.org/10.2747/0020-6814.46.9.839.

Clark, M.K., 2012, Continental collision slowing due to viscous mantle lithosphere rather than topography: Nature, v. 483, p. 74–77, https://doi.org/10.1038/nature10848.

Clark, M.K., Farley, K.A., Zheng, D.W., Wang, Z.C., and Duvall, A.R., 2010, Early Cenozoic faulting of the northern Tibetan Plateau margin from apatite (U-Th)/He ages: Earth and Planetary Science Letters, v. 296, p. 78–88, https://doi.org/10.1016/j.epsl.2010.04.051.

Corfu, F., Hanchar, J.M., Hoskin, P.W.O., and Kinny, P., 2003, Atlas of zircon textures, *in* Hanchar, J.M., and Hoskin, P.W.O., eds., Zircon: Berlin, De Gruyter, p. 469–502, https://doi.org/10.1515/9781501509322-019.

Cowgill, E., Yin, A., Harrison, T.M., and Wang, X.F., 2003, Reconstruction of the Altyn Tagh fault based on U-Pb geochronology: Role of back thrusts, mantle sutures, and heterogeneous crustal strength in forming the Tibetan Plateau: Journal of Geophysical Research: Solid Earth, v. 108, https://doi.org/10.1029/2002JB002080.

Cui, J.W., Zheng, Y.Y., Sun, X., Wu, S., Gao, S.B., Tian, L.M., Sun, J.Y., and Yang, C., 2016, Zircon U-Pb dating and its geological implications in Beidaban granite, northern Qilian, Gansu Province: Earth Science (Natural Science), v. 41, p. 1156–1170 [in Chinese with English abstract].

Dan, W., Li, X.H., Guo, J.H., Liu, Y., and Wang, X.C., 2012, Paleoproterozoic evolution of the eastern Alxa block, westernmost North China: Evidence from in situ zircon U-Pb dating and Hf-O isotopes: Gondwana Research, v. 21, p. 838–864, https://doi.org/10.1016/j.gr.2011.09.004.

Dan, W., Li, X., Wang, Q., Tang, G.J., and Liu, Y., 2014a, An early Permian (ca. 280Ma) silicic igneous province in the Alxa block, NW China: A magmatic flare-up triggered by a mantle-plume: Lithos, v. 204, p. 144–158, https://doi.org/10.1016/j.lithos.2014.01.018.

Dan, W., Li, X.H., Wang, Q., Wang, X.C., and Liu, Y., 2014b, Neoproterozoic S-type granites in the Alxa block, westernmost North China, and tectonic implications: In situ zircon U-Pb-Hf-O isotopic and geochemical constraints: American Journal of Science, v. 314, p. 110–153, https://doi.org/10.2475/01.2014.04.

Dan, W., Wang, Q., Wang, X.C., Liu, Y., Wyman, D.A., and Liu, Y.S., 2015, Overlapping Sr-Nd-Hf-O isotopic compositions in Permian mafic enclaves and host granitoids in Alxa block, NW China: Evidence for crust-mantle interaction and implications for the generation of silicic igneous provinces: Lithos, v. 230, p. 133–145, https://doi.org/10.1016/j.lithos.2015.05.016.

Dan, W., Li, X.H., Wang, Q., Wang, X.C., Wyman, D.A., and Liu, Y., 2016, Phanerozoic amalgamation of the Alxa block and North China craton: Evidence from Paleozoic granitoids, U-Pb geochronology and Sr-Nd-Pb-Hf-O isotope geochemistry: Gondwana Research, v. 32, p. 105–121, https://doi.org/10.1016/j.gr.2015.02.011.

DeCelles, P.G., Langford, R.P., and Schwartz, R.K., 1983, Two new methods of paleocurrent determination from trough cross-stratification: Journal of Sedimentary Research, v. 53, p. 629–642.

Deng, W.B., Shao, Z.G., Wang, Z.Z., Chen, X.H., Yi, J.J., and Xu, H.J., 2022, Geochemistry and zircon U-Pb-Hf isotopes of granodiorites in the northern Alxa area: Implications for the Middle–Late Devonian tectonic evolution of the southern Central Asian orogenic belt: International Journal of Earth Sciences, v. 111, p. 2369–2390, https://doi.org/10.1007/s00531-022-02233-x.

Dickinson, W.R., 1970, Interpreting detrital modes of graywacke and arkose: Journal of Sedimentary Research, v. 40, p. 695–707.

Dickinson, W.R., 1985, Interpreting provenance relations from detrital modes of sandstones, *in* Zuffa, G.G., ed., Provenance of Arenites: Dordrecht, Netherlands, Springer, North Atlantic Treaty Organization (NATO) Advanced Study Institute (ASI) Series 148, p. 333–361, https://doi.org/10.1007/978-94-017-2809-6_15.

Dickinson, W.R., and Suczek, C.A., 1979, Plate tectonics and sandstone compositions: The American Association of Petroleum Geologists Bulletin, v. 63, p. 2164–2182.

Dickinson, W.R., Beard, L.S., Brakenridge, G.R., Erjavec, J.L., Ferguson, R.C., Inman, K.F., Knepp, R.A., Lindberg, F.A., and Ryberg, P.T., 1983, Provenance of North American Phanerozoic sandstones in relation to tectonic setting: Geological Society of America Bulletin, v. 94, p. 222–235, https://doi.org/10.1130/0016-7606(1983)94<222:PONAPS>2.0.CO;2.

Ding, L., Kapp, P., Cai, F.L., Garzione, C.N., Xiong, Z.Y., Wang, H.Q., and Wang, C., 2022, Timing and mechanisms of Tibetan Plateau uplift: Nature Reviews: Earth & Environment, v. 3, p. 652–667, https://doi.org/10.1038/s43017-022-00318-4.

Ding, Q.F., and Huang, Z.B., 2019, U-Pb ages and geochemistry of Maozangsi granodiorite in North Qilian Mountains, China: Northwest Geology, v. 52, p. 53–62 [in Chinese with English abstract].

Dong, C.Y., Liu, D.Y., Li, J.J., Wang, Y.S., Zhou, H.Y., Li, C.D., Yang, Y.H., and Xie, L.W., 2007, Palaeoproterozoic Khondalite belt in the western North China craton: New evidence from SHRIMP dating and Hf isotope composition of zircons from metamorphic rocks in the Bayan Ul–Helan Mountains area: Chinese Science Bulletin, v. 52, p. 2984–2994, https://doi.org/10.1007/s11434-007-0404-9.

Dong, J.S., Tan, X.Y., Liu, J.D., and Yin, Z.H., 2015, The geological significance and determination of age of the metamorphic intrusion of Paleoproterozoic Tuolai rock Group in the mid-eastern part of the North Qilian Mountains: Journal of Qinghai University (Natural Science Edition), v. 33, p. 73–79 [in Chinese with English abstract].

Duan, J., Li, C.S., Qian, Z.Z., and Jiao, J.G., 2015, Geochronological and geochemical constraints on the petrogenesis and tectonic significance of Paleozoic dolerite dykes in the southern margin of Alxa block, North China craton: Journal of Asian Earth Sciences, v. 111, p. 244–253, https://doi.org/10.1016/j.jseaes.2015.07.012.

Duvall, A.R., Clark, M.K., Van Der Pluijm, B.A., and Li, C.Y., 2011, Direct dating of Eocene reverse faulting in northeastern Tibet using Ar-dating of fault clays and low-temperature thermochronometry: Earth and Planetary Science Letters, v. 304, p. 520–526, https://doi.org/10.1016/j.epsl.2011.02.028.

Fan, X.X., Kong, W.J., Yang, Z.X., Zhao, J.C., and Li, Y.X., 2020, U-Pb chronology, geochemical characteristics and petrogenesis of the Chelugou pluton in the western part of North Qilian orogenic belt: Geology in China, v. 47, p. 755–766 [in Chinese with English abstract].

Feng, J.Y., Xiao, W.J., Windley, B., Han, C.M., Wan, B., Zhang, J.E., Ao, S.J., Zhang, Z.Y., and Lin, L., 2013, Field geology, geochronology and geochemistry of mafic-ultramafic rocks from Alxa, China: Implications for late Permian accretionary tectonics in the southern Altaids: Journal of Asian Earth Sciences, v. 78, p. 114–142, https://doi.org/10.1016/j.jseaes.2013.01.020.

Feng, Z.R., Yuan, W.M., Zhao, Z.D., Dong, G.C., Li, X., Sun, W.L., Yang, L., Hong, S.J., Zhao, M.M., Hu, C.X., and Li, S.Y., 2023, Mesozoic–Cenozoic cooling, exhumation and tectonic implications of Chaqiabeishan-Shaliuquan LiBe ore district in the northeastern Qinghai-Tibet Plateau: Tectonophysics, v. 88, https://doi.org/10.1016/j.tecto.2023.230040.

Gansu Bureau of Geology and Mineral Resources (BGMR), 1969, Geologic Map of the Baoensi: Beijing, Geological House, scale 1:200,000 [in Chinese].
Gao, L., Ren, E.F., Li, J., and Kang, W.H., 2017, The geochemical characteristics and chronological significance of Baihuagou pluton at the eastern section of central Qilian: Journal of Qinghai University, v. 35, p. 1–7 [in Chinese with English abstract].
Gao, R., Wang, H., Yin, A., Dong, S., Kuang, Z., Zuza, A.V., Li, W., and Xiong, X., 2013, Tectonic development of the northeastern Tibetan Plateau as constrained by high-resolution deep seismic-reflection data: Lithosphere, v. 5, p. 555–574, https://doi.org/10.1130/L293.1.
Gehrels, G., 2014, Detrital zircon U-Pb geochronology applied to tectonics: Annual Review of Earth and Planetary Sciences, v. 42, p. 127–149, https://doi.org/10.1146/annurev-earth-050212-124012.
Gehrels, G.E., Yin, A., and Wang, X.F., 2003a, Detrital-zircon geochronology of the northeastern Tibetan Plateau: Geological Society of America Bulletin, v. 115, p. 881–896, https://doi.org/10.1130/0016-7606(2003)115<0881:DGOTNT>2.0.CO;2.
Gehrels, G.E., Yin, A., and Wang, X.F., 2003b, Magmatic history of the northeastern Tibetan Plateau: Journal of Geophysical Research: Solid Earth, v. 108, https://doi.org/10.1029/2002JB001876.
Geng, Y.S., and Zhou, X.W., 2010, Early Neoproterozoic granite events in Alax area of Inner Mongolia and their geological significance: Evidence from geochronology: Acta Petrologica et Mineralogica, v. 29, p. 779–795 [in Chinese with English abstract].
Geng, Y.S., and Zhou, X.W., 2012, Early Permian magmatic events in the Alxa metamorphic basement: Evidence from geochronology: Acta Petrologica Sinica, v. 28, p. 2667–2685 [in Chinese with English abstract].
Geng, Y.S., Wang, X.S., Wu, C.M., and Zhou, X.W., 2010, Late Paleoproterozoic tectonothermal events of the metamorphic basement in Alxa area: Evidence from geochronology: Acta Petrologica Sinica, v. 26, p. 1159–1170 [in Chinese with English abstract].
George, A.D., Marshallsea, S.J., Wyrwoll, K.H., Jie, C., and Lu, Y.C., 2001, Miocene cooling in the northern Qilian Shan, northeastern margin of the Tibetan Plateau, revealed by apatite fission-track and vitrinite-reflectance analysis: Geology, v. 29, p. 939–942, https://doi.org/10.1130/0091-7613(2001)029<0939:MCITNQ>2.0.CO;2.
Gong, J.H., Zhang, J.X., Yu, S.Y., Li, H.K., and Hou, K.J., 2012, Ca. 2.5 Ga TTG rocks in the western Alxa block and their implications: Chinese Science Bulletin, v. 57, p. 4064–4076, https://doi.org/10.1007/s11434-012-5315-8.
Gong, J.H., Zhang, J.X., Wang, Z.Q., Yu, S.Y., Li, H.K., and Li, Y.S., 2016, Origin of the Alxa block, western China: New evidence from zircon U-Pb geochronology and Hf isotopes of the Longshoushan complex: Gondwana Research, v. 36, p. 359–375, https://doi.org/10.1016/j.gr.2015.06.014.
Guo, J.J., Zhao, F.Q., Li, H.K., Li, H.M., and Zuo, Y.C., 2000, New chronological evidence of the age of the Huangyuan Group in the eastern segment of mid-Qilian massif and its geological significance: Regional Geology of China, v. 19, p. 26–31 [in Chinese with English abstract].
Guo, Z.P., Li, W.Y., Zhang, Z.W., Gao, Y.B., Zhang, J.W., Li, K., Kong, H.L., and Qian, B., 2015a, Petrogenesis of Lumanshan granites in Hualong area of southern Qilian Mountain: Constraints from geochemistry, zircon U-Pb geochronology and Hf isotope: Geology in China, v. 42, p. 864–880 [in Chinese with English abstract].
Guo, Z.P., Zhao, X.M., Bai, Y., Zhang, J.W., and Kong, H.L., 2015b, Zircon U-Pb and molybdenite Re-Os dating of the Langlike copper deposit in North Qilian Mountain and its geological implications: Geology in China, v. 42, p. 691–701 [in Chinese with English abstract].
Han, L.L., Ding, W.C., Chen, X.H., Shao, Z.G., Zhang, D., Xiao, Y.J., He, C.G., Wang, Z.Z., Li, B., Zhang, Y.P., Xu, S.L., and Wang, Y., 2023, Early Cretaceous thrust and nappe tectonics in north Qilian Shan, northern Tibetan Plateau: Evidence from field mapping, geochronology, and deep structural analysis: Acta Geologica Sinica (English Edition), v. 97, p. 1058–1077, https://doi.org/10.1111/1755-6724.15060.
He, C.C., Zhang, Y.Q., Li, J., Li, H.L., Sun, D.X., and Xiong, J.H., 2019, Kinematics of the Maxian Mountain fault, northeastern Tibetan Plateau: The history of Cretaceous–Cenozoic sedimentary and tectonic deformation: Acta Geoscientica Sinica, v. 40, p. 563–587 [in Chinese with English abstract].
He, X.Y., Yang, X.K., Wang, Y., Guo, R.H., Liao, Y.Y., and Fan, Y.H., 2020, Petrology, geochemistry and zircon U-Pb geochronology of the Chaidamushan granite from the southern margin of Qilianshan: Acta Geologica Sinica, v. 94, p. 1248–1263 [in Chinese with English abstract].
Horton, B.K., Dupont-Nivet, G., Zhou, J., Waanders, G.L., Butler, R.F., and Wang, J., 2004, Mesozoic–Cenozoic evolution of the Xining-Minhe and Dangchang basins, northeastern Tibetan Plateau: Magnetostratigraphic and biostratigraphic results: Journal of Geophysical Research: Solid Earth, v. 109, B04402, https://doi.org/10.1029/2003JB002913.
Hoskin, P.W.O., 2005, Trace-element composition of hydrothermal zircon and the alteration of Hadean zircon from the Jack Hills, Australia: Geochimica et Cosmochimica Acta, v. 69, p. 637–648, https://doi.org/10.1016/j.gca.2004.07.006.
Hou, R.N., Wang, S.H., Zhang, X., Hou, K.X., Zhang, C., and Wang, J.R., 2015, Geochemical characteristics and tectonic significance of the granitoids in the western section of the Mid-Qilian: Advances in Earth Science, v. 30, p. 1034–1094 [in Chinese with English abstract].
Hou, Y.C., Wang, H.Y., Fan, T.L., Zhang, H.G., Yang, R.Z., Li, Y.F., and Long, S.F., 2020, Rift-related sedimentary evolution and its response to tectonics and climate changes: A case study of the Guaizihu sag, Yingen-Ejinaqi Basin, China: Journal of Asian Earth Sciences, v. 195, https://doi.org/10.1016/j.jseaes.2020.104370.
Hu, C.S., Li, W.B., Xu, C., Zhong, R.C., Zhu, F., and Qiao, X.Y., 2015, Geochemistry and petrogenesis of Permian granitoids in the northwestern margin of the North China craton: Insights from the Dongshengmiao pluton, Inner Mongolia: International Geology Review, v. 57, p. 1843–1860, https://doi.org/10.1080/00206814.2015.1039087.
Hu, W.L., Jia, Z.L., Wang, J.R., Hou, K.X., and Wang, S.H., 2016, Geochronology and geochemistry characteristics of the granites from the Huashigou area, south Qilian, and their tectonic significance: Geological Journal of China Universities, v. 22, p. 242–253 [in Chinese with English abstract].
Huang, H., Niu, Y.L., Nowell, G., Zhao, Z.D., Yu, X.H., and Mo, X.X., 2015, The nature and history of the Qilian block in the context of the development of the Greater Tibetan Plateau: Gondwana Research, v. 28, p. 209–224, https://doi.org/10.1016/j.gr.2014.02.010.
Huang, H., Niu, Y.L., and Mo, X.X., 2017, Garnet effect on Nd-Hf isotope decoupling: Evidence from the Jinfosi batholith, northern Tibetan Plateau: Lithos, v. 274–275, p. 31–38, https://doi.org/10.1016/j.lithos.2016.12.025.
Huang, Z.B., Li, B.H., Jin, X., and Liu, M.Q., 2010, Discussion on the petrogenesis and tectonic setting of Beidaban granitic pluton in north Qilian Mountains: Journal of Mineral Petrology, v. 30, p. 62–68 [in Chinese with English abstract].
Huang, Z.B., Zheng, J.P., Li, B.H., Wei, Z.J., Qi, W., and Xu, Y.L., 2014, The discovery of late Cambrian adakite in the western central Qilian Mountains and its geological implications: Acta Petrologica et Mineralogica, v. 33, p. 1008–1018 [in Chinese with English abstract].
Huang, Z.B., Zheng, J.P., Li, B.H., Dong, X.Y., Fu, T.Y., Xu, L., and Gao, K.L., 2018, U- Pb ages, Hf isotopic composition and geochemistry of alkaline complex from the Ganshaebo REE deposit in north Qilian Mountains, China: Acta Geologica Sinica, v. 92, p. 2420–2436 [in Chinese with English abstract].
Ingersoll, R.V., Bullard, T.F., Ford, R.L., Grimm, J.P., Pickle, J.D., and Sares, S.W., 1984, The effect of grain size on detrital modes: A test of the Gazzi-Dickinson point-counting method: Journal of Sedimentary Research, v. 54, p. 103–116.
Ji, B., Huang, B.T., Li, X.M., and Wang, L., 2019, Geochronology and geochemical characteristics of the Early Ordovician granite from Hongmiaogou area in northwest margin of south Qilian and its geological significance: Northwest Geology, v. 52, p. 63–75 [in Chinese with English abstract].
Jia, Z.L., Chen, W.F., Sha, X., and Wang, J.R., 2017, Discovery of middle Permian adakitic rocks in south Qilian area, Gansu, and implications for tectonics and Cu (Au): Geotectonica et Metallogenia, v. 41, p. 222–234 [in Chinese with English abstract].
Jolivet, M., Brunel, M., Seward, D., Xu, Z., Yang, J., Roger, F., Tapponnier, P., Malavieille, J., Arnaud, N., and Wu, C., 2001, Mesozoic and Cenozoic tectonics of the northern edge of the Tibetan Plateau: Fission-track constraints: Tectonophysics, v. 343, p. 111–134, https://doi.org/10.1016/S0040-1951(01)00196-2.
Li, B., Hu, D.G., Chen, X.H., Zhang, Y.L., Wu, H.H., and Wang, C.Q., 2017, Zircon U-Pb age of granite porphyry within Youhulugou ophiolite in the suture zone of north Qilian Mountains and its geological implications: Geoscience, v. 31, p. 1170–1176 [in Chinese with English abstract].
Li, B., Chen, X.H., Zuza, A.V., Hu, D.G., Ding, W.C., Huang, P.H., and Xu, S.L., 2019a, Cenozoic cooling history of the north Qilian Shan, northern Tibetan Plateau, and the initiation of the Haiyuan fault: Constraints from apatite- and zircon-fission track thermochronology: Tectonophysics, v. 751, p. 109–124, https://doi.org/10.1016/j.tecto.2018.12.005.
Li, B., Zuza, A.V., Chen, X.H., Hu, D.G., Shao, Z.G., Qi, B.S., Wang, Z.Z., Levy, D.A., and Xiong, X.S., 2020a, Cenozoic multi-phase deformation in the Qilian Shan and out-of-sequence development of the northern Tibetan Plateau: Tectonophysics, v. 782–783, https://doi.org/10.1016/j.tecto.2020.228423.
Li, B., Zuza, A.V., Chen, X.H., Wang, Z.Z., Shao, Z.G., Levy, D.A., Wu, C., Xu, S.L., and Sun, Y.J., 2021, Pre-Cenozoic evolution of the northern Qilian orogen from zircon geochronology: Framework

for early growth of the northern Tibetan Plateau: Palaeogeography, Palaeoclimatology, Palaeoecology, v. 562, https://doi.org/10.1016/j.palaeo.2020.110091.

Li, J.F., Zhang, Z.C., and Han, B.F., 2010, Geochronology and geochemistry of early Paleozoic granitic plutons from Subei and Shibaocheng areas, the western segment of central Qilian, and their geological implications: Acta Petrologica Sinica, v. 26, p. 2431–2444 [in Chinese with English abstract].

Li, M., Wang, C., Li, R.S., and Peng, Y., 2015, Petrogenesis and LA-ICP-MS zircon U-Pb dating of late Neoproterozoic granitic gneisses in western Qilian Mountain: Geological Bulletin of China, v. 24, p. 1438–1446 [in Chinese with English abstract].

Li, Q., 2012, Study of the Precambrian Metamorphic-Plutonic Rocks in the Alatengaobao Region of Aixayouoi, Inner Mongolia [M.A. thesis]: Beijing, China University of Geosciences (Beijing), 60 p.

Li, W.F., Zhang, X.Y., Cao, J.S., Wang, G.L., Wang, W., Qiao, G.D., and Liu, J.D., 2020b, Geochemical characteristics and chronological significance of Middle Ordovician granite in Halahu area of southern Qilian Mountain: Geological Bulletin of China, v. 39, p. 215–223 [in Chinese with English abstract].

Li, X., Su, L., Song, B., and Liu, D., 2004, SHRIMP U-Pb zircon age of the Jinchuan ultramafic intrusion and its geological significance: Chinese Science Bulletin, v. 49, p. 420–422, https://doi.org/10.1007/BF02900329.

Li, X.H., Su, L., Chung, S.-L., Li, Z.X., Liu, Y., Song, B., and Liu, D.Y., 2005, Formation of the Jinchuan ultramafic intrusion and the world's third largest Ni-Cu sulfide deposit: Associated with the ~825 Ma south China mantle plume?: Geochemistry, Geophysics, Geosystems, v. 6, Q11004, https://doi.org/10.1029/2005GC001006.

Li, Y.S., Xu, L.J., Yu, S.Y., Zhang, J.X., Guo, J., Peng, Y.B., and Zhou, G.S., 2019b, Partial melting of thickened lower crust in post-collisional setting: Evidence from high silicon adakitic granites in the north Qilian orogen: Geological Journal, v. 55, p. 3990–4007, https://doi.org/10.1002/gj.3645.

Liao, H., Hu, D.G., Zhang, X.J., Yu, W.L., and Guo, T., 2014, Zircon U-Pb age for granite of the Ordovician formation and its tectonic significance in the southern Qilian: Journal of Geodynamics, v. 20, p. 292–298 [in Chinese with English abstract].

Lin, L.N., Xiao, W.J., Wan, B., Windley, B.F., Ao, S.J., Han, C.M., Feng, J.Y., Zhang, J., and Zhang, Z.Y., 2014, Geochronologic and geochemical evidence for persistence of south-dipping subduction to late Permian time, Langshan area, Inner Mongolia (China): Significance for termination of accretionary orogenesis in the southern Altaids: American Journal of Science, v. 314, p. 679–703, https://doi.org/10.2475/02.2014.08.

Liu, B.S., Cai, J.F., Lei, X.Q., Wang, T.S., and Meng, H., 2016a, Zircon U-Pb age for granite of the Ordovician formation and its tectonic significance in the southern Qilian: Northwest Geology, v. 49, p. 43–50 [in Chinese with English abstract].

Liu, J.D., Wang, C.T., Li, W.F., Zhang, X.Y., and Dong, J.S., 2015, Geological characteristics and formation of Proterozoic basement, north Qilian Langshidang area: Gansu Metallurgy, v. 37, p. 96–102 [in Chinese with English abstract].

Liu, J.N., Yin, C.Q., Zhang, J., Qian, J.H., Li, S., Xu, K.Y., Wu, S.J., and Xia, Y.F., 2020a, Tectonic evolution of the Alxa block and its affinity: Evidence from the U-Pb geochronology and Lu-Hf isotopes of detrital zircons from the Longshoushan belt: Precambrian Research, v. 344, https://doi.org/10.1016/j.precamres.2020.105733.

Liu, J.N., Yin, C.Q., Zhang, J., Qian, J.H., Xu, K.Y., Wu, S.J., and Xu, N.Q., 2020b, Detrital zircon U-Pb and Hf isotopes study of the Longshoushan belt in the southwestern margin of the Alxa block: Constraints on the tectonic evolution and affinity of the Alxa block: EGU General Assembly Online, v. 2020, https://doi.org/10.5194/egusphere-egu2020-22176.

Liu, M., Zhang, Z.M., Xiang, J.F., Cao, D.Z., and Yanf, G.H., 2014, Zircon U-Pb isotopic dating and lithogeochemical features of the biotite monzonitic granite in Daheishan tungsten deposit, Qinghai Province, China: Acta Petrologica Sinica, v. 30, p. 139–151 [in Chinese with English abstract].

Liu, M., Zhang, D., Xiong, G.Q., Zhao, H.T., Di, Y.J., Wang, Z., and Zhou, Z.G., 2016b, Zircon U-Pb age, Hf isotope and geochemistry of Carboniferous intrusions from the Langshan area, Inner Mongolia: Petrogenesis and tectonic implications: Journal of Asian Earth Sciences, v. 120, p. 139–158, https://doi.org/10.1016/j.jseaes.2016.01.005.

Liu, M.Q., 2013, Single-grain zircon U-Pb ages and geological significance of the Lianhuashan granites from Wuwei (Gansu) in the northern Qilian orogenic belt: Journal of Lanzhou University (Natural Sciences), v. 49, p. 448–452 [in Chinese with English abstract].

Liu, Q., Zhao, G.C., Sun, M., Han, Y.G., Eizenhöfer, P.R., Hou, W.Z., Zhang, X.R., Zhu, Y.L., Wang, B., Liu, D.X., and Xu, B., 2016c, Early Paleozoic subduction processes of the Paleo-Asian Ocean: Insights from geochronology and geochemistry of Paleozoic plutons in the Alxa terrane: Lithos, v. 262, p. 546–560, https://doi.org/10.1016/j.lithos.2016.07.041.

Liu, Q., Zhao, G.C., Han, Y.G., Eizenhöfer, P.R., Zhu, Y.L., Hou, W.Z., and Zhang, X.R., 2017, Timing of the final closure of the Paleo-Asian Ocean in the Alxa terrane: Constraints from geochronology and geochemistry of late Carboniferous to Permian gabbros and diorites: Lithos, v. 274–275, p. 19–30, https://doi.org/10.1016/j.lithos.2016.12.029.

Liu, Q., Wang, G., and Wang, D.K., 2019, Geochronology and its geological significance for granodiorite porphyry in the Songshunangou Au deposit: Acta Geologica Sinica, v. 39, p. 15–21 [in Chinese with English abstract].

Liu, X.H., Gao, R., Guo, X.Y., and Ding, L., 2023, Detrital zircon U-Pb geochronology of the Lunpola Basin strata constrains the Cenozoic tectonic evolution of central Tibet: Gondwana Research, v. 113, p. 179–193, https://doi.org/10.1016/j.gr.2022.10.019.

Liu, X.T., 2019, Spatial-Temporal Distribution and Tectonic Implications of the Granitoids from Qilian Block [Ph.D. thesis]: Qinghai, China, Qinghai Institute of Salt Lakes, Chinese Academy of Sciences, 138 p.

Liu, Y.X., Sha, X., Ma, Z., and Wang, J.R., 2018, Geochemical characteristics and tectonic implication of the Shuanglong mafic-ultramafic rocks in western section of the north Qilian: Acta Petrologica Sinica, v. 34, p. 3383–3397 [in Chinese with English abstract].

Lu, X.X., Sun, Y.G., Zhang, X.T., Xiao, Q.H., Wang, X.X., Wei, X.D., and Gu, D.M., 2007, The SHRIMP age of Tatalin rapakivi granite at the north margin of Qaidam Basin: Acta Geologica Sinica, v. 81, p. 626–634 [in Chinese with English abstract].

Ludwig, K.R., 2003, User's Manual for Isoplot 3.00: A Geochronological Toolkit for Microsoft Excel: Berkeley Geochronology Center Special Publication, 74 p., revised 27 August 2003.

Luo, Z.W., Zhang, Z.C., Li, J.F., Feng, Z.S., and Tang, W.H., 2015, Geochronology of two kinds of Paleozoic granitic plutons from Sangewatang in Subei, western margin of central-south Qilian, and their geological implications: Acta Petrologica Sinica, v. 31, p. 176–188 [in Chinese with English abstract].

Lv, D.Y., Ren, E.F., Yang, Q.P., and Xiong, W.S., 2021, Geochemical characteristics and geochronological significance of the rock mass of Shangmoji in the eastern part of the middle Qilian mountains: Journal of Qinghai University, v. 39, p. 101–108 [in Chinese with English abstract].

Ma, J.J., Wang, H., He, C., Wang, Q.Y., and Chen, N.S., 2018, Neoproterozoic post-collision magmatism in south Qilian orogen, China: Evidenced by geochronology and geochemistry: Journal of Earth Sciences and Environment, v. 40, p. 133–154 [in Chinese with English abstract].

Mao, J.W., Zhang, Z.H., Bernd, L.M., Zhang, Z.C., Yang, J.M., and Wang, Z.L., 2000, The Yeniutan granodiorite in Sunan County, Gansu Province, China: Petrological features, geological setting and relationship to tungsten mineralization: Episodes, v. 23, p. 163–171, https://doi.org/10.18814/epiiugs/2000/v23i3/003.

McDonough, W.F., and Sun, S.S., 1995, The composition of the Earth. Chemical Geology: Chemical Evolution of the Mantle, v. 120, p. 223–253, https://doi.org/10.1016/0009-2541(94)00140-4.

Meyer, B., Tapponnier, P., Bourjot, L., Métivier, F., Gaudemer, Y., Peltzer, G., Guo, S.M., and Chen, Z.T., 1998, Crustal thickening in Gansu-Qinghai, lithospheric mantle subduction, and oblique, strike-slip controlled growth of the Tibet Plateau: Geophysical Journal International, v. 135, p. 1–47, https://doi.org/10.1046/j.1365-246X.1998.00567.x.

Murphy, M.A., Yin, A., Harrison, T.M., Dürr, S.B., Chen, Z., Ryerson, F.J., Kidd, W.S.F., Wang, X., and Zhou, X., 1997, Did the Indo-Asian collision alone create the Tibetan Plateau: Geology, v. 25, p. 719–722, https://doi.org/10.1130/0091-7613(1997)025<0719:DTIACA>2.3.CO;2.

Nordsvan, A.R., Kirscher, U., Kirkland, C.L., Barham, M., and Brennan, D.T., 2020, Resampling (detrital) zircon age distributions for accurate multidimensional scaling solutions: Earth-Science Reviews, v. 204, https://doi.org/10.1016/j.earscirev.2020.103149.

Pan, G.T., Ding, J., Yao, D., and Wang, L., 2004, Geological Map of Qinghai-Xiang (Tibet) Plateau and Adjacent Areas: Chengdu, China, Chengdu Institute of Geology and Mineral Resources, China Geological Survey, scale 1:1,500,000.

Paton, C., Woodhead, J.D., Hellstrom, J.C., Hergt, J.M., Greig, A., and Maas, R., 2010, Improved laser ablation U-Pb zircon geochronology through robust downhole fractionation correction: Geochemistry, Geophysics, Geosystems, v. 11, Q0AA06, https://doi.org/10.1029/2009GC002618.

Paton, C., Hellstrom, J., Paul, B., Woodhead, J., and Hergt, J., 2011, Iolite: Freeware for the visualisation and processing of mass spectrometric data: Journal of Analytical Atomic Spectrometry, v. 26, p. 2508, https://doi.org/10.1039/c1ja10172b.

Pearce, N.J.G., Perkins, W.T., Westgate, J.A., Gorton, M.P., Jackson, S.E., Neal, C.R., and Chenery, S.P., 1997, A compilation of new and published major and trace element data for NIST SRM 610 and NIST SRM 612 glass reference materials: Geostandards Newsletter, v. 21, p. 115–144, https://doi.org/10.1111/j.1751-908X.1997.tb00538.x.

Peng, N., Kuang, H.W., and Liu, Y.Q., 2011, Sedimentary evolution and palaeogeography of the Early Cretaceous basins from the northern Qilian Mountains to Jiuxi areas: Earth Science Frontiers, v. 18, p. 77–87 [in Chinese with English abstract].
Peng, R.M., Zhai, Y.S., Li, C.S., and Ripley, E.M., 2013, The Erbutu Ni-Cu deposit in the Central Asian orogenic belt: A Permian magmatic sulfide deposit related to boninitic magmatism in an arc setting: Economic Geology, v. 108, p. 1879–1888, https://doi.org/10.2113/econgeo.108.8.1879.
Peng, Y.B., Yu, S.Y., Zhang, J.X., Li, S.Z., Sun, D.Y., and Tong, L.X., 2017, Early Paleozoic arc magmatism and metamorphism in the northern Qilian block, western China: A case study of Menyuan-Kekeli: Acta Petrologica Sinica, v. 33, p. 3925–3941 [in Chinese with English abstract].
Peng, Y.B., Yu, S.Y., Li, S.Z., Zhang, J.X., Liu, Y.J., Li, Y., and Santosh, M., 2019, Early Neoproterozoic magmatic imprints in the Altun-Qilian-Kunlun region of the Qinghai-Tibet Plateau: Response to the assembly and breakup of Rodinia supercontinent: Earth-Science Reviews, v. 199, https://doi.org/10.1016/j.earscirev.2019.102954.
Pi, Q.H., Liu, C.Z., Chen, Y., Li, Y.L., and Li, D.P., 2010, Formation epoch and genesis of intrusive rocks in Huogeqi orefield of Inner Mongolia and their relationship with copper mineralization: Mineral Deposits, v. 29, p. 437–451 https://doi.org/10.16111/j.0258-7106.2010.03.007 [in Chinese with English abstract].
Qi, B.S., Hu, D.G., Yang, X.X., Zhang, Y.L., Tan, C.X., Zhang, P., and Feng, C.J., 2016, Apatite fission track evidence for the Cretaceous–Cenozoic cooling history of the Qilian Shan (NW China) and for stepwise northeastward growth of the northeastern Tibetan Plateau since early Eocene: Journal of Asian Earth Sciences, v. 124, p. 28–41, https://doi.org/10.1016/j.jseaes.2016.04.009.
Qi, R.R., 2012, LA-ICP-MS zircon U-Pb ages and geological implications for the Bagadeerji granitic plutons in the central Qilian Mountains, Gansu: Sedimentary Geology and Tethyan Geology, v. 32, p. 86–93 [in Chinese with English abstract].
Qian, Q., Wang, Y.M., Li, H.M., Jian, X.Q., Han, S., and Zhang, Q., 1998, Geochemical characteristics and genesis of diorites from Laohushan, Gansu Province: Acta Petrologica Sinica, v. 14, p. 520–528 [in Chinese with English abstract].
Qin, H.P., Wu, C.L., Wang, C.S., Lei, M., Liu, C.H., and M.Z., 2014a, LA-ICP-MS zircon U-Pb geochronology and geochemical characteristics of Xiagucheng granite in north Qilian: Acta Geologica Sinica, v. 88, p. 1832–1842 [in Chinese with English abstract].
Qin, H.P., Wu, C.L., Wang, C.S., Li, X., Lei, M., Liu, C.H., and Li, M.Z., 2014b, LA-ICP-MS zircon U-Pb dating and geochemical characteristics of high Sr/Y-type granite from Xigela, eastern Qilian area: Acta Petrologica Sinica, v. 30, p. 3759–3771 [in Chinese with English abstract].
Qin, Y., 2018, Neoproterozoic to Early Paleozoic Tectonic Evolution in the South Qilian Orogen [Ph.D. thesis]: Xi'an, China, Northwest University, 153 p.
Qing, H., 2012, Petrology of Early Paleozoic Granites and Their Relation to Tectonic Evolution Orogen in the North Qilian Orogenic Belt [Ph.D. thesis]: Beijing, Chinese Academy of Geological Sciences, 150 p.
Ran, H., Zhang, W.J., and Liu, Z.B., 2012, Geochemical characteristics and LA-ICP-MS zircon U-Pb dating of the late Permian monzogranite in Hanggale, Alxa Right Banner, Inner Mongolia: Geological Bulletin of China, v. 31, p. 1565–1575 [in Chinese with English abstract].
Ren, J.S., Niu, B.G., Wang, J., He, Z.J., Jin, X.C., Xie, L.Z., Zhao, L., Liu, R.Y., Jiang, X.J., Li, S., and Yang, F.L., 2013, 1:5 million [scale] international geological map of Asia: Acta Geoscientica Sinica, v. 34, p. 24–30 [in Chinese with English abstract].
Royden, L.H., Burchfiel, B.C., and Van Der Hilst, R.D., 2008, The geological evolution of the Tibetan Plateau: Science, v. 321, p. 1054–1058, https://doi.org/10.1126/science.1155371.
Saylor, J.E., and Sundell, K.E., 2016, Quantifying comparison of large detrital geochronology data sets: Geosphere, v. 12, p. 203–220, https://doi.org/10.1130/GES01237.1.
Shao, H.H., Chen, X.H., and Zhang, D., 2019, The Early Cretaceous tectonic deformation stages and detrital zircon U-Pb ages of Pingshanhu Basin in Hexi Corridor: Geology in China, v. 46, p. 1079–1093 [in Chinese with English abstract].
Shi, J.P., Huo, T.F., Lai, Q., Peng, X.H., Du, S.Y., and Yang, D.B., 2015, Petrogenesis of early Silurian Gangchadasi granites in the eastern segment of the northern South Qilian block: Constraints from LA-ICP-MS zircon U-Pb geochronology and geochemistry: Acta Geoscientica Sinica, v. 36, p. 781–789 [in Chinese with English abstract].
Shi, J.P., Han, X.Z., Qiao, S.Y., Wang, Z.S., Huo, T.F., Yang, H.T., and Yang, D.B., 2017, The Late Ordovician tectonic evolution of the eastern section of the northern margin of the South Qilian block: Evidences from geochronology, geochemistry and mineral chemistry of the Duozang hornblende gabbro: Earth Science Frontiers, v. 24, p. 46–59 [in Chinese with English abstract].
Shi, X.J., 2012, The Geochronology, Geochemistry and Petrogenesis of Granitoid in Qinggele Area, Northern Alxa [M.A. thesis]: Beijing, China University of Geosciences (Beijing), 59 p.
Shi, X.J., Wang, T., Zhang, L., Castro, A., Xiao, X.C., Tong, Y., Zhang, J.J., Guo, L., and Yang, Q.D., 2014a, Timing, petrogenesis and tectonic setting of the late Paleozoic gabbro-granodiorite-granite intrusions in the Shalazhashan of northern Alxa: Constraints on the southernmost boundary of the Central Asian orogenic belt: Lithos, v. 208–209, p. 158–177, https://doi.org/10.1016/j.lithos.2014.08.024.
Shi, X.J., Zhang, L., Wang, T., Xiao, X.C., Ying, T., Zhang, J.J., Geng, J.Z., and Ye, K., 2014b, Geochronology and geochemistry of the intermediate-acid intrusive rocks from Zongnaishan area in northern Alxa, Inner Mongolia, and their tectonic implications: Acta Petrologica et Mineralogica, v. 33, p. 989–1007 [in Chinese with English abstract].
Sláma, J., Košler, J., Condon, D.J., Crowley, J.L., Gerdes, A., Hanchar, J.M., Horstwood, M.S.A., Morris, G.A., Nasdala, L., Norberg, N., Schaltegger, U., Schoene, B., Tubrett, M.N., and Whitehouse, M.J., 2008, Plešovice zircon—A new natural reference material for U-Pb and Hf isotopic microanalysis: Chemical Geology, v. 249, p. 1–35, https://doi.org/10.1016/j.chemgeo.2007.11.005.
Song, D.F., Xiao, W.J., Collins, A.S., Glorie, S., Han, C.M., and Li, Y.C., 2017, New chronological constraints on the tectonic affinity of the Alxa block, NW China: Precambrian Research, v. 299, p. 230–243, https://doi.org/10.1016/j.precamres.2017.07.015.
Song, D.F., Glorie, S., Xiao, W.J., Collins, A.S., Gillespie, J., Jepson, G., and Li, Y.C., 2018, Tectono-thermal evolution of the southwestern Alxa tectonic belt, NW China: Constrained by apatite U-Pb and fission track thermochronology: Tectonophysics, v. 722, p. 577–594, https://doi.org/10.1016/j.tecto.2017.11.029.
Song, D.F., Xiao, W.J., Windley, B.F., and Han, C.M., 2021, Provenance and tectonic setting of late Paleozoic sedimentary rocks from the Alxa tectonic belt (NW China): Implications for accretionary tectonics of the southern Central Asian orogenic belt: Geological Society of America Bulletin, v. 133, p. 253–276, https://doi.org/10.1130/B35652.1.
Song, S.G., Su, L., Li, X.H., Niu, Y.L., and Zhang, L.F., 2012, Grenville-age orogenesis in the Qaidam-Qilian block: The link between South China and Tarim: Precambrian Research, v. 220–221, p. 9–22, https://doi.org/10.1016/j.precamres.2012.07.007.
Song, S.G., Niu, Y.L., Su, L., and Xia, X.H., 2013, Tectonics of the North Qilian orogen, NW China: Gondwana Research, v. 23, p. 1378–1401, https://doi.org/10.1016/j.gr.2012.02.004.
Song, T.Z., Liu, J.D., Li, J., Zhang, X.Y., Liang, K.X., and Zheng, Y., 2016, LA-ICP-MS zircon U-Pb age of gabbro and basalt in the Baimuxia area of North Qilian and its geological significance: Northwest Geology, v. 49, p. 32–42 [in Chinese with English abstract].
Song, Z.B., Ren, Y.X., Li, Z.P., and Yang, J.G., 2004, A discussion on intrusion epochs of granodiorites along the Bagexia-Heidaban zone in the western part of the North Qilian Mountains: Acta Geologica Sinica, v. 25, p. 205–208 [in Chinese with English abstract].
Su, J.P., Hu, N.G., Zhang, H.F., and Feng, B.Z., 2004a, U-Pb zircon dating and genesis of the Heigouliangzi granitic intrusion in the western segment of the middle Qilian Mountains: Geoscience, v. 18, p. 70–74 [in Chinese with English abstract].
Su, J.P., Hu, N.G., Zhang, H.F., and Fu, G.M., 2004b, Single zircon U-Pb dating and geological significance of the Diaodaban granitic gneiss in the western segment of North Qilian Mountains: Geological Science and Technology Information, v. 23, p. 11–14 [in Chinese with English abstract].
Su, J.P., Zhang, X.H., Hu, N.G., Fu, G.M., and Zhang, H.F., 2004c, Geochemical characteristics and genesis of adakite-like granites at Yema Nanshan in the western segment of the central Qilian Mountains: Geology in China, v. 31, p. 65–371 [in Chinese with English abstract].
Tang, L., 2015, Granite Characteristics and Zircon LA-ICP-MS U-Pb Dating of Jiling Area in Longshoushan, Gansu Province [M.A. thesis]: Shanghai, East China Institute of Technology, 81 p.
Tang, Q.Y., Li, C.S., Zhang, M.J., Ripley, E.M., and Wang, Q.L., 2014, Detrital zircon constraint on the timing of amalgamation between Alxa and Ordos, with exploration implications for Jinchuan-type Ni-Cu ore deposit in China: Precambrian Research, v. 255, p. 748–755, https://doi.org/10.1016/j.precamres.2014.08.015.
Tao, G., Zhu, L.D., Ouyang, H.Z., Xie, L., Yang, W.G., and Yang, Z., 2017, Petrogenesis and geological significance of the North Liuhuangkuang granodiorite in the west segment of the Qilian terrane: Evidences from geochronology, geochemistry, and Hf isotopes: Earth Science, v. 42, p. 2258–2275 [in Chinese with English abstract].
Tapponnier, P., Zhiqin, X., Roger, F., Meyer, B., Arnaud, N., Wittlinger, G., and Yang, J.S., 2001, Oblique stepwise rise and growth of the Tibet Plateau: Science, v. 294, p. 1671–1677, https://doi.org/10.1126/science.105978.
Taylor, M., Yin, A., Ryerson, F.J., Kapp, P., and Ding, L., 2003, Conjugate strike-slip faulting along the Bangong-Nujiang suture zone accommodates coeval east-west extension and north-south shortening in the interior of the Tibetan Plateau: Tectonics, v. 22, 1044, correction available at https://agupubs.onlinelibrary.wiley.com/doi/10.1029/2003TC001580.

Tseng, C.Y., Yang, H.Y., Wan, Y.S., Liu, D.Y., Wen, D.J., Lin, T.C., and Tung, K.A., 2006, Finding of Neoproterozoic (~775 Ma) magmatism recorded in metamorphic complexes from the North Qilian orogen: Evidence from SHRIMP zircon U-Pb dating: Chinese Science Bulletin, v. 51, p. 963–970, https://doi.org/10.1007/s11434-006-0963-1.

Tseng, C.Y., Yang, H.J., Yang, H.Y., Liu, D.Y., Wu, C.L., Cheng, C.K., Chen, C.H., and Ker, C.M., 2009, Continuity of the North Qilian and North Qinling orogenic belts, Central orogenic system of China: Evidence from newly discovered Paleozoic adakitic rocks: Gondwana Research, v. 16, p. 285–293, https://doi.org/10.1016/j.gr.2009.04.003.

Tung, K.A., Yang, H.J., Yang, H.Y., Liu, D.Y., Zhang, J.X., Wan, Y.S., and Tseng, C.Y., 2007, SHRIMP U-Pb geochronology of the zircons from the Precambrian basement of the Qilian block and its geological significances: Chinese Science Bulletin, v. 52, p. 2687–2701, https://doi.org/10.1007/s11434-007-0356-0.

Tung, K.A., Yang, H.Y., Liu, D.Y., Zhang, J.X., Yang, H.J., Shua, Y.H., and Tseng, C.Y., 2013, The Neoproterozoic granitoids from the Qilian block, NW China: Evidence for a link between the Qilian and South China blocks: Precambrian Research, v. 235, p. 163–189, https://doi.org/10.1016/j.precamres.2013.06.016.

Vermeesch, P., 2013, Multi-sample comparison of detrital age distributions: Chemical Geology, v. 341, p. 140–146, https://doi.org/10.1016/j.chemgeo.2013.01.010.

Vincent, S.J., and Allen, M.B., 1999, Evolution of the Minle and Chaoshui Basins, China: Implications for Mesozoic strike-slip basin formation in Central Asia: Geological Society of America Bulletin, v. 111, p. 725–742, https://doi.org/10.1130/0016-7606(1999)111<0725:EOTMAC>2.3.CO;2.

Wan, Y.S., Xu, Z.Q., Yang, J.S., and Zhang, J.X., 2001, Ages and compositions of the Precambrian high-grade basement of the Qilian terrane and its adjacent areas: Acta Geologica Sinica, v. 75, p. 375–384, https://doi.org/10.1111/j.1755-6724.2001.tb00055.x [in Chinese with English abstract].

Wan, Y.S., Xu, Z.Q., Yang, J.S., and Zhang, J.X., 2003, The Precambrian high-grade basement of the Qilian terrane and neighboring areas: Its ages and compositions: Acta Geoscientia Sinica, v. 24, p. 319–324 [in Chinese with English abstract].

Wang, C.S., Dai, J.G., Zhao, X.X., Li, Y.L., Graham, S.A., He, D.F., Ran, B., and Meng, J., 2014, Outward-growth of the Tibetan Plateau during the Cenozoic: A review: Tectonophysics, v. 621, p. 1–43, https://doi.org/10.1016/j.tecto.2014.01.036.

Wang, C.S., Yu, S.Y., Sun, D.Y., Lv, P., Feng, Z., Wang, G., and Gou, J., 2021, Mesoproterozoic tectonic-thermal events in the Oulongbuluke block, NW China: Constraints on the transition from supercontinent Columbia to Rodinia: Precambrian Research, v. 352, https://doi.org/10.1016/j.precamres.2020.106010.

Wang, G.L., Chen, F.B., Li, W.F., Cao, J.S., Han, H.C., Liu, R., and Bao, G.P., 2018a, Discussion on the relationship between the Longwangshan granite mass and the Huashixia W-Mo deposit in the transitional belt of northern-central Qilian: Northwest Geology, v. 51, p. 227–243 [in Chinese with English abstract].

Wang, J., Xie, G., and Shi, G.H., 2018b, Geochronology of the Chuancigou A-type granite in the North Qilian belt and its significances: Acta Petrologica Sinica, v. 34, p. 1657–1668 [in Chinese with English abstract].

Wang, N., Wu, C.L., Lei, M., Cai, H.J., Li, M.Z., and Zheng, W.H., 2017a, Geochronology and petrogenesis of granite in Shibaocheng area from the North Qilian orogenic belt: Acta Petrologica Sinica, v. 33, p. 3909–3924 [in Chinese with English abstract].

Wang, Q.H., Luo, Y.H., and Li, Z.P., 2017b, Geochemistry characteristics and tectonic setting analysis of Zhahuaqiangzi granite in western Qilian, Gansu: Gansu Science and Technology, v. 33, p. 25–25 [in Chinese with English abstract].

Wang, W.T., Zheng, D.W., Li, C.P., Wang, Y., Zhang, Z.Q., Pang, J.Z., Wang, Y., Yu, J.X., Wang, Y.Z., Zheng, W.J., Zhang, H.P., and Zhang, P.Z., 2020a, Cenozoic exhumation of the Qilian Shan in the northeastern Tibetan Plateau: Evidence from low-temperature thermochronology: Tectonics, v. 39, https://doi.org/10.1029/2019TC005705.

Wang, X.J., 2012, The Geochemical Characters and Tectonic Implications of Ophiolites in Alax Area, Inner Mongolia [Ph.D. thesis]: Beijing, China University of Geosciences (Beijing), 208 p.

Wang, Y., Chen, X.H., Zhang, Y.Y., Yin, Z., Zuza, A.V., Yin, A., Wang, Y.C., Ding, W.C., Xu, S.L., Zhang, Y.P., Li, B., and Shao, Z.G., 2022, Superposition of Cretaceous and Cenozoic deformation in northern Tibet: A far-field response to the tectonic evolution of the Tethyan orogenic system: Geological Society of America Bulletin, v. 134, p. 501–525, https://doi.org/10.1130/B35944.1.

Wang, Y., Chen, X.H., He, C.G., Xiao, Y.J., Shao, Z.G., Han, J.E., Li, B., Zhang, Y.P., Ding, W.C., Xu, S.L., and Han, L.L., 2023, Active tectonics and paleo-earthquakes in north Yumu Shan, northern Tibetan Plateau: Insights from structural analysis and radiocarbon dating: Frontiers of Earth Science, v. 11, https://doi.org/10.3389/feart.2023.1057936.

Wang, Z.Z., Han, B.F., Feng, L.X., and Liu, B., 2015, Geochronology, geochemistry and origins of the Paleozoic–Triassic plutons in the Langshan area, western Inner Mongolia, China: Journal of Asian Earth Sciences, v. 97, p. 337–351, https://doi.org/10.1016/j.jseaes.2014.08.005.

Wang, Z.Z., Chen, X.H., Shao, Z.G., Li, B., Ding, W.C., Zhang, Y.P., Xu, S.L., and Qin, X., 2020b, Petrogenesis of the late Silurian–Early Devonian granites in the Longshoushan-Helishan area, Gansu Province, and its tectonic implications for the early Paleozoic evolution of the southwestern Alxa block: Acta Geologica Sinica, v. 94, p. 2243–2261 [in Chinese with English abstract].

Wei, Q.Q., Hao, L.B., Lu, J.L., Zhao, X.Y., and Shi, H.L., 2013, LA-MC-ICP-MS zircon U-Pb dating of Hexipu granite and its geological implications: Bulletin of Mineralogy Petrology and Geochemistry, v. 32, p. 729–735 [in Chinese with English abstract].

Wiedenbeck, M., Allé, P., Corfu, F., Griffin, W.I., Meier, M., Oberli, F., Quadt, A.V., Roddick, J.C., and Spiegel, W., 1995, Three natural zircon standards for U-Th-Pb, Lu-Hf, trace element and REE analyses: Geostandards Newsletter, v. 19, p. 1–23, https://doi.org/10.1111/j.1751-908X.1995.tb00147.x.

Worley, B.A., and Wilson, C.J.L., 1996, Deformation partitioning and foliation reactivation during transpressional orogenesis, an example from the central Longmen Shan, China: Journal of Structural Geology, v. 18, p. 395–411, https://doi.org/10.1016/0191-8141(95)00095-U.

Wu, C., Zuza, A.V., Yin, A., Liu, C.F., Reith, R.C., Zhang, J.Y., Liu, W.C., and Zhou, Z.G., 2017, Geochronology and geochemistry of Neoproterozoic granitoids in the central Qilian Shan of northern Tibet: Reconstructing the amalgamation processes and tectonic history of Asia: Lithosphere, v. 9, p. 609–636, https://doi.org/10.1130/L640.1.

Wu, C., Zuza, A.V., Zhou, Z.G., Yin, A., McRivette, M.W., Chen, X.H., Ding, L., and Geng, J.Z., 2019a, Mesozoic–Cenozoic evolution of the Eastern Kunlun Range, central Tibet, and implications for basin evolution during the Indo-Asian collision: Lithosphere, v. 11, p. 524–550, https://doi.org/10.1130/L1065.1.

Wu, C., Zuza, A.V., Li, J., Haproff, P.J., Yin, A., Chen, X.H., Ding, L., and Li, B., 2021a, Late Mesozoic–Cenozoic cooling history of the northeastern Tibetan Plateau and its foreland derived from low-temperature thermochronology: Geological Society of America Bulletin, v. 133, p. 2393–2417, https://doi.org/10.1130/B35879.1.

Wu, C., Zuza, A.V., Yin, A., Chen, X.H., Haproff, P.J., Li, J., Li, B., and Ding, L., 2021b, Punctuated orogeny during the assembly of Asia: Tectonostratigraphic evolution of the North China craton and the Qilian Shan from the Paleoproterozoic to early Paleozoic: Tectonics, v. 40, https://doi.org/10.1029/2020TC006503.

Wu, C., Li, J., Zuza, A.V., Haproff, P.J., Chen, X.X., and Ding, L., 2022a, Proterozoic–Phanerozoic tectonic evolution of the Qilian Shan and Eastern Kunlun Range, northern Tibet: Geological Society of America Bulletin, v. 134, p. 2179–2205, https://doi.org/10.1130/B36306.1.

Wu, C., Li, J., Zuza, A.V., Haproff, P.J., Yin, A., and Ding, L., 2022b, Paleoproterozoic–Paleozoic tectonic evolution of the Longshou Shan, western North China craton: Geosphere, v. 18, p. 1177–1193, https://doi.org/10.1130/GES02491.1.

Wu, C.L., Yang, J.S., Yang, H.Y., Wooden, J.L., Shi, R.D., Chen, S.Y., and Zheng, Q.G., 2004, Dating of two types of granite from North Qilian, China: Acta Petrologica Sinica, v. 2, p. 425–432 [in Chinese with English abstract].

Wu, C.L., Gao, Y.H., Wu, S.P., Chen, Q.L., Wooden, J.L., Mazadab, F.K., and Mattinson, C., 2007, Zircon SHRIMP U-Pb dating of granites from the Da Qaidam area in the north margin of Qaidam Basin, NW China: Acta Petrologica Sinica, v. 23, p. 1861–1875 [in Chinese with English abstract].

Wu, C.L., Wooden, J.L., Robinson, P.T., Gao, Y.H., Wu, S.P., Chen, Q.L., Mazdab, F.K., and Mattinson, C., 2009, Geochemistry and zircon SHRIMP U-Pb dating of granitoids from the west segment of the North Qaidam: Science China Earth Sciences, v. 52, p. 1771–1790, https://doi.org/10.1007/s11430-009-0147-3.

Wu, C.L., Xu, X.Y., Gao, Q.M., Li, X.M., Lei, M., Gao, Y.H., Frost, R.B., and Wooden, J.L., 2010, Early Paleozoic granitoid magmatism and tectonic evolution in North Qilian, NW China: Acta Petrologica Sinica, v. 26, p. 1027–1044 [in Chinese with English abstract].

Wu, C.L., Gao, Y., Frost, B.R., Robinson, P.T., Wooden, J.L., Wu, S.P., Chen, Q.L., and Lei, M., 2011, An early Palaeozoic double-subduction model for the North Qilian oceanic plate: Evidence from zircon SHRIMP dating of granites: International Geology Review, v. 53, p. 157–181, https://doi.org/10.1080/00206810902965346.

Wu, K.L., 2011, Geochemical Characteristics and Tectonic Setting of Late Varisian Period in Alashan Block [M.A. thesis]: Xi'an, China, Chang'an University, 70 p.

Wu, S.J., Hu, J.M., Ren, M.H., Gong, W.B., Liu, Y., and Yan, J.Y., 2014, Petrography and zircon U-Pb isotopic study of the Bayanwulashan complex: Constraints on the Paleoproterozoic evolution of the Alxa block, westernmost North China craton: Journal of Asian Earth Sciences, v. 94, p. 226–239, https://doi.org/10.1016/j.jseaes.2014.05.011.
Wu, W.Z., Ma, R.Y., Zhang, X.D., Ma, F.H., Pan, J.L., and Wang, Z.J., 2019b, Geochemical characteristics, zircon U-Pb ages of the gabbro in Xiji region in the eastern segment northern Qilian Mountains and their significance: Geological Review, v. 65, p. 211–220 [in Chinese with English abstract].
Wu, Y.F., Zeng, J.N., Cao, J.J., Wu, Z.Q., Chen, J.H., Zhou, S.D., Lu, S.F., and Li, X.F., 2013, Zircon U-Pb ages and Hf isotope of Hercynian intrusion in Dongshengmiao, Inner Mongolia: Geological Science and Technology Information, v. 32, p. 22–30 [in Chinese with English abstract].
Xiao, J., Sun, P., and Xu, L., 2016, LA-ICP-MS zircon U-Pb age, geochemical characteristics and genesis of the early Permian gabbro in Nuoergong area, northern Alxa: Western Resources, p. 55–60, https://doi.org/10.16631/j.cnki.cn15-1331/p.2016.04.020.
Xiao, Z.B., Kang, J.L., Wang, H.C., Gao, Z.R., Xiang, Z.Q., Chu, H., and Ren, Y.W., 2015, Formation age of Alxa Group-complex (Special) in Alxa area, Inner Mongolia: Geological Survey and Research, v. 38, p. 182–191 [in Chinese with English abstract].
Xie, F.Q., 2014, Study of Granites Rock Mass of ZongnaiShalaza and Bayinnuoergong [M.A. thesis]: Beijing, China University of Geosciences (Beijing), 70 p.
Xie, F.Q., Wang, L.D., Li, Q., Shi, Z.X., Chen, X.B., and Wei, A., 2015, Zircon LA-ICP-MS dating of granites from the southeastern Zongnai Mountain, Alxa, and its geochemical characteristics: Rock and Mineral Analysis, v. 34, p. 375–382, https://doi.org/10.15898/j.cnki.11-2131/td.2015.03.019 [in Chinese with English abstract].
Xie, Q.F., Zhou, L.F., and Liu, Y., 2014, LA-ICP-MS zircon U-Pb ages of Gangchadasi granite in Qinghai Province and their geological significance: Geological Bulletin of China, v. 33, p. 1379–1390 [in Chinese with English abstract].
Xiong, Z.L., Zhang, H.F., and Zhang, J., 2012, Petrogenesis and tectonic implications of the Maozangshi and Huangyanghe granitic intrusions in Lenglongling area, the eastern part of North Qilian Mountains, NW China: Earth Science Frontiers, v. 19, p. 214–227 [in Chinese with English abstract].
Xiu, Q.Y., Lu, S.N., Yu, H.F., and Yang, C.L., 2002, The isotopic age evidence for main Longshoushan Group: Progress in Precambrian Research, v. 25, p. 93–96 [in Chinese with English abstract].
Xiu, Q.Y., Yu, H.F., Li, Q., Zuo, G.C., Li, J.W., and Cao, C.J., 2004, Discussion on the petrogenic time of Longshoushan Group, Gansu Province: Acta Geologica Sinica, v. 78, p. 366–373 [in Chinese with English abstract].
Xu, B., Charvet, J., Chen, Y., Zhao, P., and Shi, G.Z., 2013, Middle Paleozoic convergent orogenic belts in western Inner Mongolia (China): Framework, kinematics, geochronology and implications for tectonic evolution of the Central Asian orogenic belt: Gondwana Research, v. 23, p. 1342–1364, https://doi.org/10.1016/j.gr.2012.05.015.
Xu, D.Z., Zhang, W.J., Zhou, H.T., and Sun, Q.K., 2014, Characteristics, zircon dating and tectonic significance of the gabbros along the north-central segments of the Alxa block, Inner Mongolia: Geological Bulletin of China, v. 33, p. 661–671 [in Chinese with English abstract].
Xu, L., and Xiao, J., 2015, Zircon U-Pb age and geochemical characteristics of late Permian volcanic rocks in Alakkert, northern Alxa, Inner Mongolia: Western Resources, p. 107–111 [in Chinese].
Xu, L., and Xie, Q.X., 2015, LA-ICP-MS zircon U-Pb age and geochemical characteristics of the Bayannuorigong quartz diorite in Alxa, Inner Mongolia: Xinjiang Geology, v. 33, p. 529–536 [in Chinese].
Xu, W., Zhang, H.F., and Liu, X.M., 2007, U-Pb zircon dating constraints on formation time of Qilian high-grade metamorphic rock and its tectonic implications: Chinese Science Bulletin, v. 52, p. 531–538, https://doi.org/10.1007/s11434-007-0082-7.
Xu, Y.L., Ba, J., Wang, Q.L., Zhang, L., Wang, X.Y., and Chen, N.S., 2011, LA-ICP-MS zircon U-Pb age of the Halihadeshan granite-gneiss in northeastern Dulan, Qinghai, and its tectonic implications: Geological Bulletin of China, v. 3, p. 1037–1042 [in Chinese with English abstract].
Xue, N., Wang, J., Tan, S.X., Lin, H., Li, W.F., Ren, J.Q., and Liu, S.J., 2009, Geological significance of granite of Jinningian age in Yeniugou-Tuole region on the northern margin of central Qilian block: Journal of Qinghai University (Natural Science), v. 27, p. 23–28 [in Chinese with English abstract].
Xue, S., Ling, M.X., Liu, Y.L., Zhang, H., and Sun, W.D., 2017, The genesis of early Carboniferous adakitic rocks at the southern margin of the Alxa block, North China: Lithos, v. 278–281, p. 181–194, https://doi.org/10.1016/j.lithos.2017.01.012.
Yan, Z., Aitchison, J., Fu, C.L., Guo, X.Q., Niu, M.L., Xia, W.J., and Li, J.L., 2015, Hualong complex, South Qilian terrane: U-Pb and Lu-Hf constraints on Neoproterozoic micro-continental fragments accreted to the northern Proto-Tethyan margin: Precambrian Research, v. 266, p. 65–85, https://doi.org/10.1016/j.precamres.2015.05.001.
Yang, H., 2016, Early Paleozoic Intrusive Magmatism and Geodynamic Processes in the Eastern Segment of the Central Qilian [Ph.D. thesis]: Wuhan, China, China University of Geosciences, 154 p.
Yang, H., Zhang, H.F., Xiao, W.J., Luo, B.J., Gao, Z., Tao, L., Zhang, L.Q., and Guo, L., 2020, Petrogenesis of early Paleozoic high Sr/Y intrusive rocks from the North Qilian orogen: Implication for diachronous continental collision: Lithosphere, v. 12, p. 53–73, https://doi.org/10.1130/L1129.1.
Yang, J.H., Du, Y.S., Cawood, P.A., and Xu, Y.J., 2009, Silurian collisional suturing onto the southern margin of the North China craton: Detrital zircon geochronology constraints from the Qilian orogen: Sedimentary Geology, v. 220, p. 95–104, https://doi.org/10.1016/j.sedgeo.2009.07.001.
Yang, Q.D., Zhang, L., Wang, T., Shi, X.J., Zhang, J.J., Tong, Y., Guo, L., and Geng, J.Z., 2014, Geochemistry and LA-ICP-MS zircon U-Pb age of late Carboniferous Shalazhashan pluton on the northern margin of the Alxa block, Inner Mongolia and their implications: Geological Bulletin of China, v. 33, p. 776–787 [in Chinese with English abstract].
Ye, K., Zhang, L., Wang, T., Shi, X.J., Zhang, J.J., and Liu, C., 2016, Geochronology, geochemistry and zircon Hf isotopes of the Permian intermediate-acid igneous rocks from the Yabulai Mountain in western Alxa, Inner Mongolia, and their tectonic implications: Acta Petrologica et Mineralogica, v. 35, p. 901–928 [in Chinese with English abstract].
Yin, A., 2010, Cenozoic tectonic evolution of Asia: A preliminary synthesis: Tectonophysics, v. 488, p. 293–325, https://doi.org/10.1016/j.tecto.2009.06.002.
Yin, A., and Harrison, T.M., 2000, Geologic evolution of the Himalayan-Tibetan orogen: Annual Review of Earth and Planetary Sciences, v. 28, p. 211–280, https://doi.org/10.1146/annurev.earth.28.1.211.
Yin, A., Manning, C.E., Lovera, O., Menold, C.A., Chen, X.H., and Gehrels, G.E., 2007, Early Paleozoic tectonic and thermomechanical evolution of ultrahigh-pressure (UHP) metamorphic rocks in the northern Tibetan Plateau, Northwest China: International Geology Review, v. 49, p. 681–716, https://doi.org/10.2747/0020-6814.49.8.681.
Yin, A., Dang, Y.Q., Wang, L.C., Jiang, W.M., Zhou, S.P., Chen, X.H., Gehrels, G.E., and McRivette, M.W., 2008a, Cenozoic tectonic evolution of Qaidam Basin and its surrounding regions (Part 1): The southern Qilian Shan–Nan Shan thrust belt and northern Qaidam Basin: Geological Society of America Bulletin, v. 120, p. 813–846, https://doi.org/10.1130/B26180.1.
Yin, A., Dang, Y.Q., Zhang, M., Chen, X.H., and McRivette, M.W., 2008b, Cenozoic tectonic evolution of the Qaidam Basin and its surrounding regions (Part 3): Structural geology, sedimentation, and regional tectonic reconstruction: Geological Society of America Bulletin, v. 120, p. 847–876, https://doi.org/10.1130/B26232.1.
Yong, Y., Xiao, W.J., Yuan, C., Li, J.L., Yan, Z., and Mao, Q.G., 2008, LA-ICP-MS zircon U-Pb ages of granitic plutons from the eastern sector of the central Qilian and their geologic implication: Xinjiang Geology, v. 26, p. 62–70 [in Chinese with English abstract].
Yu, J.X., Zheng, D.W., Pang, J.Z., Wang, Y.Z., Fox, M., Vermeesch, P., Li, C.P., Xiao, L., Hao, Y.Q., and Wang, Y., 2019, Miocene range growth along the Altyn Tagh fault: Insights from apatite fission track and (U-Th)/He thermochronometry in the western Danghenan Shan, China: Journal of Geophysical Research: Solid Earth, v. 124, p. 9433–9453, https://doi.org/10.1029/2019JB017570.
Yu, S.Y., Zhang, J.X., del Real, P.G., Zhao, X.L., Hou, K.J., Gong, J.H., and Li, Y.S., 2013, The Grenvillian orogeny in the Altun–Qilian–North Qaidam mountain belts of northern Tibet Plateau: Constraints from geochemical and zircon U-Pb age and Hf isotopic study of magmatic rocks: Journal of Asian Earth Sciences, v. 73, p. 372–395, https://doi.org/10.1016/j.jseaes.2013.04.042.
Yu, S.Y., Zhang, J.X., Qin, H.P., Sun, D.Y., Zhao, X.L., Cong, F., and Li, Y.S., 2015, Petrogenesis of the early Paleozoic low-Mg and high-Mg adakitic rocks in the North Qilian orogenic belt, NW China: Implications for transition from crustal thickening to extension thinning: Journal of Asian Earth Sciences, v. 107, p. 122–139, https://doi.org/10.1016/j.jseaes.2015.04.018.
Yu, X.J., Fu, S.T., Wang, Z.D., Li, Q., and Guo, Z.J., 2017, The discovery of early Paleoproterozoic high-Na trondhjemite in the northeastern Qaidam Basin: Evidence from the drilling core samples: Precambrian Research, v. 298, p. 615–628, https://doi.org/10.1016/j.precamres.2017.04.002.
Yu, X.L., Cao, C.L., Wei, X.L., Liu, X.X., and Yue, X., 2018a, Zircon U-Pb geochronology, geochemical characteristics and geological significance of middle Ordovician intrusive rocks in Shulenanshan area of South Qilian: Mineral Exploration, v. 9, p. 2049–2058 [in Chinese with English abstract].
Yu, X.L., Cao, C.L., Zhang, S.L., Wei, X.L., and Liu, X.X., 2018b, Petrogenesis of early Silurian intrusive rocks in Yeniujishan area of South Qilian: Constraints from geochemistry and LA-ICP-MS zircon U-Pb geochronology: Northwest Geology, v. 51, p. 133–146 [in Chinese with English abstract].

Yuan, D.Y., Ge, W.P., Chen, Z.W., Li, C.Y., Wang, Z.C., Zhang, H.P., Zhang, P.Z., Zheng, D.W., Bi, W.J., Craddock, W.H., Dayem, K.E., Duvall, A.R., Hough, B.G., Lease, R.O., Champagnac, J.D., Burbank, D.W., Clark, M.K., Farley, K.A., Garzione, C.N., Kirby, E., Molnar, P., and Roe, G.H., 2013, The growth of northeastern Tibet and its relevance to large-scale continental geodynamics: A review of recent studies: Tectonics, v. 32, p. 1358–1370, https://doi.org/10.1002/tect.20081.

Zeng, R.Y., Lai, J.Q., Mao, X.C., Li, B., Ju, P.J., and Tao, S.L., 2016, Geochemistry, zircon U-Pb dating and Hf isotope compositions of Paleozoic granitoids in Jinchuan, NW China: Constraints on their petrogenesis, source characteristics and tectonic implication: Journal of Asian Earth Sciences, v. 121, p. 20–33, https://doi.org/10.1016/j.jseaes.2016.02.009.

Zeng, R.Y., Lai, J.Q., Mao, X.C., Yan, J., Zhang, C.G., and Xiao, W.Z., 2021, Geochemistry and zircon ages of the Yushigou diabase in the Longshoushan area, Alxa block: Implications for crust-mantle interaction and tectonic evolution: Geological Magazine, v. 158, p. 685–700, https://doi.org/10.1017/S0016756820000783.

Zhang, B.H., Zhang, J., Zhang, Y.P., Zhao, H., Wang, Y.N., and Nie, F.J., 2016a, Tectonic affinity of the Alxa block, Northwest China: Constrained by detrital zircon U-Pb ages from the early Paleozoic strata on its southern and eastern margins: Sedimentary Geology, v. 339, p. 289–303, https://doi.org/10.1016/j.sedgeo.2016.02.017.

Zhang, B.H., Zhang, J., Wang, Y.N., Zhao, H., and Li, Y.F., 2017a, Late Mesozoic–Cenozoic exhumation of the northern Hexi Corridor: Constrained by apatite fission track ages of the Longshoushan: Acta Geologica Sinica (English Edition), v. 91, p. 1624–1643, https://doi.org/10.1111/1755-6724.13402.

Zhang, C.C., Wang, H., Chen, S., Yu, J.J., Liao, Y.T., Lu, Z.S., and Wei, J., 2019a, Lacustrine basin fills in an Early Cretaceous half-graben, Jiuquan Basin, NW China: Controlling factors and implications for source rock depositional processes and heterogeneity: Journal of Earth Science, v. 30, p. 158–175, https://doi.org/10.1007/s12583-017-0953-z.

Zhang, C.Y., Wu, L., Chen, W.K., Zhang, Y.S., Xiao, A.C., Zhang, J.Y., Chen, S.Y., and Chen, H.L., 2020, Early Cretaceous foreland-like northeastern Qaidam Basin, Tibetan Plateau, and its tectonic implications: Insights from sedimentary investigations, detrital zircon U-Pb analyses and seismic profiling: Palaeogeography, Palaeoclimatology, Palaeoecology, v. 557, https://doi.org/10.1016/j.palaeo.2020.109912.

Zhang, G.D., Xu, Z.Q., Gong, J., Feng, J., Han, Y.B., Zhang, J.W., Zhou, Y., Huang, Z.S., Zeng, X.F., Zhang, K.J., Wang, J.K., and Cheng, J., 2016b, Geochronology and significance of intermediate-acid intrusive rocks in Quanji area, Gangcha, Qinghai: Geological Journal of China Universities: Geological Journal of China Universities, v. 22, p. 113–126 [in Chinese with English abstract].

Zhang, H.R., Zhao, J.I., and Yu, H.Y., 2019b, Petrogenesis and tectonic implications of the Laohushan quartz diorite from the eastern part of North Qilian orogen: Geological Journal of China Universities, v. 25, p. 641–653 [in Chinese with English abstract].

Zhang, J., Li, J.Y., Xiao, W.X., Wang, Y.N., and Qi, W.H., 2013a, Kinematics and geochronology of multistage ductile deformation along the eastern Alxa block, NW China: New constraints on the relationship between the North China plate and the Alxa block: Journal of Structural Geology, v. 57, p. 38–57, https://doi.org/10.1016/j.jsg.2013.10.002.

Zhang, J., Wang, Y.N., Qu, J.F., Zhang, B.H., Zhao, H., Yun, L., Li, T.Y., Niu, P.F., Nie, F.J., Hui, J., and Zhang, Y.P., 2021, Mesozoic intracontinental deformation of the Alxa block in the middle part of Central Asian orogenic belt: A review: International Geology Review, v. 63, p. 1490–1520, https://doi.org/10.1080/00206814.2020.1783583.

Zhang, J.J., Wang, T., Zhang, Z.C., Tong, Y., Zhang, L., Shi, X.J., Guo, L., Li, S., and Zeng, T., 2012a, Magma mixing origin of Yamatu granite in Nuoergong-Langshan area, western part of the northern margin of North China craton: Petrological and geochemical evidences: Geological Review, v. 58, p. 53–66 [in Chinese with English abstract].

Zhang, J.J., Wang, T., Zhang, L., Tong, Y., Zhang, Z.C., Shi, X.J., Guo, L., Huang, H., Yang, Q.D., Huang, W., Zhao, J.X., Ye, K., and Hou, J.Y., 2015a, Tracking deep crust by zircon xenocrysts within igneous rocks from the northern Alxa, China: Constraints on the southern boundary of the Central Asian orogenic belt: Journal of Asian Earth Sciences, v. 108, p. 150–169, https://doi.org/10.1016/j.jseaes.2015.04.019.

Zhang, J.J., Wang, T., Castro, A., Zhang, L., Shi, X.J., Tong, Y., Zhang, Z.C., Guo, L., Yang, Q.D., and Maria Iaccheri, L., 2016c, Multiple mixing and hybridization from magma source to final emplacement in the Permian Yamatu pluton, the northern Alxa block, China: Journal of Petrology, v. 57, p. 933–980, https://doi.org/10.1093/petrology/egw028.

Zhang, J.M., Chen, G.T., Cai, H.J., and Fu, Y.W., 2018a, Zircon U-Pb age dating of the diorite in the Suli area of central Qilian Mountains: Its geological significance: Journal of Mineral Petrology, v. 38, p. 20–26 [in Chinese with English abstract].

Zhang, J.X., and Gong, J.H., 2018, Revisiting the nature and affinity of the Alxa block: Acta Petrologica Sinica, v. 34, p. 940–962 [in Chinese with English abstract].

Zhang, J.X., Mattinson, C.G., Meng, F., Wan, Y., and Tung, K., 2008, Polyphase tectonothermal history recorded in granulitized gneisses from the north Qaidam HP/UHP metamorphic terrane, western China: Evidence from zircon U-Pb geochronology: Geological Society of America Bulletin, v. 120, p. 732–749, https://doi.org/10.1130/B26093.1.

Zhang, J.X., Gong, J.H., Yu, S.Y., Li, H.K., and Hou, K.J., 2013b, Neoarchean–Paleoproterozoic multiple tectonothermal events in the western Alxa block, North China craton, and their geological implication: Evidence from zircon U-Pb ages and Hf isotopic composition: Precambrian Research, v. 235, p. 36–57, https://doi.org/10.1016/j.precamres.2013.05.002.

Zhang, L., Shi, X.J., Zhang, J.J., Yang, Q.D., Tong, Y., and Wang, T., 2013c, LA-ICP-MS zircon U-Pb age and geochemical characteristics of the Taohaotuoxiquan gabbro in northern Alxa, Inner Mongolia: Geological Bulletin of China, v. 32, p. 1536–1547 [in Chinese with English abstract].

Zhang, L.L., 2014, The Geochemistry and Tectonic Significance of Granitic Rocks in Danghenanshan Region, South Qilian Mountains [M.A. thesis]: Lanzhou, China, Lanzhou University, 93 p.

Zhang, L.Q., Zhang, H.F., Zhang, S.S., Xiong, Z.L., Luo, B.J., Yang, H., Pan, F.B., Zhou, X.C., Xu, W.C., and Guo, L., 2017b, Lithospheric delamination in post-collisional setting: Evidence from intrusive magmatism from the North Qilian orogen to southern margin of the Alxa block, NW China: Lithos, v. 288–289, p. 20–34, https://doi.org/10.1016/j.lithos.2017.07.009.

Zhang, L.T., Yu, J.P., Zhao, J.C., Fan, X.X., and Chen, S.X., 2018b, LA-ICP-MS zircon U-Pb age and geochemistry of Chaidano Mountain granite mass in the western part of North Qilian: Gansu Geology, v. 37, p. 8–16 [in Chinese with English abstract].

Zhang, M.J., Kamo, S.L., Li, C.S., Hu, P.Q., and Ripley, E.M., 2010, Precise U-Pb zircon-baddeleyite age of the Jinchuan sulfide ore-bearing ultramafic intrusion, western China: Mineralium Deposita, v. 45, p. 3–9, https://doi.org/10.1007/s00126-009-0259-x.

Zhang, S.H., Liu, C.Y., Wang, J.Q., Bai, J.K., Zhao, X.C., Zhang, L., Jia, N., Song, L.J., and Peng, H., 2022, Zircon U-Pb-Hf isotopes, biotite $^{40}Ar/^{39}Ar$ geochronology, and whole-rock geochemistry of the Baogeqi gabbro in the northern Alxa, southernmost Central Asian orogenic belt: Minerals (Basel), v. 12, p. 656, https://doi.org/10.3390/min12050656.

Zhang, W., Wu, T.R., Feng, J.C., Zheng, R.G., and He, Y.K., 2013d, Time constraints for the closing of the Paleo-Asian Ocean in the northern Alxa region: Evidence from Wuliji granites: Science China Earth Sciences, v. 56, p. 153–164, https://doi.org/10.1007/s11430-012-4435-y.

Zhang, W., Wang, J.R., Chen, W.F., Zhai, X.W., and Ma, J.L., 2014, The discovery of the carboniferous adakite and its tectonic implications in Alxa Youqi: Geological Journal of China Universities: Geological Journal of China Universities, v. 20, p. 378–387 [in Chinese with English abstract].

Zhang, X., Zhang, L.L., Wang, L.B., Liu, B., Dai, S., Jin, Z.P., Meng, Z., and Yang, H.Y., 2015b, Zircon U-Pb geochronology and geochemical characteristics of neutral-acidic intrusions of Wuligou in South Qilian Mountains: Their implications on forming gold deposit: Journal of Chengdu University of Technology (Science & Technology Edition), v. 42, p. 596–607 [in Chinese with English abstract].

Zhang, X.Y., Wang, C.T., Ouyang, G.W., and Li, R.B., 2018c, Zircon U-Pb ages and their geological significance of Aoguotunwulan pluton in South Qilian, China: Journal of Earth Sciences and Environment, v. 40, p. 546–562 [in Chinese with English abstract].

Zhang, Z.Q., Wang, K.X., Wang, G., Liu, X.D., Liu, W.H., and Wu, B., 2018d, Petrogenesis and tectonic significances of the Paleozoic Jiling syenite in the Longshou Mountain area, Gansu Province: Geological Review, v. 64, p. 1017–1029 [in Chinese with English abstract].

Zhang, Z.W., Li, W.Y., Gao, Y.B., Zhang, J.W., Guo, Z.P., and Li, K., 2012b, ID-TIMS zircon U-Pb age of Yulonggou intrusive rocks in southern Qilian Mountain and its geological significance: Geological Bulletin of China, v. 31, p. 455–462 [in Chinese with English abstract].

Zhang, Z.W., Li, W.Y., Wang, Y.L., and Gao, Y.B., 2015c, The genesis study on Xiashentang basic-ultrabasic intrusion associated with Ni-Cu mineralization in Hualong, southern Qilian Mountains: Zircon geochronology, geochemistry and Sr-Nd isotopic constraints: Acta Petrologica Sinica, v. 25, p. 2539–2548 [in Chinese with English abstract].

Zhao, G.B., Yang, H.Q., Ren, H.N., Jia, J., Wang, Y.H., Li, J.C., and Zhou, H., 2013, LA-ICP-MS zircon U-Pb ages of Heishishan granite bodies in North Qilian and their geological significance: Geological Bulletin of China, v. 32, p. 1575–1583 [in Chinese with English abstract].

Zhao, X.C., Liu, C.Y., Wang, J.Q., Zhao, Y., Wang, L., and Zhang, Q.H., 2016, Detrital zircon U-Pb ages of Paleozoic sedimentary rocks from the eastern Hexi Corridor belt (NW China): Provenance and geodynamic implications: Sedimentary Geology, v. 339, p. 32–45, https://doi.org/10.1016/j.sedgeo.2016.04.005.

Zhao, X.M., Zhang, Z.H., Liu, M., Li, Y.S., and Guo, S.F., 2014, Zircon U-Pb geochronology, geochemistry and petrogenesis of the granites from the Xiaoliugou deposit in the western part of the North Qilian: Acta Petrologica Sinica, v. 30, p. 16–34 [in Chinese with English abstract].

Zhao, X.M., Guo, Z.P., Wang, Y.X., Gao, Y.W., Zhang, L., Bai, Y., and Yang, S.F., 2018, Zircon U-Pb age, geochemical characteristics and geological significance of granitoids in the Maozangsi deposit, northern Qilian Mountain: Geological Bulletin of China, v. 37, p. 669–681 [in Chinese with English abstract].

Zheng, D.W., Wang, W.T., Wan, J.L., Yuan, D.Y., Liu, C.N., Zheng, W.J., Zhang, H.P., Pang, J.Z., and Zhang, P.Z., 2017a, Progressive northward growth of the northern Qilian Shan–Hexi Corridor (northeastern Tibet) during the Cenozoic: Lithosphere, v. 9, p. 408–416, https://doi.org/10.1130/L587.1.

Zheng, R.G., Wu, T.R., Zhang, W., Xu, C., Meng, Q.P., and Zhang, Z.Y., 2014, Late Paleozoic subduction system in the northern margin of the Alxa block, Altaids: Geochronological and geochemical evidences from ophiolites: Gondwana Research, v. 25, p. 842–858, https://doi.org/10.1016/j.gr.2013.05.011.

Zheng, R.G., Li, J.Y., Xiao, W.J., Liu, J.F., and Wu, T.R., 2016, Discovery of Silurian pluton in the Enger Us region in the northern margin of Alxa block: Acta Geologica Sinica, v. 90, p. 1725–1736 [in Chinese with English abstract].

Zheng, Y., Chen, G.T., Zhang, X.Y., Song, T.Z., and Liang, K.X., 2017b, Geochemical characteristics and chronology significance of Ordovician quartz diorite from Suli area in Middle Qilian Mountains: Northwest Geology, v. 50, p. 9–17 [in Chinese with English abstract].

Zhou, B., Zheng, Y.Y., Tong, H.K., Xu, R.K., Nie, X.L., Ma, C., and Liu, Q., 2014, Zircon dating of early adakitic granite on the northern margin of Qaidam Basin and its geological significance: Geoscience, v. 28, p. 875–883 [in Chinese with English abstract].

Zhou, X.C., Zhang, H.F., Luo, B.J., Pan, F.B., Zhang, S.S., and Guo, L., 2016, Origin of high Sr/Y-type granitic magmatism in the southwestern part of the Alxa block, Northwest China: Lithos, v. 256–257, p. 211–227, https://doi.org/10.1016/j.lithos.2016.04.021.

Zhu, X.H., Chen, D.L., Liu, L., Wang, C., Yang, W.Q., Cao, Y.T., and Kang, L., 2013, Geochemistry, geochronology, and Hf isotopic compositions of the Tuanyushan pluton from the western segment of the northern Qaidam: Geological Journal of China Universities: Geological Journal of China Universities, v. 19, p. 233–244 [in Chinese with English abstract].

Zhu, X.H., Wang, H.L., and Yang, M., 2016, Zircon U-Pb age of the monzogranite from the middle segment of the Qaidam Mountain composite granite on the south margin of the Qilian Mountains: Geology in China, v. 43, p. 751–767 [in Chinese with English abstract].

Zhu, X.L., Ren, E.F., Kang, W.H., Guan, S., Yang, Q.P., and Du, M., 2019, Zircon U-Pb age and geological significance of the granodiorite from the Bahan rock in the eastern part of South Qilian: Journal of Qinghai University, v. 37, p. 94–98 [in Chinese with English abstract].

Zuza, A.V., Cheng, X.G., and Yin, A., 2016. Testing models of Tibetan Plateau formation with Cenozoic shortening estimates across the Qilian Shan–Nan Shan thrust belt: Geosphere, v. 12, p. 501–532, https://doi.org/10.1130/GES01254.1

Zuza, A.V., Wu, C., Reith, R.C., Yin, A., Li, J.H., Zhang, J.Y., Zhang, Y.X., Wu, L., and Liu, W.C., 2018, Tectonic evolution of the Qilian Shan: An early Paleozoic orogen reactivated in the Cenozoic: Geological Society of America Bulletin, v. 130, p. 881–925, https://doi.org/10.1130/B31721.1.

Zuza, A.V., Wu, C., Wang, Z.Z., Levy, D.A., Li, B., Xiong, X.S., and Chen, X.H., 2019, Underthrusting and duplexing beneath the northern Tibetan Plateau and the evolution of the Himalayan-Tibetan orogen: Lithosphere, v. 11, p. 209–231, https://doi.org/10.1130/L1042.1.

Zuza, A.V., Gavillot, Y., Haproff, P.J., and Wu, C., 2020, Kinematic evolution of a continental collision: Constraining the Himalayan-Tibetan orogen via bulk strain rates: Tectonophysics, v. 797, https://doi.org/10.1016/j.tecto.2020.228642.